Long-Term Seepage Assessment Using Numerical Modeling for Upstream-Type Tailings Dams

Chengcheng Xu

A Thesis

in

The Department

of

Building, Civil and Environmental Engineering

Presented in Partial Fulfillment of the Requirements

for the Degree of

Master of Applied Science (Building, Civil and Environmental Engineering) at

Concordia University

Montreal, Quebec, Canada

February 2019

CONCORDIA UNIVERSITY

School of Graduate Studies

This is to certify that the thesis prepared by

By: Chengcheng Xu

Entitled: Long-Term Seepage Assessment Using Numerical Modeling for Upstream-Type Tailings Dams

and submitted in partial fulfillment of the requirements for the degree of

Master of Applied Science (Civil Engineering)

complies with the regulations of the University and meets the accepted standards with respect to originality and quality.

Signed by the final examining committee:

_____Chair
Dr. A. M. Hanna

_____Supervisor
Dr. A. M. Zsaki

_____Examiner External (to program)
Dr. A. Dolatabadi

_____Examiner
Dr. B. Li

_____Examiner
Dr. A. M. Hanna

Approved by _____
Dr. F. Haghighat, GPD
Department of Building, Civil and Environmental Engineering

_____
Dr. Amir Asif, Dean
Gina Cody School of Engineering and Computer Science

Date _____

Abstract

Long-Term Seepage Assessment Using Numerical Modeling for Upstream-Type Tailings Dams

Chengcheng Xu

A tailings dam, as part of a tailings storage facility, is typically constructed using waste rock or mine tailings, which are the waste created during extraction of ore from mining or by-products from mineral beneficiation and manufacturing. These dams are often raised continuously, as the tailings facility is expanding. The holding capacity of these facilities is needed to accommodate large volumes of tailings with the increasing demand placed on the mining industry. Thus, the topic of focus in this thesis is to investigate the seepage conditions that can ensure that the embankment can be safely constructed and operated during the raising stage and that it remains safe afterwards, beyond closure of the mine. However, according to statistics, a tailings dam must be protected against failures caused by various reasons even during its construction stage. Structural stability is the most important aspect and it should to be considered when addressing the problem of "safety" for tailings dams, which are threatened by seismic liquefaction, slope instability, overtopping and seepage. The seepage conditions of upstream-type tailings dams are the main topic of this research, which is associated with knowing the position of phreatic surface. The amount of pore water below the phreatic surface affects the stability of a tailings dam by reducing the shear strength of soil. The purpose of this thesis is to develop a seepage analysis model using a numerical modeling technique and to investigate potential means of phreatic surface control. Parameters like beach width, permeability anisotropy, raising rate of embankment and

slope inclination will be investigated to identify factors that may have a significant influence on the long-term evolution of phreatic surface within the tailings dam during the mine's life. This research will develop an uncoupled hydro-mechanical model using finite elements in which the whole process of construction is simulated in stages of embankment raising and filling of the tailings pond. The finite element model will be built using RS2, which is a comprehensive two-dimensional finite element program for soil and rock applications. It can model a wide range of engineering projects including excavation design, slope stability analysis, groundwater seepage, probabilistic analysis, and dynamic analysis. RS2 is able to carry out a finite element groundwater seepage analysis, with due consideration of both saturated and unsaturated soil states, in both steady-state and transient groundwater seepage formulations through both homogeneous and heterogeneous dams, dikes and other embankment types. However, basic finite element analysis principles will also be presented in this thesis, to aid the comprehension of the models developed. Based on the results of modeling, each identified parameter was assessed and guidelines were given regarding its contribution in the development of seepage face breakout on the downstream face of tailings embankment dams. These guidelines can serve practicing engineers in their design and evaluation of tailings dams to ensure safe and economical operation of tailings facilities.

Acknowledgments

First of all, I would like to express my deep appreciation to my research supervisor, Dr. Attila Michael Zsaki, who has provided me with a great amount of support and guidance throughout my study and research at Concordia. Thanks to his professional knowledge and patience, I was able to successfully conduct my thesis research.

I would also like to extend my sincerest appreciation and gratitude to my family, who has generously supported me financially and spiritually in the past three years, as well as all my friends, who helped me with their encouragement and love.

Authorization

I hereby declare that I am the sole author of the thesis.

I authorize the Department of Building, Civil and Environmental Engineering at Concordia University to lend this thesis to other institutions or individuals for the purpose of scholarly research.

I also authorize the Department of Building, Civil and Environmental Engineering at Concordia University to reproduce this thesis by photocopying or by other means, in total or in part, at the request of other institutions or individuals for the purpose of scholarly research.

Table of Contents

List of Tables

List of Figures

Notation

A	=	area of an element (m^2)
$[B]$	=	derivative matrix of the area coordinates
C_C	=	compression index
c_T	=	total stress – cohesion (kPa)
C_V	=	coefficient of consolidation (m^2/min)
$[D]$	=	stiffness matrix
$[E]$	=	capacitance matrix
$[F]$	=	flux vector reproducing the boundary conditions
d_{10}	=	grain size in millimeters for which 10% particles pass by weight
dx, dy	=	infinitesimal dimensions of soil element in the *x*-, *y*-direction, respectively
g	=	gravitational acceleration (9.81m/s^2)
H	=	embankment height (m)
h_w	=	hydraulic head (m)
$\{h_{wn}\}$	=	vector of hydraulic heads at the nodal points, that is $\begin{Bmatrix} h_{w1} \\ h_{w2} \\ h_{w3} \end{Bmatrix}$ for a triangular element (m)
i_x, i_y	=	hydraulic head gradient within an element in the *x*-, *y*-direction
k	=	average permeability (cm/s)
K_h / K_v	=	tailings embankment anisotropy
K_g	=	gaseous conductivity (mW/mK)
K_l	=	liquid conductivity (uS/cm)

k_s	=	saturated permeability coefficient (cm/s)
k_{sx}	=	saturated permeability coefficient in the *x*-direction (cm/s)
k_{sy}	=	saturated permeability coefficient in the *y*-direction (cm/s)
k_w	=	coefficient of permeability in the x- and y- directions (cm/s)
$[k_w]$	=	matrix of the water coefficients of permeability (cm/s)
$[K_w]$	=	tensor of the water coefficients of permeability for an element (cm/s)
k_{w1}	=	major coefficient of permeability (cm/s)
k_{w2}	=	minor coefficient of permeability (cm/s)
K_{wx} / K_{wy}	=	the ratio of variation of coefficients of permeability in the *x* and *y* directions
$k_{wx}(u_a\text{-}u_w)$, $k_{wy}(u_a\text{-}u_w)$	=	coefficient of permeability variation in the *x*-, *y*-direction (cm/s)
K_x, K_y	=	coefficients of permeability in the *x* and *y* directions (cm/s)
L	=	beach width (m)
(L)	=	element area coordinate matrix
$[L]$	=	matrix of element area coordinates
L_1, L_2, L_3	=	area coordinates of points in the element, for a triangular element (m)
m_2^w	=	coefficient of water volume change with respect to a change in matric suction
m_v	=	coefficient of volume change
S_p	=	perimeter of an element (m)
$\{u_{wn}\}$	=	matrix of pore-water pressures at nodal points for a triangular element
$\overline{v}_w$	=	external water flow rate in a direction perpendicular to the boundary of the element (cm/s)
v_{wx}, v_{wy}	=	water flow rate of soil element in the *x*-, *y*-direction, respectively (cm/s)

x, y	=	cartesian coordinates of a point within an element (m)
x_i, y_i	=	cartesian coordinates of the three nodal points (i=1,2,3) of a triangular element (m)
$\{y_n\}$	=	matrix of elevation heads at nodal points for a triangular element
φ	=	effective friction angle (degrees)
φ_T	=	total stress friction angle (degrees)
$\partial h_w / \partial y$	=	hydraulic head gradient in the *y*-direction
$\partial h_w / \partial x$	=	hydraulic head gradient in the *x*-direction
$\partial k_{wx} / \partial x$	=	change of coefficient of permeability in the *x*-direction
$\partial k_{wx} / \partial y$	=	change of coefficient of permeability in the y-direction
ρ_w	=	density of water (kg/m^3)
λ	=	$\rho_w g m_2^w$

Chapter 1: Introduction

1.1 PROBLEM STATEMENT

A tailings embankment dam is a geotechnical structure built to store adequate amount of mining waste during the life of an embankment dam using mined waste as construction material, thereby saving on cost. Due to the development of large open-pit mining operations over the past few decades, a typical tailings facilty has to be rapidly expanded in order to address the problem of storage capacity. Large open-pit mining operations can produce approximately 100,000 to 150,000 tons of tailings and/or mined waste per day, and even up to 250,000 tons are produced at the Syncrude operations at Alberta Oil Sands (Klohn, 1979).

Figure 1.1: The Mount Polley open pit copper and gold mine disaster in the Cariboo region of British Columbia (Linnitt, 2018).

Understandably, tailings dam safety issues are critical in today's mining operations, not only for structural stability, but including consideration for the environment and property. Any failures or dangerous incidents with tailings dams could result in human casualties, destruction of property, pollution of the environment and economic loss to the mining industry. Unfortunately, the frequency of major collapse events shows and increasing trend on an annual basis. Figure 1.1 illustrates the Mount Polley mine disaster that had occurred in 2014 in the Cariboo region of Central British Columbia (Chambers, 2016). About 25 million cubic meters of potentially toxic slurry waste were released into Hazeltine Creek, Quesnel Lake and Polley Lake, which removed trees in a 900 km^2 corridor on either side of Hazeltine Creek (Byrne et al., 2015). The spill widened the Haseltine Creek channel and expanded it from 2 meters to over 25 meters, and the water level of Polley Lake was raised by 170 meters. The solid tailings among this impoundment failure contained a mixture of unusual metal contaminants (arsenic, copper, gold, manganese, nickel, lead, vanadium) that may exist in regional soils and sediments for over 1000 years, and furthermore, the spill affected the regional biodiversity, water security and the livelihoods of First Nations communities (Byrne et al., 2015).

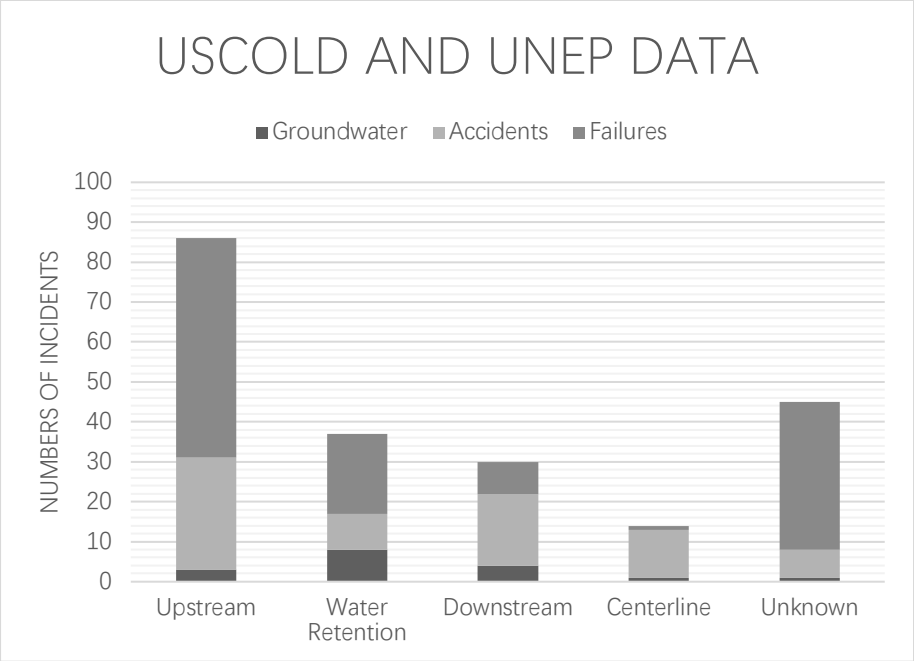

Figure 1.2: The comparison of tailings dam construction methods (ICOLD, 2001).

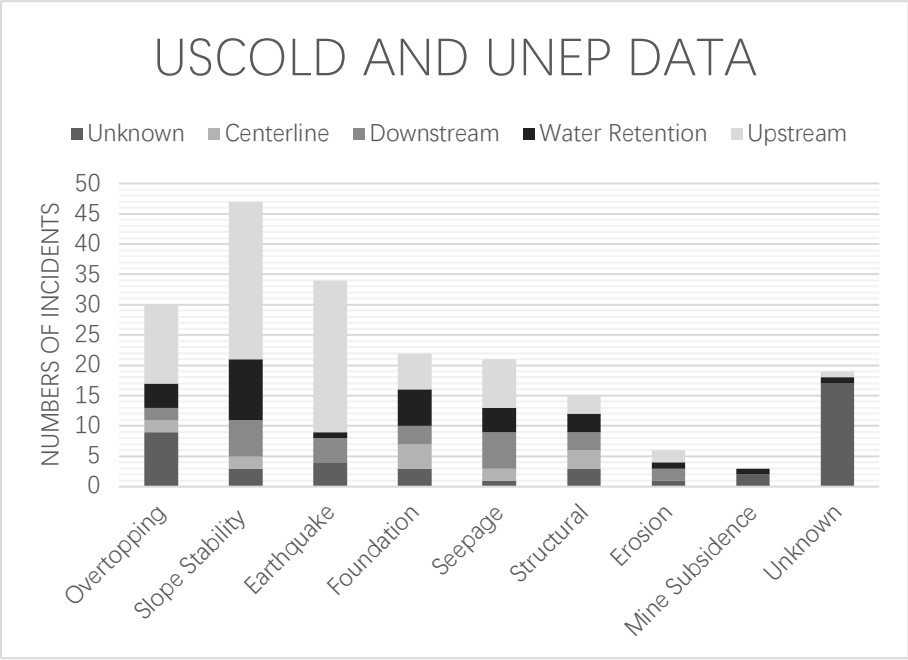

Figure 1.3: The comparison of tailings dam incident cause with incident type of active dams (ICOLD, 2001).

According to statistics provided by ICOLD, as shown in Figure 1.2, most of tailings dam failures belong to ones done by upstream construction methods and water retaining types in comparison with other methods of construction. Mittal and Morgenstern proposed the upstream construction method in 1991, becoming the oldest and most popular method, but the one with the most problems, which can be illustrated in Figure 1.3 (ICOLD, 2001).

1.2 MOTIVATION

Therefore, it is well-founded that further research is needed concerning the stability of tailings dams to provide tailings dam designers and constructors with access to effective tools and information to contribute to the design of safe tailings dams.

In this research, a detailed numerical modeling using the finite element method was carried out to investigate the major factors that affect the seepage-induced instability of tailings dam. In order to control seepage flow through tailings dams to avoid stability problems, the phreatic surface and its location are the parameters that should be investigated. The main approach of phreatic surface control is to keep the phreatic surface as low as possible in tailings embankments, particularly in their downstream shell, to minimize the possibility of seepage breakouts on the face of an embankment (Vick, 1983). A seepage breakout can lead to rapid erosion of the downstream shell, resulting in a catastrophic dam failure in a very short time.

Therefore, the objectives of this research are:

1. Identify various seepage patterns within a dam and the influence of phreatic surface on them.

2. Investigate the suitability of a numerical method to model the staged raising of a tailings dams along with the resulting transient seepage occurring within them.
3. Identify the key input parameters of these models.
4. Interpret the seepage conditions obtained from modeling and long-term evolution of phreatic surface.
5. Compare model outputs to draw conclusions and give recommendations based on them.

1.3 METHODS OF ANALYSIS

Key model parameters, soil properties and methods of phreatic surface control are presented at the beginning of this thesis. Not only the methodology and model parameters, but also the assumptions must be verified before the start of modeling to fully understand the phreatic surface conditions obtained for the control of seepage flow. In summary, the main assumptions adopted in this thesis are:

1. The permeability (in particular, the ratio of horizontal to vertical permeability) is in the range from to 2 to 10 for beach sand deposits and slimes (Vick, 1983).
2. The embankment dam slope inclination is assumed as 3 horizontal to 1 vertical and 2 horizontal to 1 vertical, which are often used in the mining industry (Vick, 1983).
3. The considered dam raising rates were 5, 10, 15 or 20 meters per year, which are typical in the industry, starting from zero-meter level at the starter dam crest, to model the whole life span of a dam (Vick, 1983).

4. The beach width to dam height ratio was varied as 3, 5, 9 and 12, covering a wide range of beach sizes, modeling various methods of deposition (spigoting, etc.) (Vick, 1983).
5. The initial dam height was chosen to be 6.1m (20ft), a very typical height of a started dam (Vick, 1983).

Models were constructed using a combination of these parameters and the seepage face breakout location was adopted as a measure of severity for seepage-induced instability. Since the seepage face breakout signifies that the downstream shell has considerable pore water pressure buildup, a set of control models were created that included an underdrain under the downstream shell. These were done to confirm that indeed an underdrain is an effective measure of controlling seepage breakout. However, the focus of this thesis is on dams that what have either no underdrain or a non-functioning one, concentrating on the long-term seepage evolution going well beyond the life of a mining operation.

1.4 BRIEF SUMMARY OF FINDINGS AND STATEMENT OF CONTRIBUTION ARISING FROM THIS THESIS

The results of modeling, considering all combinations of key parameters, have revealed that the beach width to dam height ratio does not affect the seepage face breakout to the extent as initially though. The most influential parameter was found to be the rate of embankment raising, while the slope inclination and permeability do impact the development of seepage face breakout under certain combination of parameters. Upon analyzing the data obtained from modeling, this thesis presents a comprehensive comparison of model parameters affecting the long-term seepage performance of tailings dams. This thesis also raises issues that tailings facility designers and

operators need to consider seepage face breakout both during and after the mining operation to ensure a safe and viable tailings storage while maintaining maximum production rates.

Chapter 2: Literature Review

This chapter will review the background of tailings dams along with the basic characteristics of tailings, concentrating on the upstream-type of tailings dams, which are the main focus of this research.

2.1 TAILINGS

2.1.1 Introduction

Tailings are residues produced as a by-product of mining operations, mineral beneficiation and chemical processing in civil works (Singh et al., 2015). Figure 2.1 illustrates a typical process in an open pit mine, from excavation to waste disposal. Tailings can be in a form of liquids, solids, or a slurry of fine particles, which are discharged as slurry into impoundments. Solid residues are usually used as part of the dam structure itself, forming tailings dams (EPA, 1994). Depending on the composition of tailings, the potential pollution hazards can be elevated; for example, due to high sulfide content. These tailings must be stored under water, because once exposed to air, the sulfide will leach acid into the environment. Therefore, a tailings dam must safely contain mine tailings and the process water not only during the operation of the mines, but for almost perpetuity.

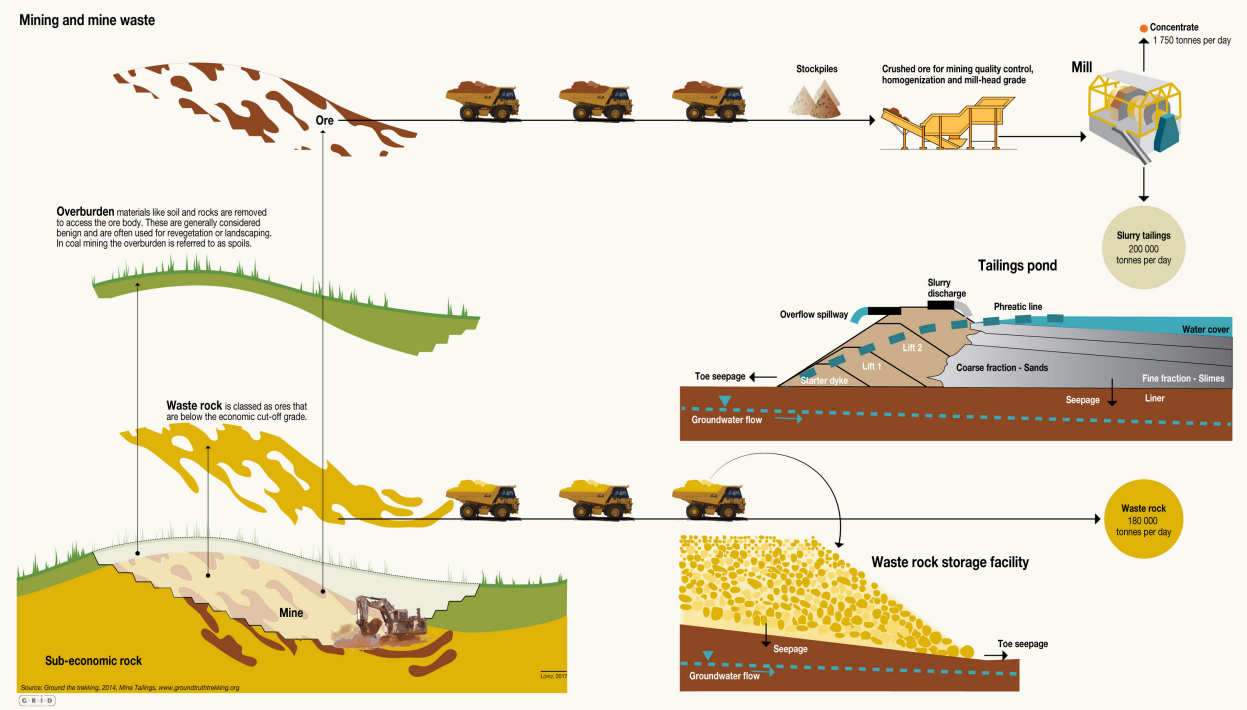

Figure 2.1: A mining operation, from excavation to waste disposal (Thygesen, 2017).

2.1.2 Characteristics of Tailings

The characteristics of tailings can vary widely and depend on the kind of ore being milled and the particular processing operation (physical or chemical processes) (El-Salam, 2012). Also, the composition of tailings mainly depends on the original ore or ore-bearing rock.

For example, Ritcey (1989) pointed out that the same type of tailings may have different mineralogical characteristics and thus have different physical and chemical characteristics. Due to the specific processing and hydraulic emission (or deposition) methods of the tailings, together with the tailings undergoing hydraulic classification and sedimentation, tailings deposits can be layered in both vertical and horizontal directions. So, it is not surprising why the characteristics of tailings have considerable variations in vertical and horizontal directions.

2.1.3 Basic Engineering Properties of Tailings

Although the ore production rate and construction methods determine the depth of each layer, however the tailings' mechanical behavior in a structural layer depends on the deposition method (e.g. spigotting), the deposition process (e.g. segregation), and the consolidation rate (Mittal & Morgenstern, 1975). Engineering properties of tailings can significantly affect the stability of a tailings dam. The most important properties are the permeability, consolidation constants, compressibility, shear strength and so on. Thus, it is necessary to know those engineering properties and their behavior of selected materials of the dam and foundations before the impoundment construction has begun.

In more detail, the engineering properties of tailings are as follows:

a) Permeability

The permeability of a tailings material is related to the seepage through the entire tailings dam, which directly affects the stability of a tailings dam. Many tailings dam collapse accidents occur because of the deformation caused by seepage that reduces the stability conditions of a tailings dam (Vick, 1983).

Permeability can vary in both vertical and horizontal directions due to deposition and layered nature of tailings. For a uniform beach sand deposit, the ratio of horizontal to vertical (anisotropy ratio) permeability (k_h/k_v) is generally in range of 2-10 (Vick, 1983). Compared with other engineering properties of tailings, permeability is the most difficult one to define and generalize. Permeability varies as a function of grain size and depth in deposit, plasticity as well as method of deposition (Vick, 1983). Moreover, a permeability parameter can span more than five orders of

magnitude from 10^{-4} m/sec for clean, coarse, or cycloned sand tailings to 10^{-9} m/sec for well-consolidated slimes (Vick, 1983). In general, the permeability of the tailings is also related to the fine particles size as an aspect of composition of tailings. Generally, finer the particles, lower the permeability (Vick, 1983). Mittal and Morgenstern (1975) demonstrated that Hazen's Formula can be used to calculate the average tailings permeability, which is one of the classic methods for determination of permeability and is written as

$$k=d_{10}^{2}. \tag{2-1}$$

Where k is the average permeability (cm/s) and d_{10} represents the grain size in millimeters for which 10% particles pass by weight. However, this method is only an estimate, based on particle size, but it cannot explain several important factors that control the permeability of an entire tailings deposit. In determining the overall permeability of a deposit, the effects of other important factors such as anisotropy ratio, void ratio and distance from discharge cannot be ignored (Vick, 1983). Given the method of tailings deposition via spigotting or cycloning, coarse particles settle near the point of discharge and finer and colloidal particles settle in the decantation pond located farther away. According to Kealy and Busch's suggestion (1971), a tailings dam can be divided into three different functional areas according to this graded gradient: a zone close to the point of discharge with high-permeability sands, an intermediate permeability zone, and a zone of low permeability slimes. The conceptual model of permeability variation within a tailings deposit is shown in Figure 2.2.

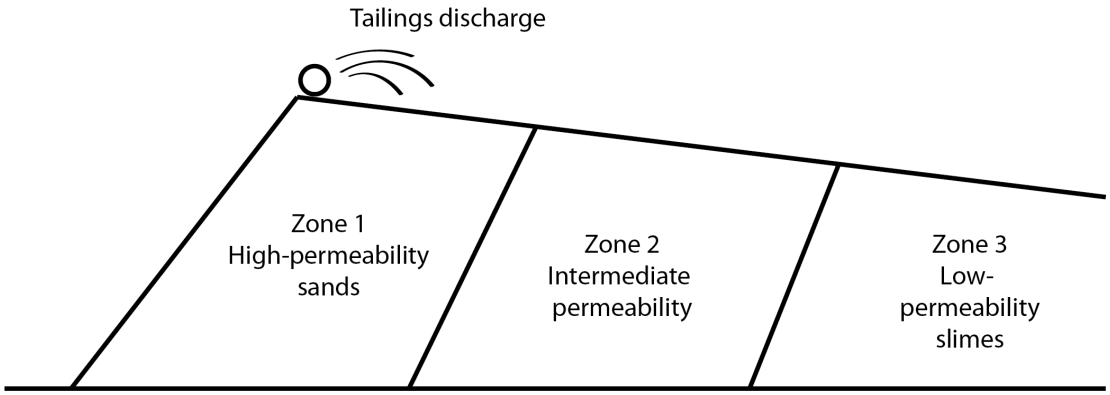

Figure 2.2: Conceptual model of permeability variation within a tailings deposit, after Vick (1983).

b) Compressibility

Like density, the compressibility of tailings is highly dependent on their composition. Whether the tailings are sands or slimes, their loosely deposited state, high angularity and grading properties make them more compressible than most natural soils (Vick, 1983). This kind of deformation of tailings deposits is mainly due to the pore water and air expelled from the space between material particles. In traditional soil mechanics, one-dimensional compression (consolidation) tests are widely used to measure soil compressibility. The difference between tailings sands and tailings slimes is a basic factor affecting the compression index, C_C. The general variation of C_C for sand tailings is in the range from 0.05 to 0.10. The C_C of most low plasticity tailings slimes is generally 3 to 4 times higher than the former, in the range of 0.20 to 0.30 (Bhanbhro, 2014). Another important factor is the density and void ratio of tailings sands and tailings slimes in sediments. The looser or softer the initial state, the greater the compression under load.

c) Consolidation

Terzaghi, who first laid the foundation for soil consolidation theory, believed that the soil consolidation process can be divided into two phases (Lambe & Whitman, 1969). Under constant loading, the porosity of tailings decreases, and thus there is less volume available for the pore water. Thus, pore water is squeezed out of the tailings in this process, which is called primary consolidation. After the excess pore water pressure is completely dissipated and the effective stress is basically constant, the process in which the settlement amount continues to increase over time is the secondary consolidation process. The reason that the deformation continues to occur may be due to the involvement of grain-to-grain slippage and particle rearrangement (Vick, 1983). However, most of the effects of secondary consolidation of tailings are very small compared to primary consolidation and are often considered negligible. Frequently, the process of primary consolidation occurs too rapidly to be measured in the laboratory. The coefficient of consolidation C_V is an indicator that is regularly used to reflect this. For tailings slimes, the coefficient of consolidation is reported to vary between 10^{-5} to 10^{2} cm^2/sec which is six orders of magnitude slower than that of a beach sand deposit (Vick, 1983). In addition, the change of C_V with the void ratio can also be reflected by the function of change in permeability and the rate of change in stress.

d) Drained Shear Strength

The strength of a tailings material is an important factor when considering the stability of tailings dams. As mentioned earlier, the particles of tailings have a high degree of angularity, so that they have a higher drainage shear strength (Mittal & Morgenstern 1975; Vick, 1983). In a same density and stress condition, the effective friction angle（φ）of the tailings is generally 3 ~ 5° higher than similar natural soils (Vick, 1983). When raising a tailings dams, the increase of pore water

pressures can cause a lower consolidation rate, that affects the strength of the whole tailings dam. It is common to use a consolidated drained (CD) test in a laboratory for determine the tailings friction angle φ. Vick (1983) described that the tailings are basically cohesion-less materials. Therefore, the effective cohesive force equals to zero, which was usually shown in the laboratory test results as well. In this sense, the shear strength of tailings is determined by the effective stress and the internal friction angle. Typically, values of φ fall, for most materials, in the range between 28° and 39°.

e) Undrained Shear Strength

Vick (1983) describes that the undrained shear strength considers pore pressure generated by a rapid application of shear stress, which is very important for evaluating the flowlike behavior of many tailings deposits failures. The undrained strength can be measured by using a consolidated undrained (CU) triaxial test, which produces the total stress friction angle (φ_T) and the total stress cohesion c_T. In general, the total stress friction angle of tailings varies, with the range from 14° to 28°.

2.1.4 Tailings Impoundments

A tailings impoundment is a storage used to prevent tailings from flowing into waterways and solves the issue of waste storage. As long as there is a tailings operation, there will be a tailings impoundment facility to hold the tailings. Each tailings impoundment is unique in its site, requirements and nature. Basically, there are two common types of impounding structures for retaining tailings in impoundments; water retaining type dams and raised embankments, which can be formed into different types or configurations of tailings impoundments. Ring-dikes, valley

impoundments, in-pit, and specially dug pits are the four main types of impoundments that are often used (Vick, 1983). Figure 2.3 and Figure 2.4 gives examples of basic types of impoundments. Due to increasing demand for metals and other minerals, the mining industry produces enormous quantities of fine rock particles. This has greatly increased the amount of tailings and other wastes generated by individual mining projects and by the mining industry as a whole.

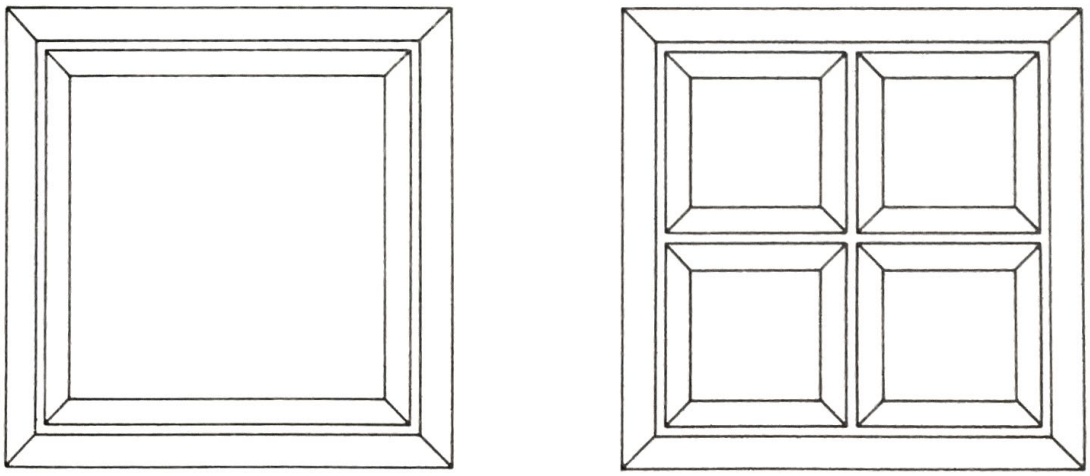

Figure 2.3: Ring dike configuration of single impoundment and segmented impoundment (Vick, 1983).

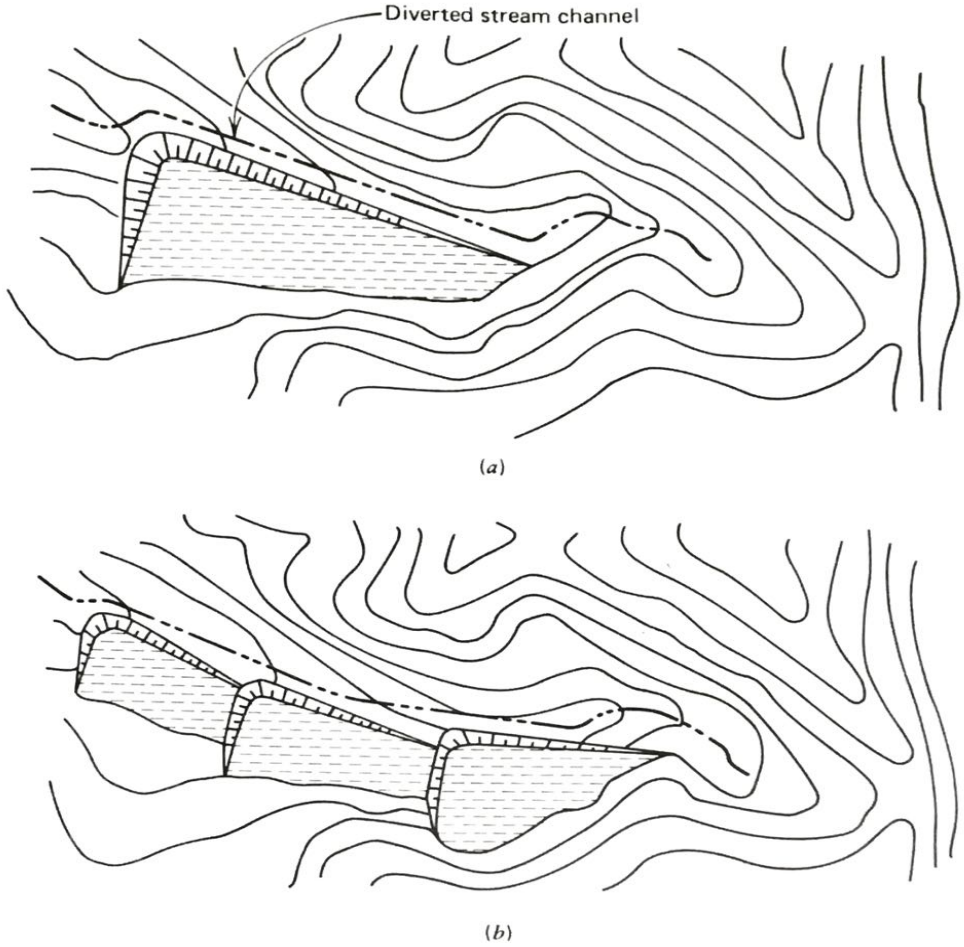

Figure 2.4: Valley-bottom impoundment; (a) single impoundment (b) multiple impoundments (Vick, 1983).

2.2 TAILINGS DAMS

2.2.1 Introduction

A tailings dam is a retaining structure that tailings impoundments use to block the outflow of tailings and ponded water. Before the existence of tailings dams, large amounts of waste generated from the mines was discharged directly into rivers and soils. The purpose of tailings dam construction is not only to protect the surrounding environment, but also to ensure that the water

passes through the dam in a controlled manner. The initial structure of a typical tailings dam is composed of a starter dam. With the expansion of tailings storage capacity, the height of the dam (and its slopes) continues to increase, and the tailings dam volume increases gradually. According to the relative position of the dam crest and the starter dyke, there are three methods for depositing the tailings and building a dam: upstream method, centerline method, and downstream method.

2.2.2 Upstream Method

This construction typically starts with a pervious starter dike foundation by using the coarse fraction of tailings as shown in Figure 2.5. Followed by distributing the spigots on the top of a dam crest to discharge tailings. When the tailings sand filled in to the impoundment height and reaching its initial capacity, the second dike is constructed on these settled and consolidated tailings. In this way, the structure is built cyclically and piled up, layer by layer. Granular particles settle closest to the spigots of discharge and fines and colloidal particles settle out of solution farther away. Affected by this mine discharge method, upstream designed dams contain more fine-grained particles, poorer permeability, and a higher saturation line location, resulting in generally poorer dam stability. However, this method has many advantages, such as simple construction of dams, ease of management, low operating costs while being highly economical. Also, there are only few requirements to choose the areas of a site, so it is widely used around the world.

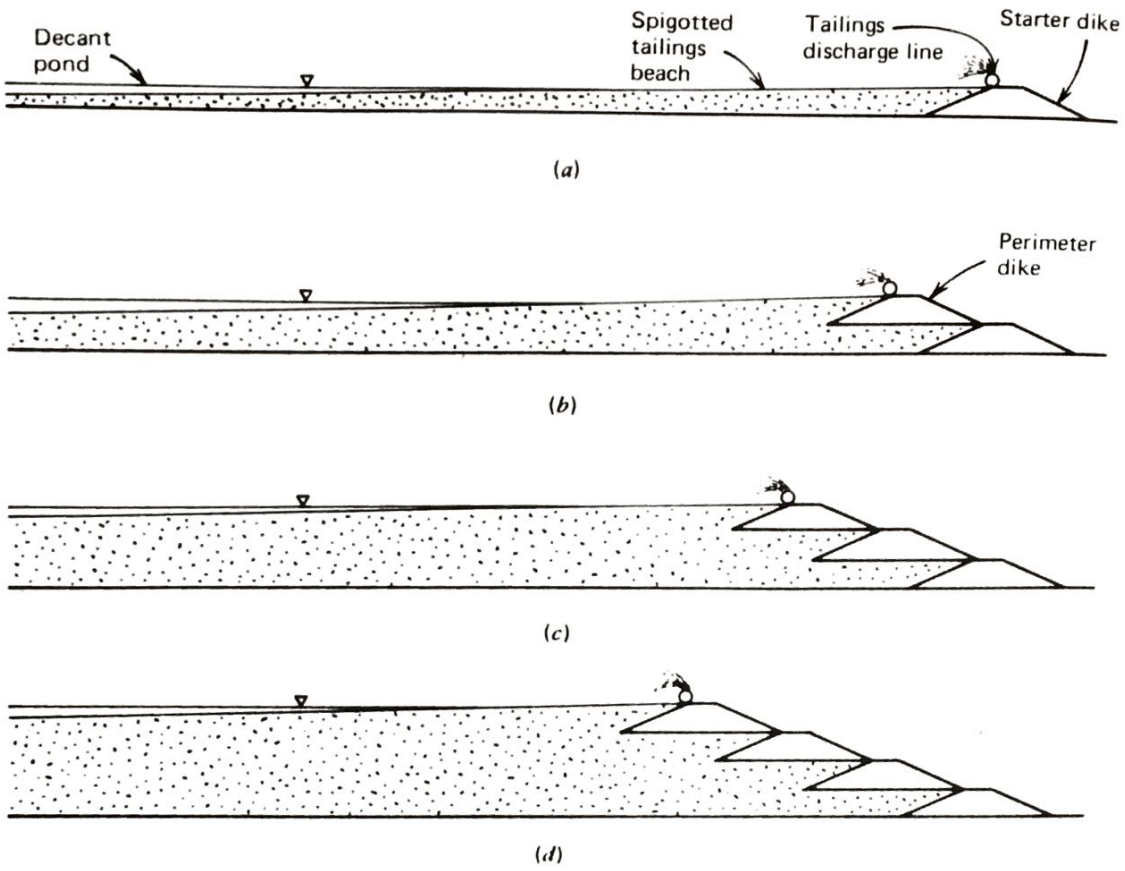

Figure 2.5: Upstream method of construction (Vick, 1983).

The application of upstream method is limited by three main factors: control of phreatic surface, water storage capacity within a dam and susceptibility of seismic liquefaction. Among them, the position of the phreatic surface governs the stability of a tailings embankment.

Figure 2.6 indicates three main factors that affect the position of phreatic surface for upstream tailings dams: a.) pond water location, b.) beach grain size segregation and lateral permeability variation and c.) foundation permeability. Figure 2.6 (a) shows that the increase of pond water level near the embankment can endanger the stability of tailings dams. An elevated phreatic surface may cause the seepage to breakout high on the embankment face, which threatens overall stability

of an embankment (Vick, 1983). Due to the application of cycloning in the upstream method of construction, coarse particles settle closest to embankment and fines and colloidal particles towards the beach. The position of phreatic surface rises as the decrease of tailings segregation, as shown in Figure 2.6 (b). Thus, higher permeability materials can lower the phreatic surface as shown in Figure 2.6 (c).

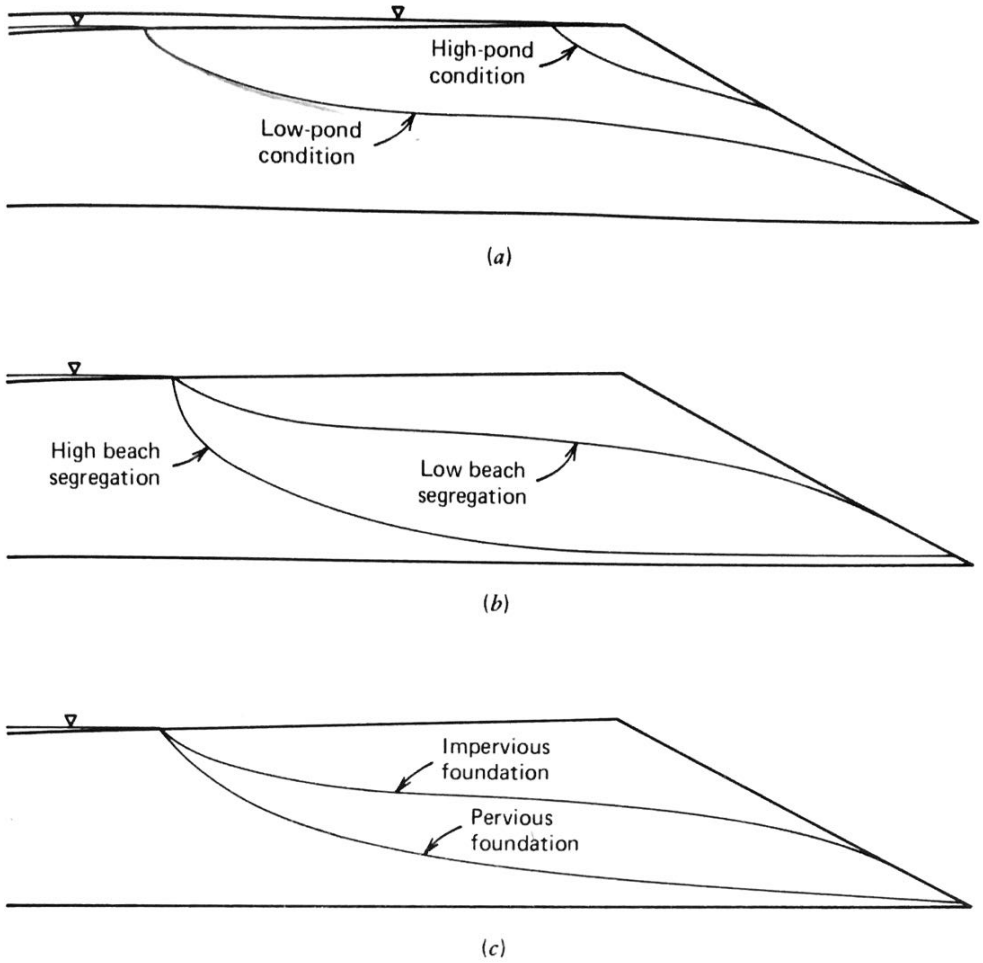

Figure 2.6: Factors that affect the position of phreatic surface for upstream tailings dams. (a) Influence of pond water location, (b) Influence of beach grain-size segregation and lateral permeability variation, (c) Influence of foundation permeability (Vick, 1990).

Based on the above, the upstream tailings dam is the most economical and widely used type, but it is also the type that is prone to the most problems. Thus, the stability conditions for upstream-type tailings dams will be discussed in Chapter 3.

2.2.3 Downstream Method

On-dam cycloning can be utilized in the downstream dam construction for grading tailings. As shown in Figure 2.7, thin layers of fine particles are spread to the upstream direction of the starter dike and coarse tailings comprised of granular particles are discharged to the downstream direction. As the dike stage gradually increases, these subsequent stages are constructed by placing embankment fill on the downstream slope of the previous raise, and the center line of the top of the dam will be continuously moving in the downstream direction with each new stage. Because each raise is constructed independently, the foundation is stable and the height of dam is relatively unrestricted. This method can set drainage facilities in the dam as needed, such as impervious cores and internal drains so that the phreatic surface and seepage is easier to control. Therefore, the downstream method can be applied to sites with large amounts of stored water and tailings. One advantage is that the dam has good stability and is resistant to liquefaction because the dam's fill can be compacted, making it very popular in a high-seismicity zone.

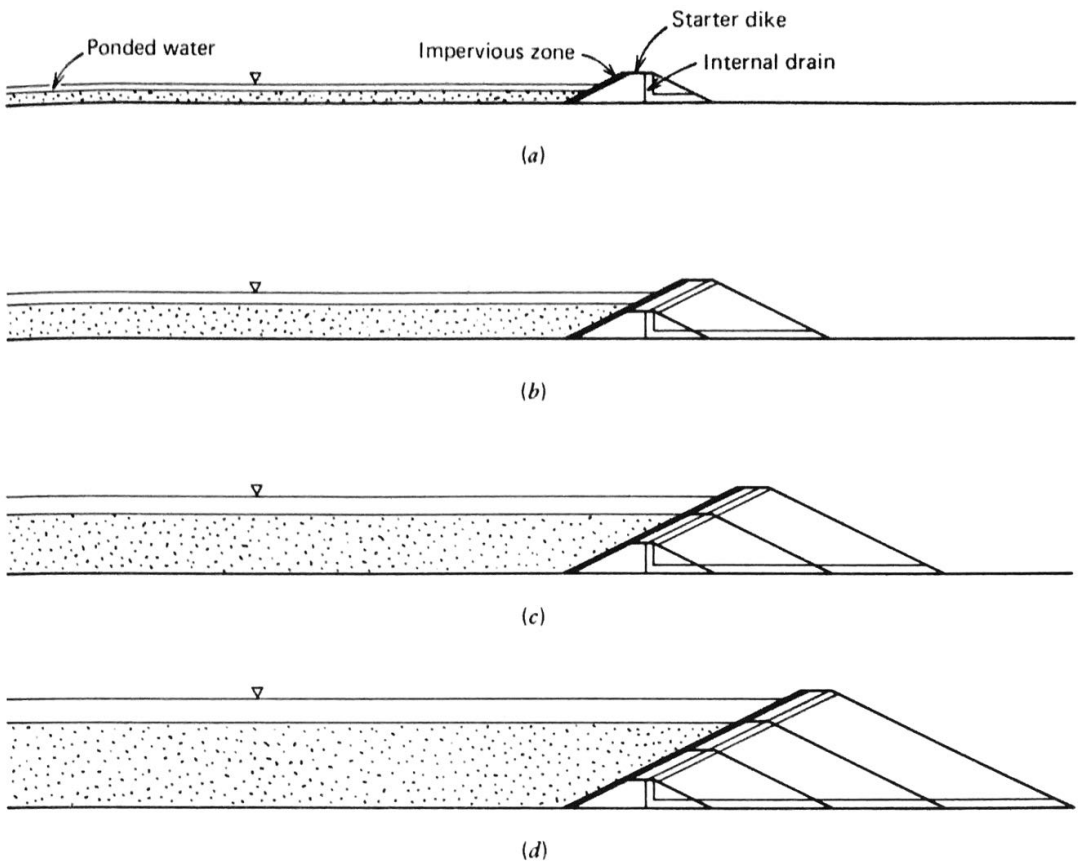

Figure 2.7: Downstream method of construction (Vick, 1983).

The main disadvantage of the downstream method of construction is that large amounts of coarse-grained tailings are needed to build dams, especially at the early stage of use of a tailings pond, often resulting in a problem of insufficient amount of coarse-grained tailings available. The solution is to use other materials to supplement or increase the height of the initial dam, such as the use of waste stones to supplement the tailings but this greatly increases the cost. In addition, downstream dam slopes are constantly changing, resulting in serious water and soil loss on the dam surface; this also results in a high operating cost of the method.

2.2.4 Centerline Method

The centerline raising method is essentially a compromise between the upstream and downstream designs in many aspects. Therefore, it not only shares the advantages but also reduces the shortcoming of both. Initially, the starting embankment is built, and the tailings discharged by spigots from the top of the dike crest to form a beach. Figure 2.8 shows a centerline raising of an embankment (Vick, 1983).

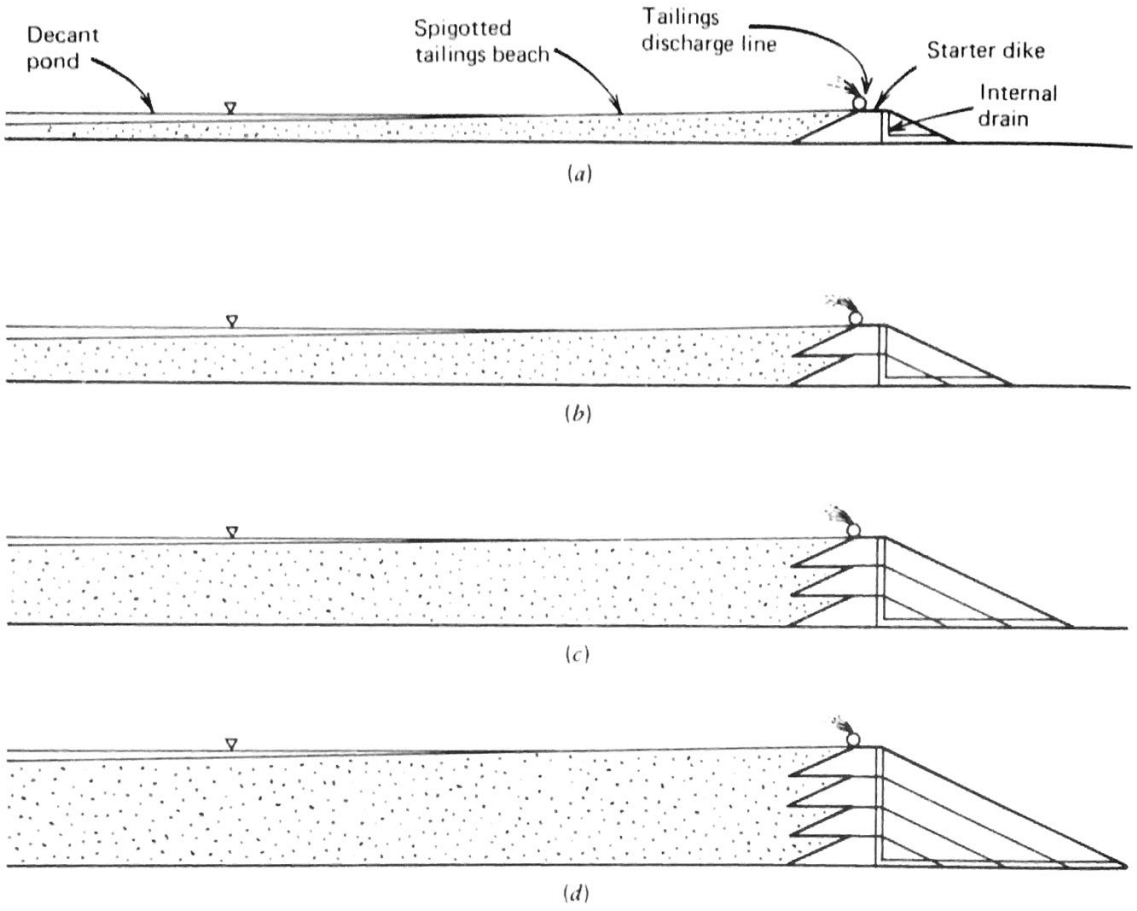

Figure 2.8: Centerline method of construction (Vick, 1983).

If subsequent raising is required, embankment fill is placed onto the beach and the downstream slope of the previous dike. In this respect, the method is basically similar to the downstream dam

construction method. However, compared with the downstream method, the dike rises faster and requires less material for dam construction. Also, the dike body has similar degree of stability as the downstream method. Due to the slope of a downstream dam is always changing, soil erosion of the dam surface is a serious concern. Although its cost is lower than that of the downstream method, it is still higher than the upstream method.

In summary, from the standpoint of seismic stability, the downstream method is the best, but its cost is higher, so this method is generally used only under special circumstances. For the centerline method, both the construction cost and earthquake resistance of the dam are a compromise between the upstream and downstream dam types. This type is the most economic and safe dam-building method that can best meet sustainable development in the current mining industry. However, seen from the aspect of material volume requirements and cost, the upstream method is the most economical. In general, upstream raising methods are well suited to areas where there is minimal storage of water in the impoundment, because the water storage capacity is too small to hold a large volume. But the low relative density of the tailings and poor water management in upstream dams may increase the liquefaction-induced flow of tailings.

Key considerations in the design concepts of tailings dams and impoundments are stability, cost and environmental performance. Even if the upstream method is less stable and problematic than the other two methods, but it is still the most popular due to its low cost. Nevertheless, it has to be kept in mind that each built tailings dam is unique, no matter what method was used in its construction.

2.3 TAILINGS DAM SITING

2.3.1 Site Selection Criteria

The selection of a tailings dam site plays an important role in the tailings facilities design process, since the location may affect the dynamic strength behavior of a tailings dam. It is because different locations could have different tailings characteristics that affect stability and seepage quantity. There are many constraints imposed on the selection of location, such as the nature of the on-site tailings material, locally available soils or rocks, storage capacity required of the facility, operating cost, tailings-specific factors and site-specific factors (topography, hydrology, geology, and hydrogeology) (Vick, 1983). As to the mill location, the site should be as close as possible to the mill, that is because the shorter the distance of tailings transmission, the lower the cost of a piping system. Ideally the tailings impoundment should be located within four to five kilometers of the processing plant, but for special situations where large amounts of tailings disposal need to be handled, it needs to be closer (Vick, 1983). In addition , the elevation difference of the mine relative to the tailings storage will also affect the operating costs and should be reduced as much as possible. Ideally, the disposal site should be downhill from the mine to take advantage of the gravity flow of tailings, thereby reducing pumping costs (EPA, 1994).

Other factors that need to be considered in the site selection process include environmental hazards, land ownership, rights and boundaries, distance and elevation of processing plants, location of future ore bodies, large residential areas, water and water production bases, protected places of interest, rare or protected animals and plants, etc. (Tan, 2008).

2.3.2 Facility Layout

Tailings impoundment layout is a part of the tailings site selection process and depends on natural topography and man-made engineering characteristics (Ritcey, 1989). To a certain extent, there are a variety of tailings layout options, but the one selected must be compatible with a wide range of topographical factors, and it has little to do with the types of dams used. As mentioned above, the types of layouts that currently exist in the industry include: valley impoundment, ring-dike and in-pit. Different impoundment layouts are chosen by different geographical and topographical locations of a mine.

2.4 SURFACE WATER

2.4.1 Introduction

One of the key issues in the design of surface tailings is to adapt the amount of water that needs to be treated to the type of dam selected. For this reason, in the early stages of planning, the amount of inflow of tailings solids, beneficiation wastewater, precipitation and runoff into the tailings impoundment must be estimated, and appropriate water control methods must be considered. Properly designed surface water control measures for dam safety are very important. Almost all failures of tailings storage facilities are related to water directly and indirectly, such as seepage, piping, internal and external erosion, liquefaction and overtopping. Each type of failure mode may weaken the embankment and may even be the main cause of dam collapse. These common failure modes are the potential failure surfaces of the dam and they should be included in the analysis when the dam's factor safety is calculated (U.S. Environmental Protection Agency, Office of Solid Waste, 1994).

2.4.2 Surface Water Control and Water Balance

In the control of surface water, the treatment of normal inflow of tailings impoundment water must first be considered, i.e. the liquid component of tailings discharged from normal ore processing operations into tailings impoundment, precipitation, and surface runoff water under normal climatic conditions. The key to normal inflow water treatment is the water balance between inflow and outflow, which means that the amount of water in the impoundment has to remains relatively stable during the entire period of ore processing operations. The main sources of water flowing into the tailings impoundment include direct rainfall on the sedimentary beach and sedimentation tank, precipitation into the pond (including storm events), run-on (including flood events), peak inflow and the liquid component of tailings discharged from normal ore processing operations into the tailings impoundment. Among them, rainfall is not controllable, but it can be roughly estimated based on the local average annual rainfall. If the facility is located in a mountainous area, the actual rainfall may vary greatly due to elevation and topography.

In order to design an effective water control system, it is also necessary to examine the outflow of tailings. Variables include the water returned from tailings impoundment, evaporation, seepage, recycling tailings water, the retention of water in the tailings and direct drainage.

Among them, the amount of water retained in the pores of tailings can be estimated based on the concept of unit void ratio. Evaporation can be estimated from a regional annual average evaporation. It is generally assumed that evaporation only occurs on the surface of a sedimentation tank. Evaporation in the sediment pool is difficult to estimate and is often neglected. Obviously, the controlling factor of evaporation is the scale of the sedimentation tank.

Most control measures are one or more of the following combinations: flood events, recirculation, seepage control, and dewatering processes. The main threat of flooding in tailings dams is the

danger of over-toping. A tailings dam is subjected to rapid down-cut and erosion once the water reaches the top of a dam, and the dam can be completely destroyed in a short time. The best avoidance method is to select a reasonable site at the design stage to achieve the inflow control of the impoundment (U.S. Environmental Protection Agency, Office of Solid Waste, 1994). The main method of dealing with floods is to accumulate flood water in the impoundment, which means that the tailings impoundment can receive an assumed amount of flood inflow volume with sufficient volume at any time and the raising of a dam still maintains an appropriate excess height. However, the dam's inflow plus the storage available should equal to the outflow. When the inflow is equal to the outflow, the amount of storage reaches its maximum.

The most commonly used drainage method is to set a series of drainage wells in the impoundment, based on site-specific factors (topography, hydrology, geology, hydrogeology, etc.), tailings dam elevation and flood discharge capacity requirements. Diversion ditches are often used to divert normal runoff, but they can also be used as flood discharges around tailings ponds. Experience has shown that some tailings dams may withstand the destruction of slopes, damage caused by seepage, and even partial liquefaction, but almost no dam could survive overtopping damage caused by inadequate flood protection measures. On the other hand, setting the impoundment as far as possible in the high valley and diverting streams can minimize run-on so that to minimize the volume of inflow and seepage.

The above methods are used to simply estimate some of the major naturally occurring inflows and outflows. In addition, hydrogeological modeling and analysis can also be used to estimate natural inflow and outflow, such as precipitation and evaporation, but this process is relatively

complicated and seldom implemented (U.S. Environmental Protection Agency, Office of Solid Waste, 1994).

2.5 SEEPAGE

2.5.1 Introduction

Seepage is a quantity of fluid passing through or move around a dam or impoundment. It is inevitable to control seepage to prevent internal erosion and instability for all types of embankments and most of concrete dams. Zero-discharge of seepage from a tailings facility remains a difficult challenge even with complex liner systems (Vick, 1983). Uncontrolled seepage may cause specific problems such as piping erosion or excess water losses that threaten the stability of slopes. Thus, the control of seepage is a critically important requirement in a design. However, the two major factors which affect the measures of seepage control are the volume and the quality of water.

The quality of seepage, as the most important environmental impact, should be evaluated in the early stage of a design. Complex geochemical methods are also suitable for simulating the quality of seepage. As mentioned above, the methods of ore being milled, ore-bearing rock, and the particular operation (physical or chemical processes) determine the characteristics of tailings, thus affect seepage. Not all wastewaters contain toxic components, thus the characteristics of tailings can vary widely due to the kind of ore being milled, the pH and beneficiation process (physical or chemical processes). Also, the composition of tailings mainly depends on the original ore or ore-bearing rock. Many similar reactions (precipitation adsorption, neutralization, oxidation/reduction, biological reactions, and ion exchange) are used to extract the desired mineral during a milling operation (Vick, 1983).

Ritcey (1989) pointed out that the same type of tailings may have different mineralogical characteristics and thus have different physical and chemical characteristics.

2.5.2 Seepage Control Measures

a) The seepage return system

A seepage return system, as a method of reducing seepage, can collect wastewater that has leaked out of the dam and return it to the tailings pond, thereby eliminating or reducing the migration of contaminants in the groundwater. According to Vick (1983), collector ditches and collector wells are the major forms of return system operations. Collector ditches are generally used in the first line of defense because their cost is relatively economical and can be used either alone or in combination with other leakage control measures. An anti-filter layer is provided in the ditch to prevent piping surges. It can be installed in permeable upstream dams, downstream dams, or centerline dams. Collector wells intercept the contaminated seepage water by drilling a drainage well along the downstream side of a dam. Collector wells are relatively expensive and generally used as a remedial measure to prevent the contaminated aquifer from being further damaged (Vick, 1983).

b) Seepage barriers

Seepage barriers require the tailings dam to be constructed with impervious core and be well connected with barriers. The seepage barrier is also the main method for controlling seepage, including cutoff trenches, slurry walls and grout curtains (Zardari, 2011). In order to effectively reduce the amount of seepage, a seepage barrier must pass through the pervious foundation layer to an impervious stratum.

As shown in Figure 2.9, seepage barriers categorized by cutoff trenches, slurry walls and grout curtains. Cutoff trenches are the most economical and most widely used seepage control methods in tailings dams. In the case of saturated, fine-grained, shallower, and flatter foundations, where previous materials are not suitable for excavating cutoff trenches, slurry walls can be used to limit seepage.

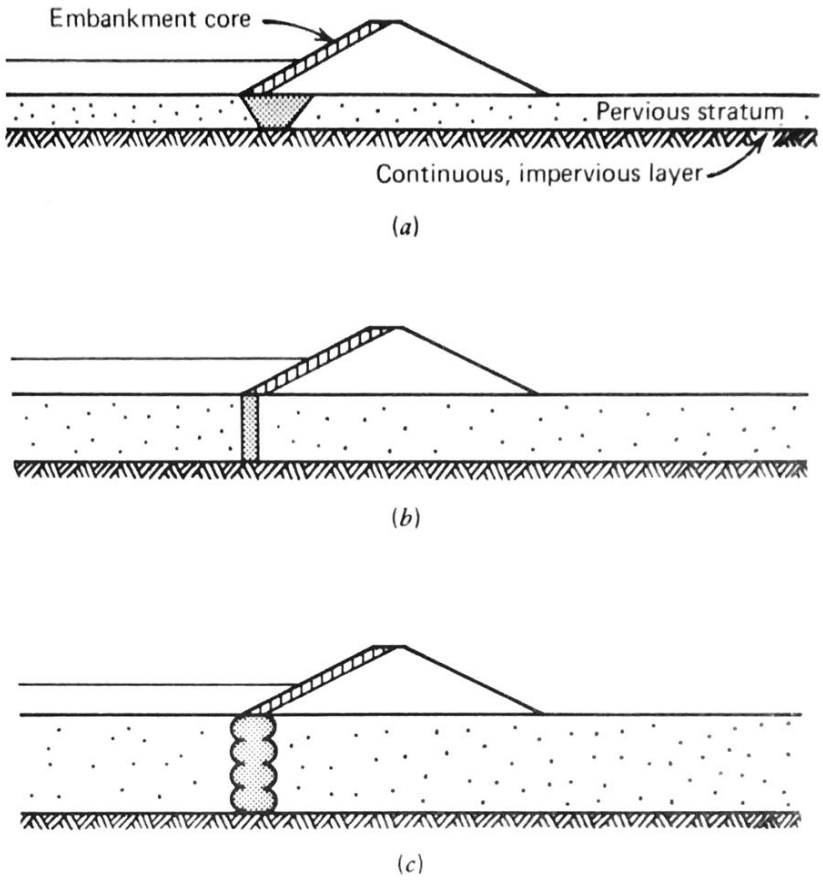

Figure 2.9: Seepage barriers (a) Cutoff trench, (b) Slurry walls, (c) Grout curtains (Vick, 1983).

c) Liners

Liners are often used as a final strategy for seepage control to minimize seepage and thus minimize pollutant emissions. There are three types liners that are widely used: tailings slimes liners, clay liners and synthetic liners (including synthetic rubber film, thermal plastic film, spray film, asphalt concrete). Figure 2.10 illustrates the comparison of clay liners and slimes liners (Vick, 1983).

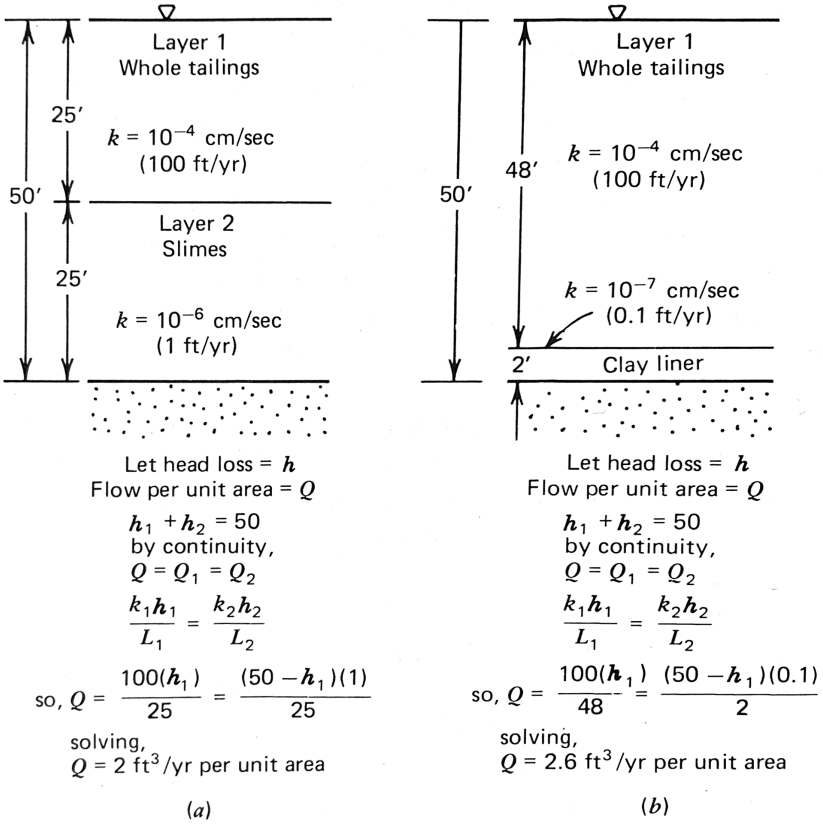

Figure 2.10: Example of liner seepage comparison; (a) Slimes liners (b) Clay liners (Vick, 1983).

Different liners contain different materials; each having their relative advantages and disadvantages. The cost of a liner is high as compared to the permeability barrier or permeation reflow system, but it is indeed more efficient than the other two methods. They are usually required to be used under relatively high concentrations of toxic components in the wastewater. Unlike the seepage barrier system and seepage return system, the feasibility of a liner construction does not depend on the existence of the lower impermeable layer and the nature of soil layer that passes through it. It is completely independent of the underground conditions, so it is not restricted by underground soil, nature of bedrock or groundwater. The liners also have the property of resistance to chemical corrosion and various physical fractures.

Chapter 3: Theoretical foundations of modeling and analysis of seepage through tailings embankment dams

3.0 KEY MODEL PARAMETERS

Seepage flow through tailings embankment dams may lead to stability problems of the dam's slopes. In light of what was described in the previous chapter, the phreatic surface and its breakout location on the slope face are the parameters that control the tailings dam's stability under seepage conditions. Thus, these two will be used in this thesis to assess the implied stability since understanding their evolution with time can lead to their inclusion in limit equilibrium or finite element-based analysis tools. Also, the use of a drainage zone and filters, as critical aspects in lowering the position of a phreatic surface (Vick, 1983), will be evaluated as well. Various published solutions are available for governing the stability of upstream tailings embankments, and this chapter will lay the foundation of using numerical solutions, to comprehend their effectiveness.

3.1 PHREATIC SURFACE

Phreatic surface is defined as the internal water level that resides between the zone of saturation and the zone of aeration in a tailings dam (EC, 2004). The exact location of phreatic surface is closely related to the seepage and governs the stability of an entire tailings embankment under static and seismic loading conditions. An elevated phreatic surface may cause the seepage to break out high on the downstream embankment face, which threatens overall stability of an embankment (Vick, 1983).

The major objective of phreatic surface control is to keep the phreatic surface as low as possible in tailings embankments to minimize the possibility of seepage breakouts on the face of an embankment that might induce seepage problems (Vick, 1983). In general, an upstream tailings dam is pervious, with permeability of the various zones gradually increasing along the direction of seepage, thus ensuring that the phreatic surface remains inside an embankment. Phreatic surface control can be achieved by using materials of differing permeability filled in the embankment to zone phreatic surface, and available materials that are adequate for seepage control (Vick, 1983). In the case of low permeability materials being filled in a dam, cores and internal drainage can be used to collect seepage flows, thereby providing a safe exit for a phreatic line (Klohn, 1979). However, the application of low-permeability-core is the most appropriate for dams which are centerline-type or downstream-type. The objective of this research is the seepage condition of upstream-type tailings dams. Thus, for those, the following methods, as discussed in the subsections, can be used to contribute to limit or collect seepage flows.

3.1.1 Drainage Zone

Drainage always performs an important role of controlling a phreatic surface in tailings dams. There are two types of drains that can be used to limit and collect seepage flows: blanket and chimney. As shown in Figure 3.1(a), horizontal blanket drains always have a beneficial effect on the phreatic surface for upstream-type dams. In addition, a pervious starter dike is needed by an upstream-type dam due to the permeability as an important factor that affects the position of phreatic surface. The application of chimney drains is always incorporated with blankets in downstream and centerline-type dams. Figure 3.1(b) and Figure 3.1(c) show the use of chimney-

blanket drains in the downstream and centreline-type embankments. The combination of chimney-blanket drains is flexible in selection of materials that are used to construct them (Vick, 1983).

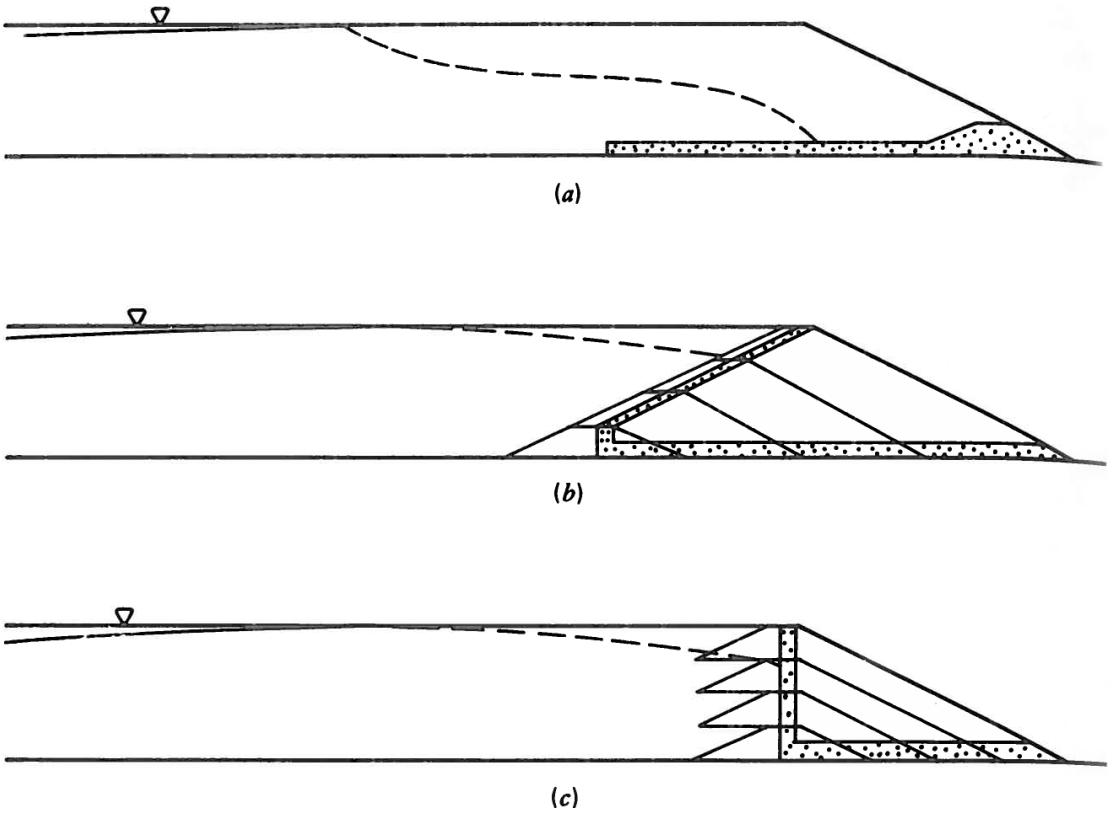

Figure 3.1: Use of internal drainage zones in raised embankments. (a) Upstream embankment using pervious starter dike with upstream blanket drain, (b) Downstream embankment using inclined chimney drain and blanket drain, (c) Centreline embankment with vertical chimney drain and blanket drain (Vick, 1983).

However, the use of drains will involve the risk and problems such as piping, erosion, sloughing, etc., and keeping the draining system clear, which is necessary over the entire life of the operation (Klohn, 1979). The prerequisite to the application of internal zoning as a phreatic surface control method is, of course, that the range of materials is available and obtainable.

3.1.2 Use of Materials

Phreatic surface control can be achieved by using materials of differing permeability filled in the embankment to zone a phreatic surface. The various zones must be gradually increased along the direction of seepage flow to allow lower-permeability in the upstream portion and higher-permeability in the downstream portion of an embankment. Hence, the sand and slimes must be separated from tailings materials by cycloning (Vick, 1983). Figure 3.2 illustrates the application of tailings to control phreatic surface in three different types of tailings dams. As shown in Figure 3.2(a), sands are cycloned on the embankment in an upstream dam, slimes are discharged farther out on the beach to form two different permeability zones. Similar process occurs in downstream and centerline embankments, as shown in Figure 3.2 (b) and (c).

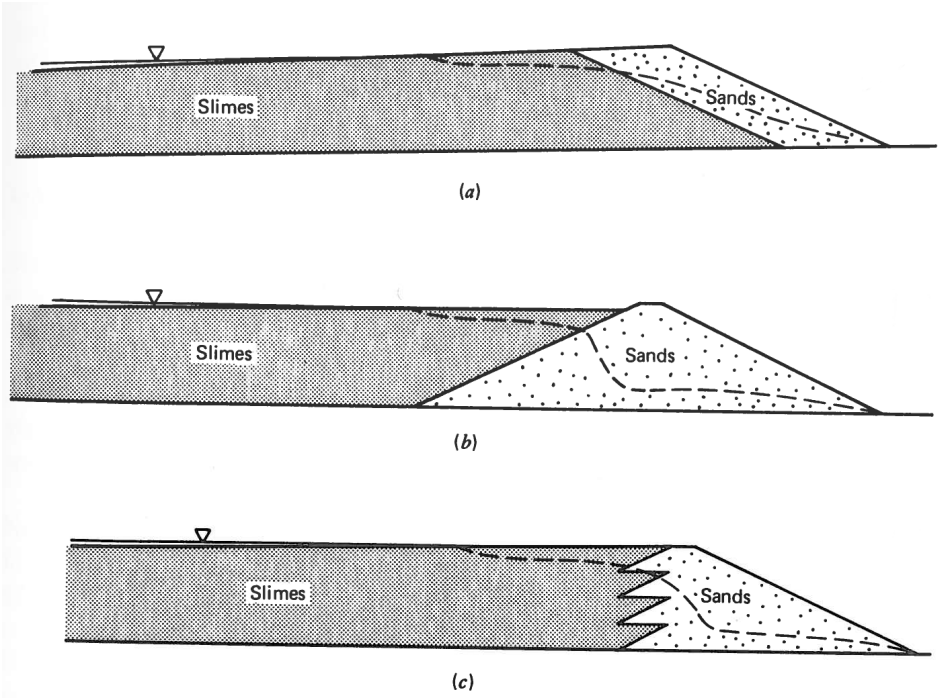

Figure 3.2: Use of tailings to control phreatic surface: (a) Upstream embankment (b) Downstream embankment (c) Centerline embankment (Vick, 1983).

3.1.3 Filters

The design of drainage should also be considered as part of filtering requirements. The objective of a filter is to permit the passage of seepage water but to prevent migration of soil particles. Most drains are graded by function; e.g. an internal zone with high permeability, which can let seepage pass through. Each graded filter must satisfy the filter criteria relative to the zones of others to prevent soil particles from the outer zone migrating to the inner zone. Materials in the various zones need to be in accordance with the requirements of a graded filter, so that they can be smoothly graded (Klohn, 1979). The material of filters needs to be fine enough and with high permeability to be a prerequisite for drainage. It also needs to be cohesionless enough to prevent crack formation in the core (U.S. Environmental Protection Agency, Office of Solid Waste, 1994).

3.1.4 Phreatic Surface Solutions for Upstream Embankments

As mentioned in Chapter 2, the position of phreatic surface is a critical aspect, which influences the stability of an embankment. Some factors affect the phreatic surface location such as pond location (beach width), anisotropic permeability of tailings and boundary conditions. In more detail:

a) Beach Width

Position of the pond relative to the crest of an embankment, or the width of the exposed tailings beach is important for the phreatic surface location. Figure 3.3 illustrates the effect of beach width on phreatic surface for an anisotropic, homogeneous upstream embankment. Assuming several values of beach width (L) normalized by embankment height (H), let a normalized beach width

L/H be a measurement within the assumed condition. Once the L/H is much less than 9, the corresponding phreatic surface location would be breaking out on the slope face, thus creating a hazardous situation.

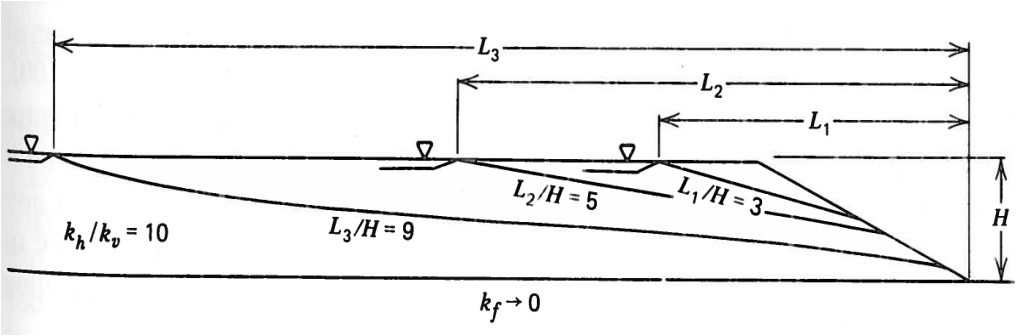

Figure 3.3: The effect of beach width on phreatic surface for an anisotropic, homogeneous upstream embankment on an impermeable foundation (Vick, 1983).

b) Permeability Variation

The range of degree of permeability variation is widely dependent on factors such as the gradation of mill tailings, and pulp density of discharge, which are related to the grain-size distribution and segregation. Figure 3.4 shows the effect of lateral permeability variation for upstream embankments by comparisons of different assumed conditions.

Figures 3.4 (a) and 3.4 (b) show that a low phreatic surface can be achieved by a combination of beach permeability variations and beach width. Figure 3.1.4.2(b) shows a lesser permeability variation may be useful, combined with a wider beach to produce a low phreatic surface. Figure 3.4 (c) illustrates the degree of beach permeability variation to be critical to control phreatic surface location even though the beach width and isotropic tailings permeability are intermediate.

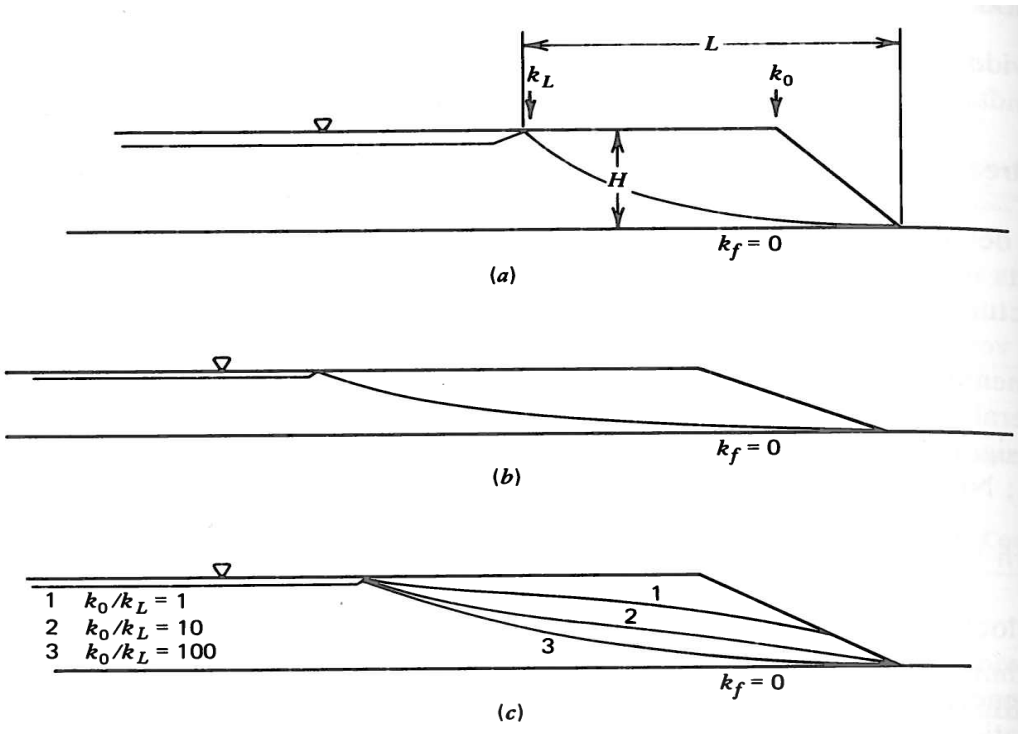

Figure 3.4: Influence of beach permeability for nonhomogeneous upstream embankments. (a) k_0/k_L (beach permeability variation) = 100, L/H (beach width) ≅3, k_h/k_v= 10. (b) k_0/k_L= 5, L/H≅7, k_h/k_v= 2.5. (c) Variable k_0/k_L, L/H≅5, k_h/k_v= 1 (Vick, 1983).

c) Anisotropy of Permeability

The effects of anisotropy are illustrated for a homogeneous embankment in Figure 3.5 (a) and for a nonhomogeneous embankment in Figure 3.5 (b). The influence of anisotropy on phreatic surface is insignificant due to greater degrees of beach permeability variation, as shown in Figure 3.5 (b).

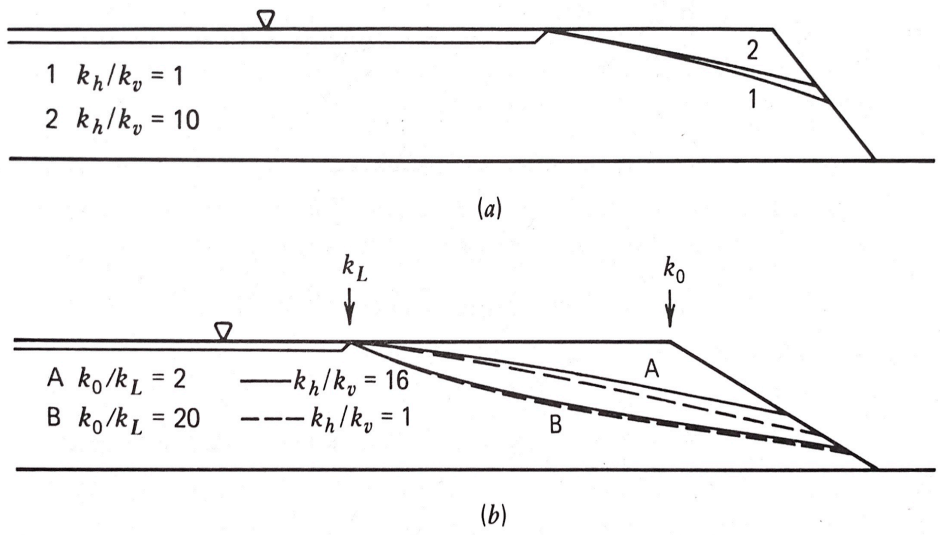

Figure 3.5: The effects of anisotropy for homogeneous and nonhomogeneous upstream embankments on impermeable foundations. (a) Homogeneous embankment, $L/H \cong 3$, (b) Nonhomogeneous embankment, $L/H \cong 3$ (Vick, 1983).

However, if the phreatic surface breaks out on or near the embankment face, even a small rise in the phreatic surface can result in “wet spots" to move up the embankment face (Vick, 1983).

d) Boundary Conditions

Boundary flow conditions affect the phreatic surface dramatically, particularly for the permeability condition of foundation and starter dike. Figure 3.6 (a) illustrates the influence of different foundation permeability on phreatic surface location. On the other hand, a higher-permeability starter dam lowers the position of phreatic surface, as shown in Figure 3.6 (b).

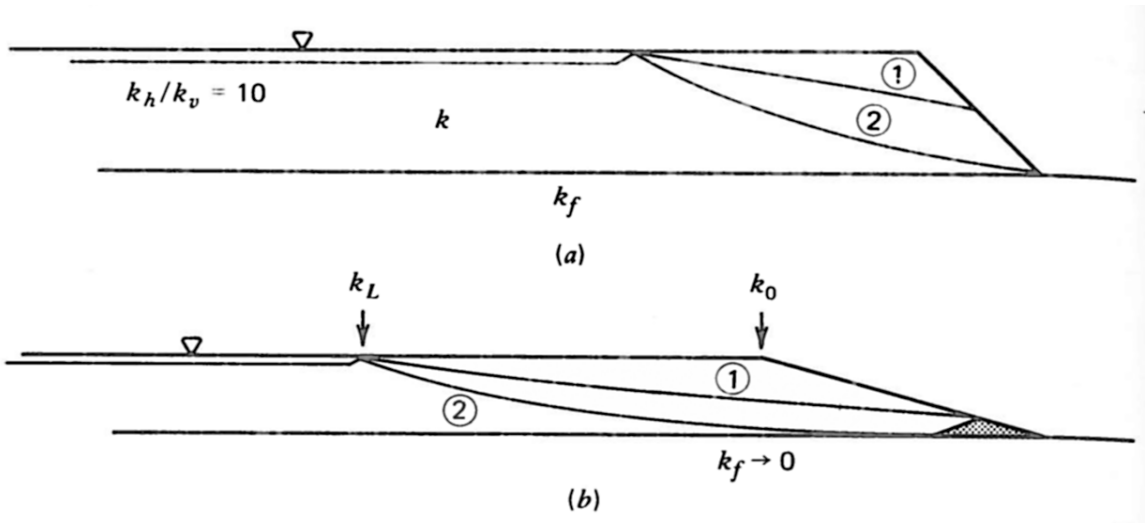

Figure 3.6: Effects of boundary flow condition on phreatic surface for upstream embankments: (a) Effects on foundation permeability, homogeneous upstream embankment, $L/H \cong 3$; ① $k_f=0$; ② $k_f=10k$. (b) Effects on starter dam permeability, nonhomogeneous upstream embankment, $k_0/k_L \cong 5$, $L/H \cong 7$: ① Impervious starter dam; ② Pervious starter dam (Vick, 1983).

3.2 NUMERICAL METHODS FOR MODELING SEEPAGE FLOWS IN EMBANKMENT DAMS

Mathematical models were initially used for groundwater analysing as early as 1800s. With the wide use of high-speed digital computers in the 1960s, numerical models have been developed to become the most popular type of method for analysing groundwater flows.

Generally, a mathematical model describes groundwater flow by specifying the governing differential equations (Wang & Anderson, 1982). Thus, a mathematical solution of differential equations in a physical domain (defined as homogenous, porous medium, with its isotropic or anisotropic permeabilities) is constrained to boundary conditions which are express as head, water content, pore water pressures, or flow rates (Chapuis & Aubertin, 2001).

A considerable advantage of using numerical methods is that they can handle realistic situations for actual groundwater problems. Some types of models can provide solutions for unsaturated seepage problems, and many can take both steady state and transient groundwater flow into account. There are three broad categories of model types: sand tank models, analog models, and mathematical models (Wang & Anderson, 1982).

This research used a mathematical model, implemented as a numerical method using finite elements (FEM), with a focus on the internal seepage within embankment dams under the influence of drainage.

3.2.1 Finite Element Groundwater Seepage Analyses

FEM is a type of numerical technique in which the solution of governing general differential equation is obtained by an approximate solution (Asadzadeh, 2010). Early numerical analysis of this type began with the first evaluation of seepage conditions of tailings embankments using the finite element method (Chapuis & Aubertin, 2001). Proponents of FEM point out that it is flexible when it comes to realistic problems in which the boundary conditions are irregular or the medium is heterogeneous or anisotropic (Wang & Anderson, 1982).

Generally, the FEM is implemented by discretizing the soil mass into element types such as triangular and quadrilateral element shapes in 2D. Triangular elements are defined by three nodes at their corners at which the groundwater head is specified (Fredlund et al., 2012). Each element is the fundamental building block, but when assembled, these elements can develop an approximation to the underlying differential equations (Wang & Anderson, 1982).

A finite element representation (mesh) for the computation of steady-state saturated-unsaturated seepage through an earth-fill dam in two-dimension is shown in Figure 3.7 (a). Figure 3.7 (b) shows the computed hydraulic heads for steady-state seepage through an earth-fill dam. The nodal points are vertices where the elements corners meet and are connected by element edges. The governing flow equation can be used to solve for, using the boundary conditions, the hydraulic head at each nodal point (Fredlund et al., 2012).

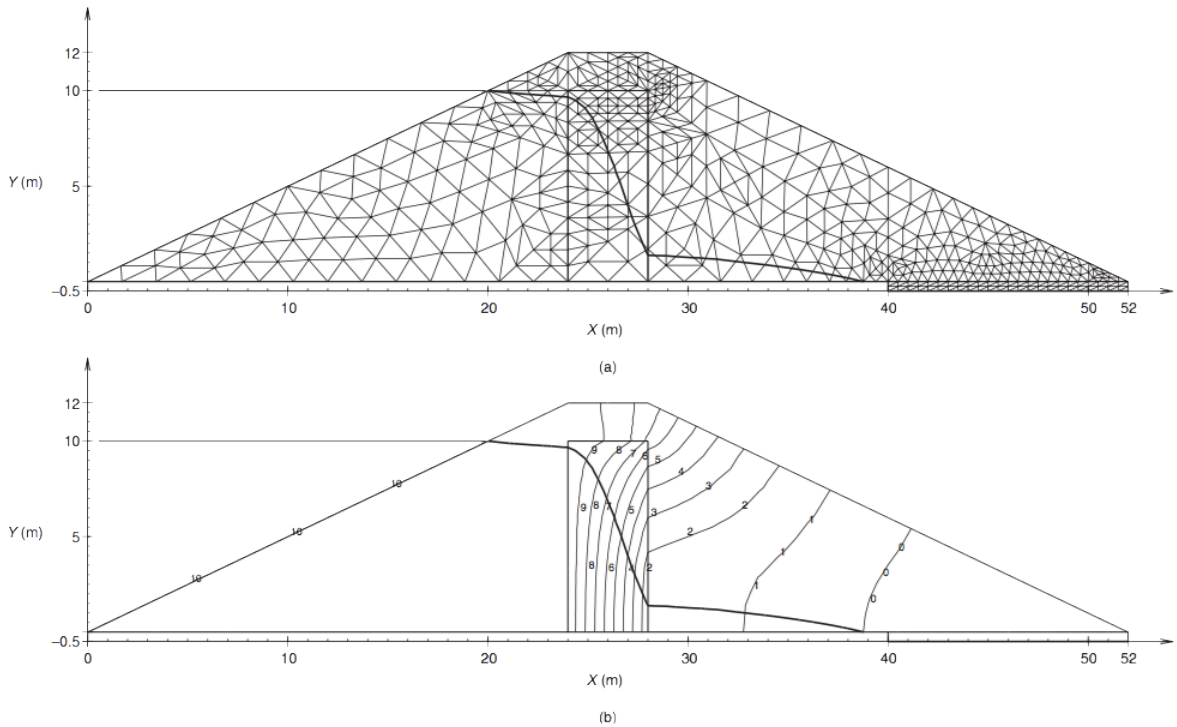

Figure 3.7: A cross section of analysis of seepage through an earth-fill dam with a clay core in two-dimension. (a): Final optimized mesh of FEM with triangular elements. (b): Computed hydraulic head contours.

3.2.2 Finite Element Analysis Software – Rocscience's RS2

RS2 (Rocscience Inc., 2018), which is an implementation of FEM, was used in this research. RS2 is a comprehensive two-dimensional finite element program for soil and rock applications. Pore-

water pressures will be computed using RS2's groundwater seepage analysis option. Although RS2 is capable to perform coupled seepage-stress analysis (Biot's equation), this thesis only included seepage since most literature, including Vick's seminal work (1983), only considers the flow of water through the tailings dam when giving recommendations. In addition, RS2 can be used in a wide range of engineering projects including excavation design, slope stability analysis, groundwater seepage, probabilistic analysis, and dynamic analysis capabilities.

RS2 can carry out a finite element groundwater seepage analysis, with due consideration of both saturated and unsaturated soil states, in both steady-state and transient groundwater seepage formulations through both homogeneous and heterogeneous dams, dikes and other embankment types.

3.2.3 Simplified Steady State Fluid Flow

Seepage flow through a dam involves water migration in both saturated and unsaturated areas. The quantity and directions of groundwater seepage flow through porous media are always needed to be known together for a comprehensive understanding of the flow regime, so seepage flows through both saturated and unsaturated soils are governed by the same flow law and permit the application of Darcy's Law (Fredlund et al., 2012).

Henzel et al. (1999) showed the difference between saturated and unsaturated soil is their dissimilar permeability by a study of both saturated and unsaturated permeability based on experimental and theoretical approaches.

The permeability, as an inherent characteristic of porous medium, depends on the degree of saturation. Figure 3.8 illustrates the dependence of permeability coefficient on saturation degree.

The medium is defined by the fibre element (*f*), the liquid element (*l*) and the gaseous element (*g*) as used for subscripts in Figure 3.8.

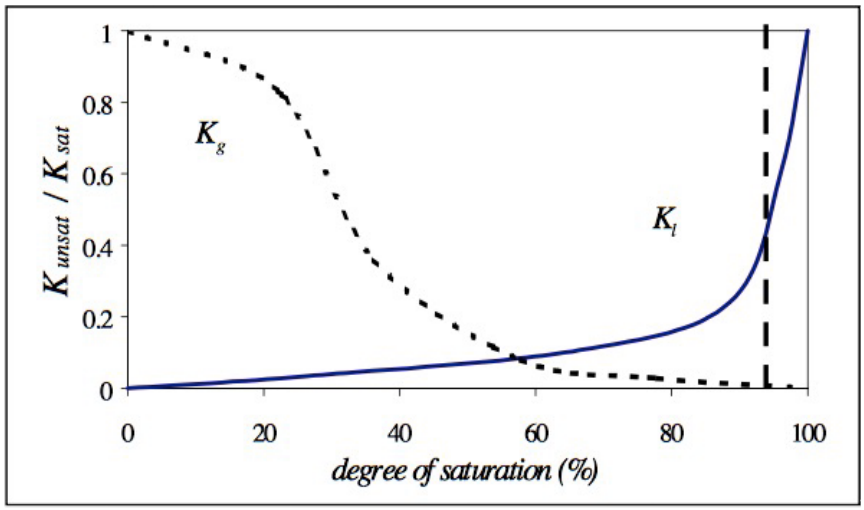

Figure 3.8: Soil permeability as a function of degree of saturation, where K_g: gaseous conductivity, K_l: liquid conductivity. The vertical dashed line in the figure indicates that complete saturation of the porous medium is not possible (Henzel et al., 1999).

a) Flow Through Unsaturated Soils

The coefficient of permeability at each point in a soil is assumed to be a constant in a steady-state fluid flow. However, the variation in the volume distribution of pore-water leads to heterogeneous distribution in the unsaturated soil, which is due to the difference in permeability at each point in soil mass, to be attributed to the spatial variation of permeability coefficient. The permeability coefficient at one point can also vary with respect to direction, and this condition is called anisotropy. Figure 3.9 shows two rules for the variation of permeability condition in unsaturated soils. Figure 3.9 (a) indicates the water coefficient of permeability conditions in heterogeneous

isotropic soils, the coefficients of permeability are identical in the *x* and *y* directions at any point. The coefficient of permeability K_x and K_y at a point in an anisotropic condition may vary with respect to direction, as shown in Fig. 3.9 (b).

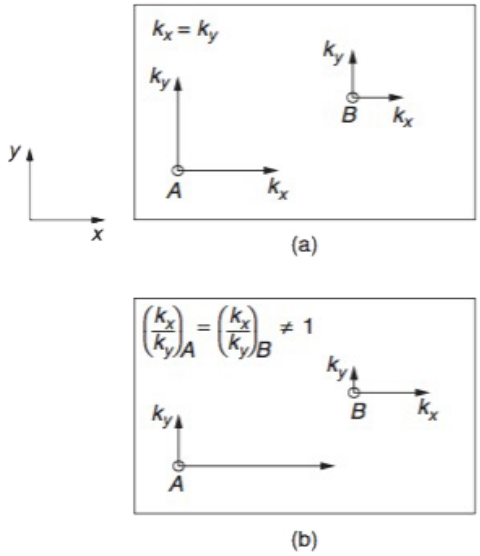

Figure 3.9: Variation of permeability in unsaturated soils; (a) heterogeneous isotropic soils and (b) heterogeneous anisotropic soils (Fredlund et al., 2012).

The magnitude of the coefficients of permeability in both direction K_x and K_y depends on the matric suction. The ratio (K_{wx} / K_{wy}) of variation remains constant, though the coefficients of permeability K_x and K_y can vary from one point to another.

For a two-dimensional, steady-state flow through an unsaturated soil element, as shown in Figure 3.10, the situation is:

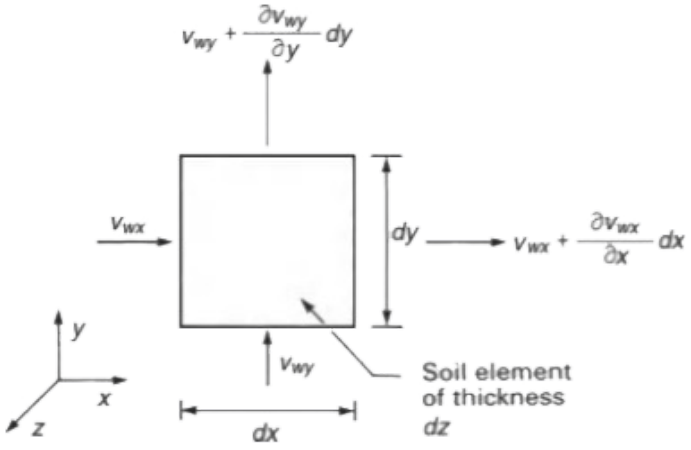

Figure 3.10: Steady-state water flow through a soil element in two dimensions (Fredlund et al., 2012).

The positive and negative sign of flow rate depends on the flow direction of water flow. The flow rate v_{wx} is positive when water flows toward the positive x-direction. Similarly, the flow rate v_{wy} is assumed to be positive if flowing upward along the positive y-direction.

The following equations are the two-dimensional flow equations in unsaturated soils:

$$\left(v_{wx} + \frac{\partial v_{wx}}{\partial x} dx - v_{wx}\right) dydz + \left(v_{wy} + \frac{\partial v_{wy}}{\partial y} dy - v_{wy}\right) dxdz = 0 \qquad (3\text{-}1)$$

where:

v_{wx}, v_{wy} = water flow rate of soil element in the x-, y-direction, respectively (m/s).

dx, dy = infinitesimal dimensions of soil element in the x-, y-direction, respectively.

The net flux in the x- and y-directions can be expressed as follow:

$$\left(\frac{\partial v_{wx}}{\partial x} + \frac{\partial v_{wy}}{\partial y}\right) dxdydz = 0 \tag{3-2}$$

For the fluid flow through porous medium, Darcy's Law can be applied:

$$v_w = -k_w \frac{\partial h_w}{\partial y} \tag{3-3}$$

where:

k_w = coefficient of permeability in the x- and y- directions.

$\partial h_w / \partial y$ = hydraulic head gradient in the *y*-direction.

Substituting Darcy's Law into the net flux equation yields the following partial differential equation:

$$\frac{\partial}{\partial x}\left\{k_{wx}(u_a - u_w)\frac{\partial h_w}{\partial x}\right\} + \frac{\partial}{\partial y}\left\{k_{wy}(u_a - u_w)\frac{\partial h_w}{\partial y}\right\} = 0 \tag{3-4}$$

where:

$\partial h_w / \partial y$ = hydraulic head gradient in the *y*-direction.

$\partial h_w / \partial x$ = hydraulic head gradient in the *x*-direction.

$k_{wx}(u_a\text{-}u_w)$, $k_{wy}(u_a\text{-}u_w)$ = coefficient of permeability variation in the *x*-, *y*-direction, respectively, where (u_a-u_w) represents suction.

Simplifying the coefficients of permeability $k_{wx}(u_a\text{-}u_w)$ and $k_{wy}(u_a\text{-}u_w)$ to k_{wx} and k_{wy}, respectively, the nonlinear form of the partial differential seepage equation of heterogeneous anisotropic soils can be written as follow:

$$k_{wx}\frac{\partial^2 h_w}{\partial x^2} + k_{wy}\frac{\partial^2 h_w}{\partial y^2} + \frac{\partial k_{wx}}{\partial x}\frac{\partial h_w}{\partial x} + \frac{\partial k_{wy}}{\partial y}\frac{\partial h_w}{\partial y} = 0 \tag{3-5}$$

Where:

$\partial k_{wx}/\partial x$ = change of coefficient of permeability in the *x*-direction.

$\partial k_{wx}/\partial y$ = change of coefficient of permeability in the *y*-direction.

Note, for isotropic soils, the coefficient of permeability in the *x*-direction is the same as in y-direction, so k_w can be used for permeability:

$$k_w\left(\frac{\partial^2 h_w}{\partial x^2} + \frac{\partial^2 h_w}{\partial y^2}\right) + \frac{\partial k_w}{\partial x}\frac{\partial h_w}{\partial x} + \frac{\partial k_w}{\partial y}\frac{\partial h_w}{\partial y} = 0 \tag{3-6}$$

b) Flow Through Saturated Soils

When the soil condition is a saturated one, the water permeability coefficient k_w is approximately equal to the saturated permeability coefficient k_s (Fredlund et al., 2012).

Hence, the equations of isotropic, anisotropic heterogeneous soils can be written as follows:

$$k_{sx}\frac{\partial^2 h_w}{\partial x^2} + k_{sy}\frac{\partial^2 h_w}{\partial y^2} + \frac{\partial k_{sx}}{\partial x}\frac{\partial h_w}{\partial x} + \frac{\partial k_{sy}}{\partial y}\frac{\partial h_w}{\partial y} = 0 \tag{3-7}$$

$$k_s\left(\frac{\partial^2 h_w}{\partial x^2}+\frac{\partial^2 h_w}{\partial y^2}\right)+\frac{\partial k_s}{\partial x}\frac{\partial h_w}{\partial x}+\frac{\partial k_s}{\partial y}\frac{\partial h_w}{\partial y}=0 \qquad (3\text{-}8)$$

Where:

k_s = saturated permeability coefficient which is equal to the coefficient of permeability (k_w)

k_{sx} = saturated permeability coefficient in the *x*-direction.

k_{sy} = saturated permeability coefficient in the *y*-direction.

c) Finite Element Formulation

The application of the finite element method requires discretization of the soil mass into element types, such as triangular and quadrilateral elements. A variational principle or weighted residual principle can be applied to define the head throughout a problem domain in the FEM.

Deriving the finite element formulation for two-dimensional steady-state fluid flow can be done by applying Galerkin's method, which is based on the weighted residual principle (Fredlund et al., 2012). Thus, the finite element formulation is as follow:

$$\int_A \begin{bmatrix}\frac{\partial}{\partial x}(L)\\ \frac{\partial}{\partial y}(L)\end{bmatrix}^T \begin{bmatrix}k_{wx} & 0\\ 0 & k_{wy}\end{bmatrix} \times \begin{bmatrix}\frac{\partial}{\partial x}(L)\\ \frac{\partial}{\partial y}(L)\end{bmatrix} dA\{h_{wn}\}\int_S \{L\}^T \overline{v}_w dS_p = 0 \qquad (3\text{-}9)$$

Where:

$\begin{bmatrix}k_{wx} & 0\\ 0 & k_{wy}\end{bmatrix}$ = matrix of the water coefficients of permeability (i.e., $[k_w]$),

$\{h_{wn}\}$ = vector of hydraulic heads at the nodal points, that is $\begin{Bmatrix}h_{w1}\\ h_{w2}\\ h_{w3}\end{Bmatrix}$ for a triangular element,

$\overline{v}_w$ = external water flow rate in a direction perpendicular to the boundary of the element,

S_p = perimeter of the element,

(*L)* = element area coordinate matrix,

L_1, L_2, L_3 = area coordinates of points in the element, for a triangular element, which are dependent on Cartesian coordinates of nodal points and can be written as the following equations:

$$L_1 = 1/2A\{(x_2y_3 - x_3y_2) + (y_2 - y_3)x + (x_3 - x_2)y\}$$

$$L_2 = 1/2A\{(x_3y_1 - x_1y_3) + (y_3 - y_1)x + (x_1 - x_3)y\} \quad (3\text{-}10)$$

$$L_3 = 1/2A\{(x_1y_2 - x_2y_1) + (y_1 - y_2)x + (x_2 - x_1)y\}$$

Where:

$x_i, y_i (i = 1,2,3)$ = cartesian coordinates of the three nodal points of a triangular element,

x, y = cartesian coordinates of a point within an element,

A = area of an element.

Equation (3-9) can be simplified as follows

$$\int_a [B]^T [k_w][B] dA\{h_{wn}\} - \int_s [L]^T \overline{v}_w \, dS_p = 0 \quad (3\text{-}11)$$

Where, [B], is the derivative matrix of the area coordinates, and can be expressed as follows:

$$\frac{1}{2A}\begin{Bmatrix} y_2 - y_3 & y_3 - y_1 & y_1 - y_2 \\ x_3 - x_2 & x_1 - x_3 & x_2 - x_1 \end{Bmatrix}$$

Either Dirichlet or Neumann boundary conditions must be defined to solve for hydraulic heads at boundary nodal points.

Equation (3-11) is non-linear due to the permeability coefficient as a function of the matrix suction and is related to the hydraulic head at each node. The hydraulic head is an unknown variable in the equation and can be solved by using an iterative process. A Gaussian elimination technique can be used to linearize the flow equation.

By using the derivative of the element hydraulic head relative to the *x*-, *y*-direction, the hydraulic head gradient in the x and y directions of the element can be calculated:

$$\begin{Bmatrix} i_x \\ i_y \end{Bmatrix} = [B]\{h_{wn}\} \tag{3-12}$$

Where:

$i_x, i_y =$ hydraulic head gradient within an element in the *x*-, *y*-direction, respectively.

Using Darcy's Law to calculate the element flow rates from the hydraulic head gradients and the coefficients of permeability:

$$\begin{Bmatrix} v_{wx} \\ v_{wy} \end{Bmatrix} = [k_w][B][h_{wn}] \tag{3-13}$$

Where:

v_{wx}, v_{wy} = water flow rates within an element in the *x*-, *y*-direction, respectively.

Finally, the hydraulic head gradient and flow rate at each node point can be computed.

3.2.4 Transient Groundwater Flow

Seepage flow through a dam can be divided into two categories: steady-state and transient flow problems. The main difference between steady-state and transient flow is the hydraulic head (and possibly the permeability coefficient) changes with respect to time (Fredlund et al., 2012).

a) General Governing Flow Equations

Assuming pressures remain constant with time, the time derivatives of the total stress and the pore-air pressure are equal to zero and a partial differential equation for transient seepage in anisotropic soils can be expressed as follows:

$$\frac{\partial}{\partial_x}\left(k_{wxx}\frac{\partial h_w}{\partial x}+k_{wxy}\frac{\partial h_w}{\partial y}\right)+\frac{\partial}{\partial_y}\left(k_{wyx}\frac{\partial h_w}{\partial x}+k_{wyy}\frac{\partial h_w}{\partial y}\right)=\ m_2^w\rho_w g\frac{\partial h_w}{\partial t} \qquad (3\text{-}14)$$

Since the pore-water pressure is constant with respect to time, the major and minor coefficients of permeability directions are not identical to the x and y direction. Setting the α angle equal to zero, and the governing partial differential equation can be simplified as follows:

$$\frac{\partial}{\partial_x}\left(k_{w1}\frac{\partial h_w}{\partial x}\right)+\frac{\partial}{\partial_y}\left(k_{w2}\frac{\partial h_w}{\partial y}\right)=\ m_2^w\rho_w g\frac{\partial h_w}{\partial t} \qquad (3\text{-}15)$$

Where:

k_{w1} = major coefficient of permeability,

k_{w2} = minor coefficient of permeability,

h_w = hydraulic head,

m_2^w = coefficient of water volume change with respect to a change in matric suction,

ρ_w = density of water,

g = gravitational acceleration (9.81m/s^2).

The general governing partial differential equation can be used to solve transient flow through both saturated and unsaturated soils. Like the steady-state seepage though saturated soils, the water permeability coefficient k_w is approximately equal to the saturated permeability coefficient k_s and the coefficient of water volume change with respect to a change in matric suction (m_2^w) is approximately equal to the coefficient of volume change (m_v) (Fredlund et al., 2012).

b) Finite Element Formulation

Solving the transient flow problem requires knowing the permeability function and the water storage function of each soil layer. Both the permeability function and the water storage function use a nonlinear mathematical model to represent unsaturated soils (Fredlund et al., 2012). Deriving the finite element formulation for two-dimensional transient fluid flow by applying Galerkin's method to the governing seepage equations, which is given by the following integrals over the area and boundary surface of a triangular element:

$$\int_A [B]^T [k_w][B] dA\{h_{wn}\} + \int_A [L]^T \lambda [L] dA \frac{\partial \{h_{wn}\}}{\partial t} - \int_S [L]^T \overline{v}_w dS = 0 \qquad (3\text{-}16)$$

Where:

$[B]$ = matrix of the derivatives of area coordinates, as shown for the steady-state formulation,

$[L]$ = matrix of element area coordinates (i.e., $\{L_1L_2L_3\}$),

$\lambda = \rho_w g m_2^w$,

A = area of the element,

$\{h_{wn}\}$ = matrix of hydraulic heads at the nodal points, that is $\begin{Bmatrix} h_{w1} \\ h_{w2} \\ h_{w3} \end{Bmatrix}$, for a triangular element,

$\overline{v}_w$ = external water flow rate in a direction perpendicular to the boundary of an element,

$[K_w]$ = tensor of the water coefficients of permeability for an element, which can be written as: $\begin{bmatrix} k_{wxx} & k_{wxy} \\ k_{wyx} & k_{wyy} \end{bmatrix}$

The saturated-unsaturated seepage equation can be constructed by numerical integration of equation (3-16), in matrix form:

$$[D]\{h_{wn}\} + [E]\{h_{wn}\} = [F] \tag{3-17}$$

Where

$[D]$ = stiffness matrix, that is, $[B]^T[k_w][B]A$,

$[E]$ = capacitance matrix, that is, $\frac{\lambda A}{12}\begin{bmatrix} 2 & 1 & 1 \\ 1 & 2 & 1 \\ 1 & 1 & 2 \end{bmatrix}$,

$\{h_{wn}\} =$ matrix of time derivatives of hydraulic heads at the nodal points (i.e., $\partial\{h_{wn}\}/\partial t$),

$[F]$ = flux vector reproducing the boundary conditions (i.e., $\int_S [L]^T \overline{v}_w dS$).

Equation (3-17) can be written for each element in order to form a set of global flow equations which can be solved by using iterative methods to calculate the hydraulic head at all nodal points. Once the hydraulic head values at nodal points have been calculated, other quantities, such as pore water pressures can be calculated using the following equation:

$$\{u_{wn}\} = (\{h_{wn}\} - \{y_n\})\rho_w g \tag{3-18}$$

Where:

$\{u_{wn}\}$ = matrix of pore-water pressures at nodal points $\left(i.e. \begin{Bmatrix} u_{w1} \\ u_{w2} \\ u_{w3} \end{Bmatrix} \right)$ for a triangular element,

$\{y_n\}$ = matrix of elevation heads at nodal points $\left(i.e. \begin{Bmatrix} y_1 \\ y_2 \\ y_3 \end{Bmatrix} \right)$ for a triangular element.

Chapter 4: Modeling and analysis of transient seepage for upstream-type tailings dams by the Finite Element Method

4.1 METHODOLOGY AND SETUP

The analysis of transient seepage flow models using FEM will be accomplished in this chapter by incorporating key parameters identified in the previous chapter. It was established that a.) the permeability (in particular the ratio of horizontal to vertical permeability), b.) embankment dam slope, c.) beach-width to dam-height ratio, d.) rate of embankment raising and e.) presence/absence of underdrain are the most important factors. In general, a cross-section through the tailings dam, assuming that the length of the dam perpendicular to the section is much greater than its width, will be represented as a two-dimensional model with no out-of-plane flow conditions. This assumption is a routine one when analyzing embankments and dams.

Thus, two simulation sets were designed in this research: one for a dam with no underdrain under the downstream shell (Model Set A) and the other set for a dam with an installed under-drain (Model Set B). Note, that the models with underdrain serve as control models, since it is expected that for a functioning underdrain, there will be no seepage face breakout on the downstream embankment shell. The two model sets form the changing geometric and boundary conditions. For each simulation, it was assumed that the dam was raised at either 5, 10, 15 or 20 meters per year starting from zero-meter level at the starter dam crest, which are typical production-level raising rates. Within the two model sets, two subsets were created, which used two different, albeit typical, slope inclinations (3 horizontal to 1 vertical and 2 horizontal to 1 vertical). In addition, the beach-width to dam-height (L/H) ratio was varied as 3, 5, 9 and 12, covering a wide range of beach sizes.

The initial dam height was chosen to be 6.1m (20ft), which is a typical starter dam height. All models were constructed based on common current practices and parameters and individual models were built from values presented in Table 4.1; Table 4.1 (a) and Table 4.1 (b) for slope inclinations of 3:1 and 2:1, respectively. The 32 models form Model Set A, where the dam has no underdrain installed. The same 32 models with a continuous underdrain under the downstream slope form Model Set B. The location of the underdrain will be discussed in a subsequent section.

Model Set I				
Slope inclination	3 horizontal: 1 vertical			
Crest	6.1m (20ft)			
Embankment raising rate (m/year)	Beach width (L/H)			
	3	5	9	12
5	Model 1	Model 2	Model 3	Model 4
10	Model 5	Model 6	Model 7	Model 8
15	Model 9	Model 10	Model 11	Model 12
20	Model 13	Model 14	Model 15	Model 16

Table 4.1 (a), Input paraments of Model Set I.

Model Set II				
Slope inclination	2 horizontal : 1vertical			
Crest	6.1m (20ft)			
Embankment raising rate (m/year)	Beach width (L/H)			
	3	5	9	12
5	Model 17	Model 18	Model 19	Model 20
10	Model 21	Model 22	Model 23	Model 24
15	Model 25	Model 26	Model 27	Model 28
20	Model 29	Model 30	Model 31	Model 32

Table 4.1 (b), Input paraments of Model Set II.

As described in the previous chapter, permeability (K) is an important factor that affects the position of phreatic surface. In order to compare the phreatic surface location for different anisotropies of K, the tailings embankment anisotropy (K_h / K_v) parament was assumed to vary in each model set, while the material properties and embankment geometry was kept constant for comparison. According to Vick (1990), the anisotropy, which is measured by the ratio of horizontal to vertical permeability (K_h / K_v), generally ranges from 2 to 10 for beach sand deposits and slimes. Table 4.2 presents the considered variation of anisotropy. As three sets of typical anisotropies were

considered, there were a total of 96 models in each simulation Model Set, giving rise to 192 models analysed in total.

	Permeability Anisotropy (K_h / K_v)		
	Set 1	Set 2	Set 3
Beach Sands	1	2	5
Slimes	5	10	10

Table 4.2: Variation of anisotropy in each model set.

Once the methodology and model parameters were selected, general project settings should always be chosen at the start of the modeling, which are shown in Figure 4.1. Plane strain formulation was selected as the default type of analysis, which is typical for 2D analyses of dams, which have a constant (prismatic) cross-section. The solid-fluid interaction was uncoupled since the coupled analysis could not be used in conjunction with transient analysis in RS2. Gaussian elimination was chosen as the default solver method. Due to long time scales of mine operation, tailings generation and embankment raising measured in decades, the time units were set to years.

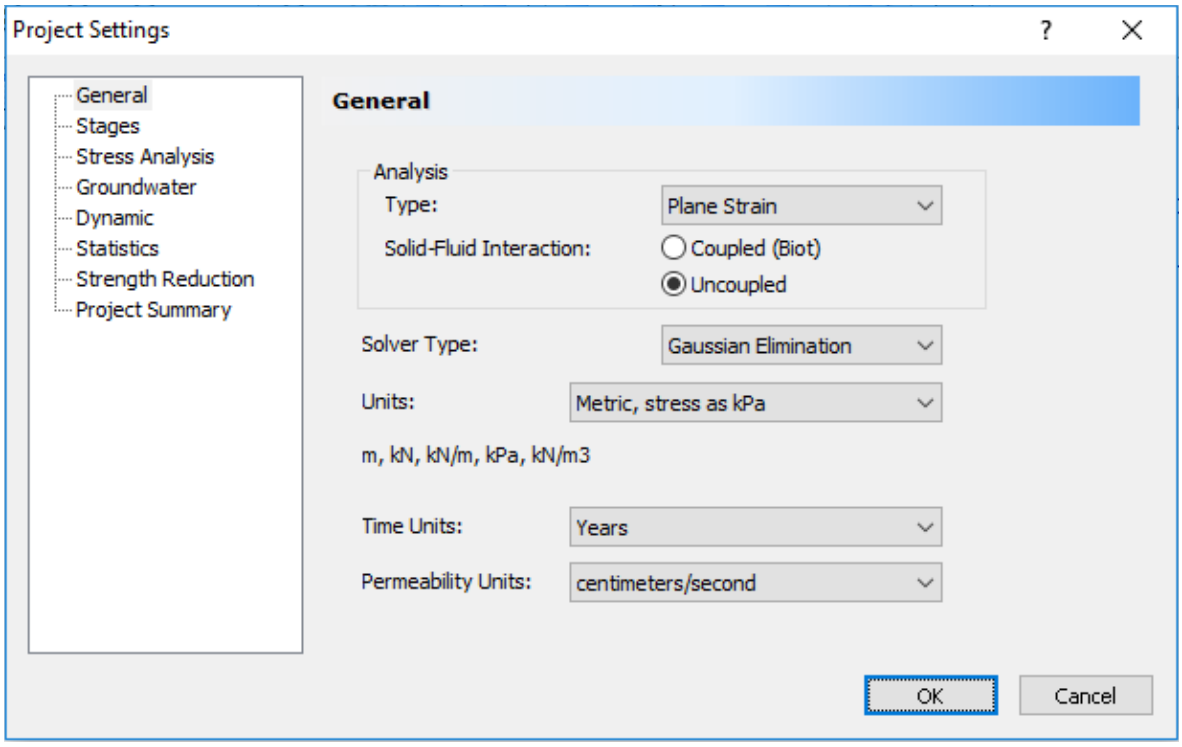

Figure 4.1: General project settings and assumptions.

Since the pore water pressure was considered in these models, hydraulic properties need to be defined, as shown in Figure 4.2, using Model 1 as an example. Hydraulic properties are used to specify the groundwater or hydraulic parameters for each material. According to the simulation, the anisotropy (K_h / K_v) is 1 for sand and 5 for slimes in Model 1, so the K_2 / K_1 is 1 for sands and 0.2 for slimes using RS2's nomenclature, as shown in Figure 4.2 (a) and (b), respectively. After which, the same procedure of hydraulic properties for the rest of 191 models was applied, based on Model 1.

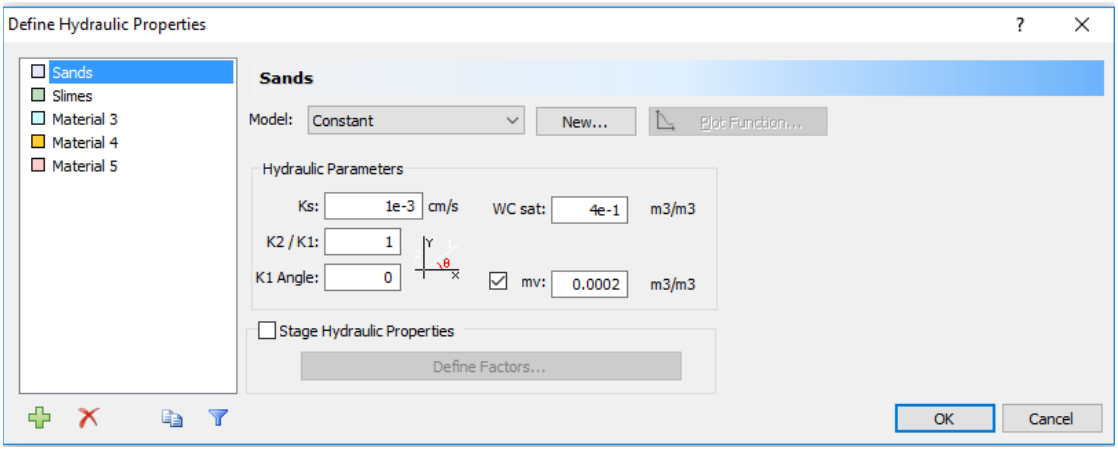

Figure 4.2 (a): Definition of hydraulic properties for sands for Model 1.

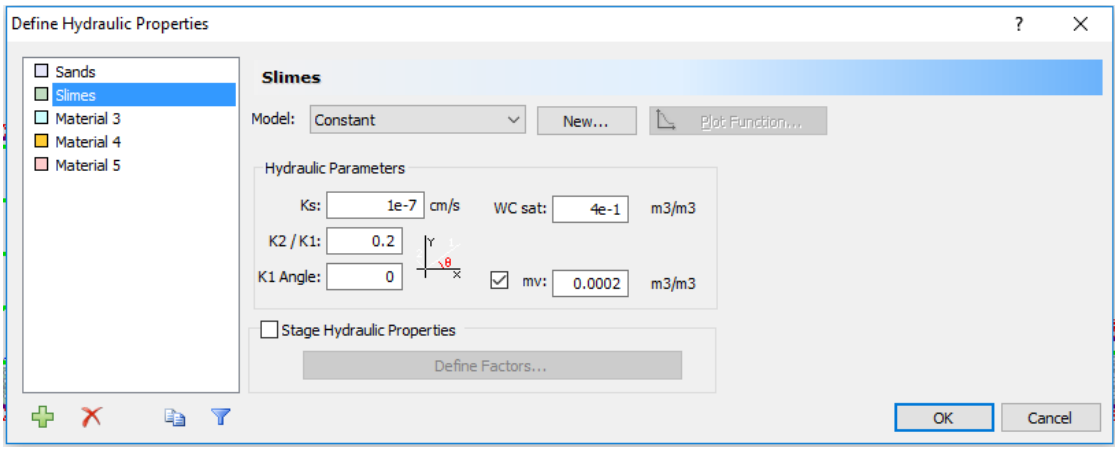

Figure 4.2 (b): Definition of hydraulic properties for slimes for Model 1.

4.2 IMPLEMENTATION OF STAGING OF DAM RAISING IN FINITE ELEMENT ANALYSIS

After defining the material properties, boundary conditions were established next. It was assumed that the tailings facility was constructed on an impervious foundation (no flow across the boundary), which is quite a reasonable assumption, since siting the pond is often done such way

to avoid any seepage under a dam. Since the location of the phreatic surface itself is an unknown, a boundary condition was defined in RS2 to search for the phreatic surface, which is where the pressure is zero. These boundary conditions are denoted by the '?' symbols on the plots. The finite element model in this thesis was built considering staged construction (dam raising) to represent the time-dependent evolution of phreatic surface condition as the embankment dam is being constructed. The whole process can be illustrated by the following stages:

1. Construction of the initial (starter) dam and filling of the tailings pond (year 0)
2. Raising the embankment dam (according to parameters in Table 4.1) and filling the tailings pond (years 1 through 4)
3. Cessation of embankment raising and pond filling, tailings storage has reached its capacity (year 5)
4. Long-term evolution of phreatic surface and seepage (years 10, 20 and 50) considering the water level is maintained at a constant level in the pond (balance of precipitation, runoff, etc.)

Each model, based on Tables 4.1 and 4.2, was generated to include the above stages. The five-year filling of a pond is an average time-span for such activity in the industry. Since the long-term evolution of phreatic surface is the goal of the research work, a time period of 45 years after the cessation of pond filing represents a good compromise. As will be discussed later in the thesis, the phreatic surface often peaks or reaches equilibrium well before 50 years, thus the time span appears to be more than adequate.

4.3 ACCURACY AND ADEQUACY OF THE FINITE ELEMENT MODEL – MESH CONVERGENCE STUDY

Having defined the model using stages to represent all major steps in the evolution of a tailings storage facility, the finite element method can compute the distribution of pressure and total heads at any given point within a domain. However, it is required to instill trust in these computed values. It is appreciated that the solution given by the finite element method approximates the physical system. However, there are errors arising from the choice of finite element formulation, discretization error and numerical errors from computation. With a finite element package like RS2, the finite element formulation is selected, as described in Chapter 3, to solve for transient seepage. The element formulation was chosen to be second-order (quadratic) triangles with 6-nodes, which are quite accurate to capture the flow field. RS2 uses sophisticated solvers to compute the unknowns with control over the residuals (Rocscience Inc., 2018), thus ensuring that numerical error is minimized. Thus, only one thing is left to the analyst to decide; the discretization of a domain. It is appreciated that if more and more elements are used (that are smaller and smaller), the solution should converge to a value that no further improvement can be achieved at a reasonable cost. RS2 attempts to give a good estimate of how many elements are required to discretize the domain into, but it does not guarantee that there will be sufficient numbers used to generate a converged mesh. This task is left to the analyst. Therefore, it is advisable to carry out a small study to find the adequate number of elements (and nodes) that result in a mesh with converged results. Three discretizations of a same model were set up, by roughly doubling the number of nodes for each model, as summarized in Table 4.3, to examine mesh convergence. These models were analyzed and the results at 50 years were plotted up at a critical section running down from the crest of the downstream shell of a starter dam, knowing that the phreatic surface

will cross this line to emerge as a seepage face. Figure 4.3 shows the plot of computed values of total head at the critical section, while Figure 4.4 shows the location of the line in the model. The results of Accepted mesh and Fine mesh plot on top of each other with the difference between them in the L_{inf} norm being 0.00317. While the Coarse mesh and the Accepted mesh gave results that differ in the L_{inf} norm by 0.0247, which is an order of magnitude higher than for the Fine mesh. Thus, it can be said that the gain attained by using the Fine mesh with respect to the Accepted mesh is minimal, while the computation effort expended is considerable (about 87 percent longer solution time for the Fine mesh). Similarly, the Coarse mesh is not a converged mesh, since by increasing the number of nodes (and the degrees of freedom), the solution accuracy can be improved. Therefore, the discretization method to achieve mesh density in the Accepted mesh was used throughout the study to generate converged meshes, ensuring a quality solution.

Model discretization	Number of elements	Number of nodes
Coarse mesh	2683	5564
Accepted mesh	4760	10769
Fine mesh	8956	21374

Table 4.3: Model parameters used in the mesh convergence study.

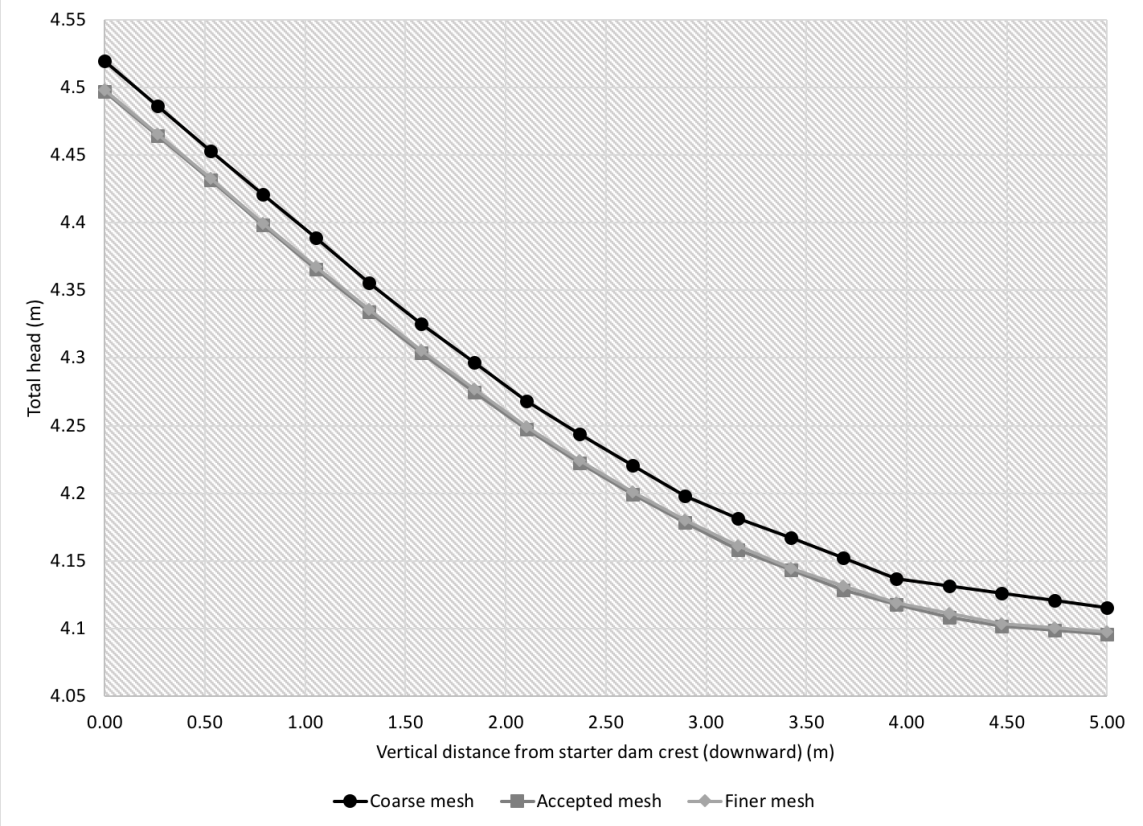

Figure 4.3: Mesh convergence - variation of total head at the downstream crest of the starter dam at 50 years

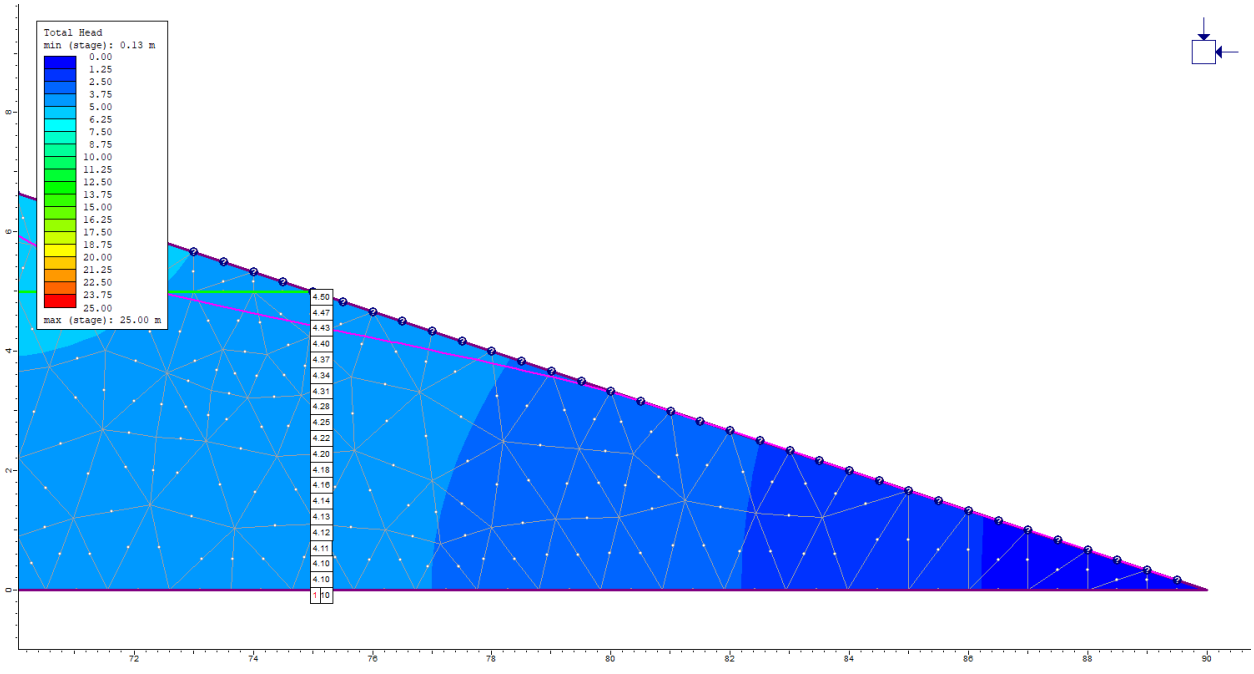

Figure 4.4: Mesh convergence – measurement line at the downstream crest of the starter dam.

4.4 RESULTS OF ANALYSIS – EVOLUTION OF PHREATIC SURFACE

As discussed earlier, the objective of numerical modeling is to assess the conditions of transient groundwater seepage flow and how it changes under the influence of variables considered in Tables 4.1 and 4.2. Moreover, the purpose is to obtain the most appropriate solution through comparisons of different variables to minimize the risk of raising phreatic surface and its break out on the downstream slope face with gradually increasing the width and height of the embankment dam.

For the sake of brevity, since there are almost 200 models, the format of Section 4.4 and its subsections will be such that the contour plots of distribution of total head within the slope will be presented for a typical model only. Followed by charts showing the evolution of seepage face for models organized by anisotropy set, slope ratio and beach width, in that order. The discussion of correlation of all parameters will be done in subsections for each parameter.

For a typical model (Model 1 – Anisotropy Set 1), after constructing the starter embankment on an impervious foundation and filling the pond, the results are presented in Figure 4.5, showing the variation of total head and the location of phreatic surface. The solid line traversing the model indicates the location of the Water Table (phreatic surface) where the position of the Pressure Head = 0 contour boundary.

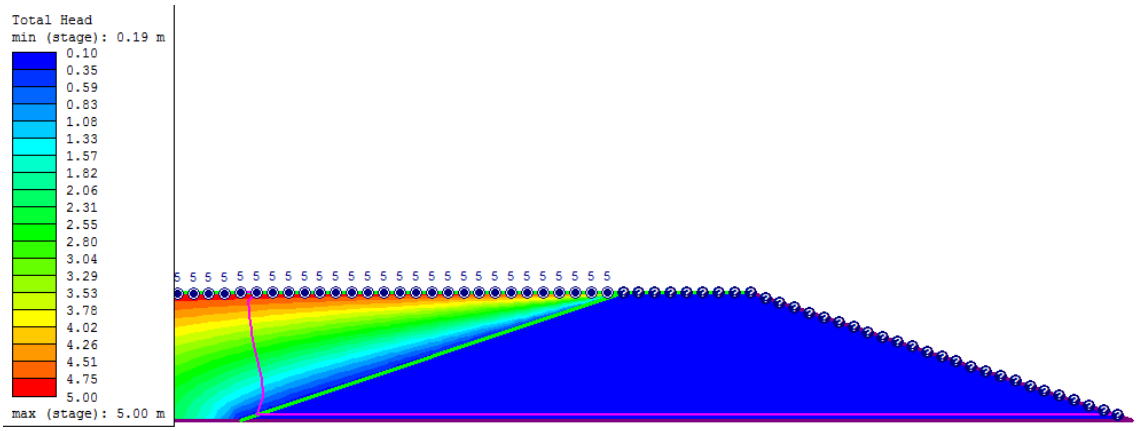

Figure 4.5: Total head distribution and phreatic surface for the initial state (starter embankment).

It is evident from Figure 4.5 that the phreatic surface suddenly drops as the seepage flow enters the embankment dam. This is due to the difference in permeability between the dam (sands) and tailings (slimes), which is about four orders of magnitude higher for the sands. The phreatic surface emerges very close to the downstream toe of the embankment, freeing the downstream shell from excess pore water pressure, thus increasing its stability. With the yearly raises of embankment and filling the tailings pond for years 1 though 5 and the subsequent cessation of embankment rising for Model 1 with Anisotropy Set 1, the evolution of total head and the location of phreatic surface can be followed through Figures 4.6 to 4.13, respectively.

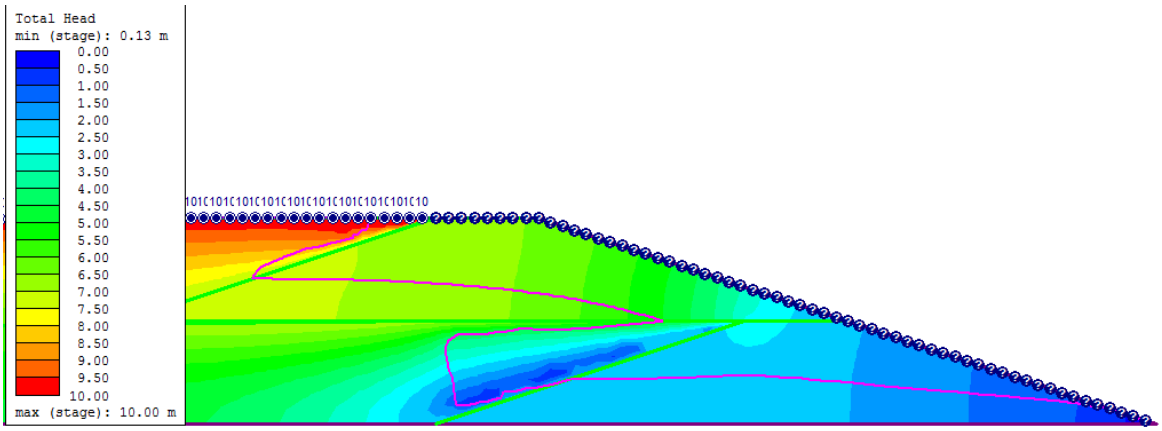

Figure 4.6: Total head distribution and phreatic surface for year 1.

The first raise of embankment and filling of tailings pond resulted in a drastic change in the shape of phreatic surface, as seen on Figure 4.6. Due to the differing orders of magnitude for permeability between sands and slimes, the seepage preferentially occurs through the sands (embankment). Thus, the phreatic surface migrates upward and the point of breakout (often called seepage face breakout) on the downstream face of dam moves uphill. This will be discussed after the total heads are presented for all stages. The location of seepage face breakout will be measured along the slope face from the downstream toe of the slope. The second dam raising, as shown on Figure 4.7, further pushed the phreatic surface upward and moved the breakout point uphill. Similar trend was observed for years 3, 4 and 5, as shown on Figures 4.8 through 4.10. Worth mentioning that the pocket of low total head on the upstream face of the dam within the tailings, eventually closes up because the seepage flow occurs in the downstream shell of the dam, circumventing the low permeability tailings.

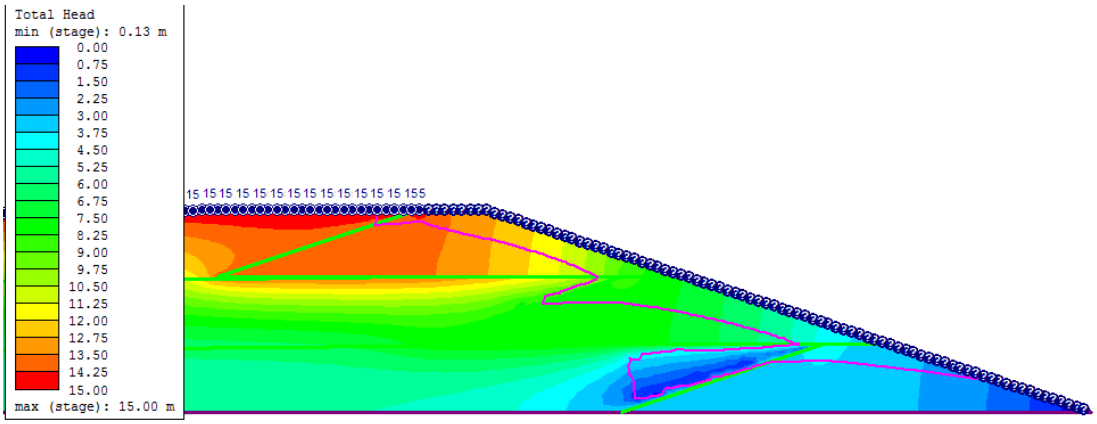

Figure 4.7: Total head distribution and phreatic surface for year 2.

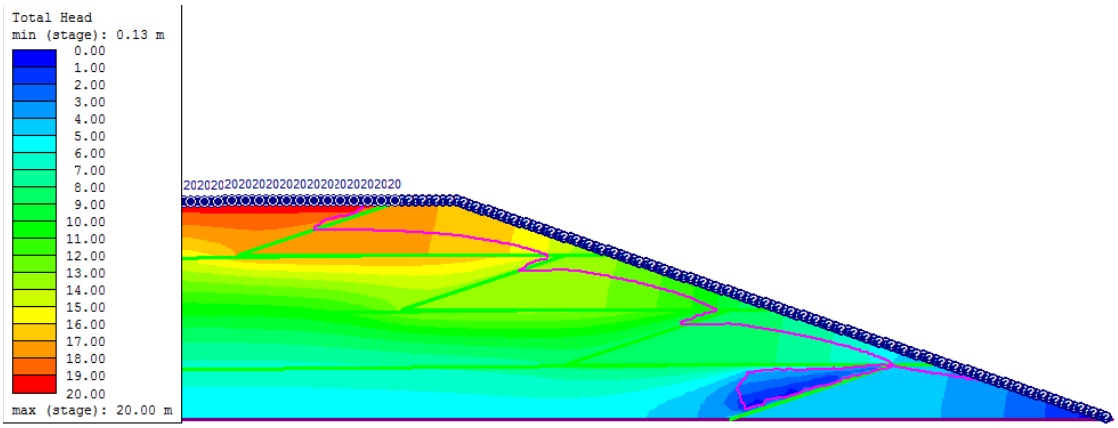

Figure 4.8: Total head distribution and phreatic surface for year 3.

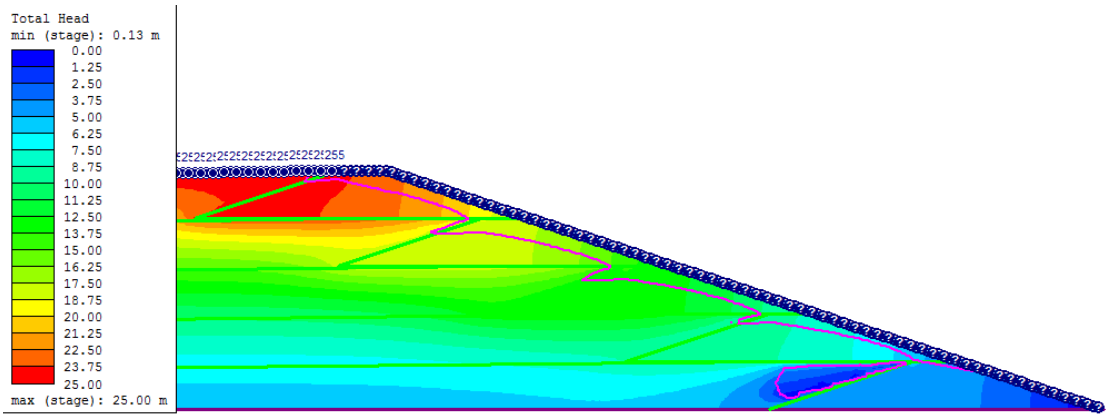

Figure 4.9: Total head distribution and phreatic surface for year 4.

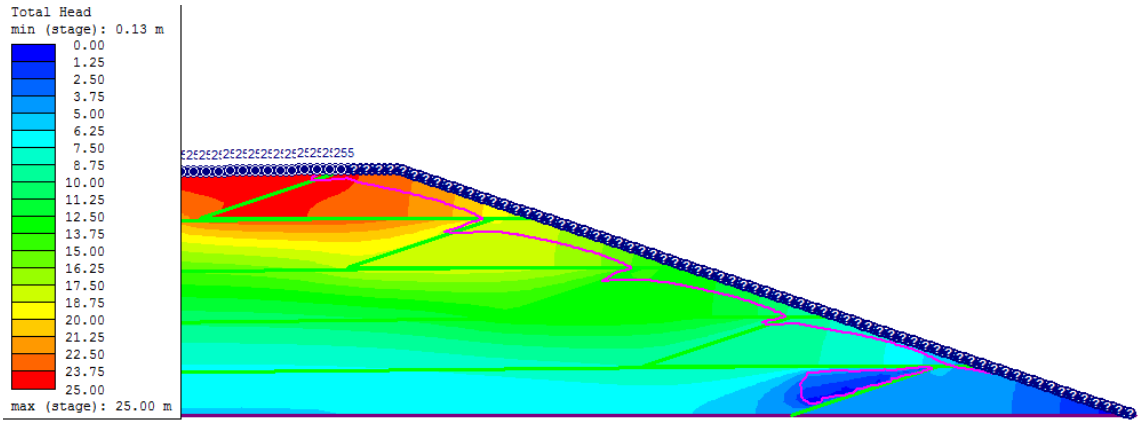

Figure 4.10: Total head distribution and phreatic surface for year 5.

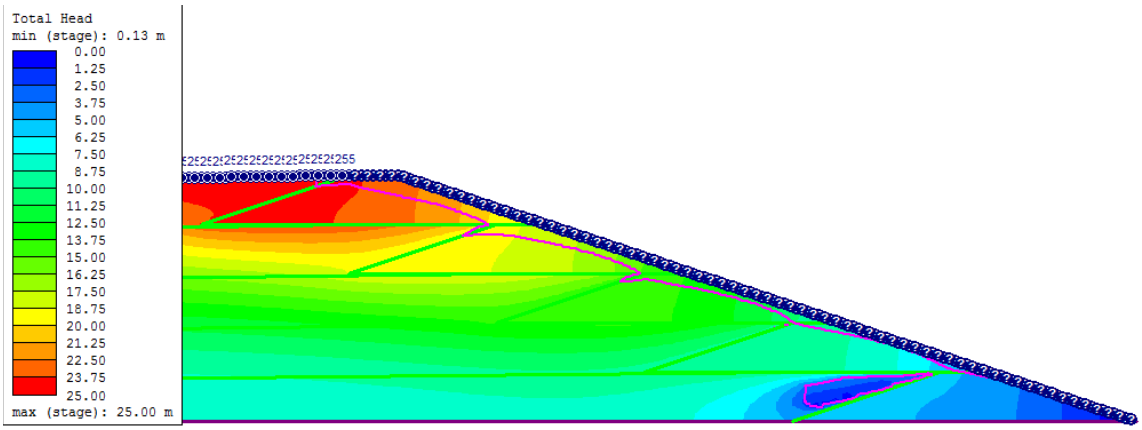

Figure 4.11: Total head distribution and phreatic surface for year 10.

In year 10, five years after the ending of embankment raising and pond filling, the upward migration of breakout point slows down, while the pocket of low total head persists in the tailings next to the starter embankment's upstream face.

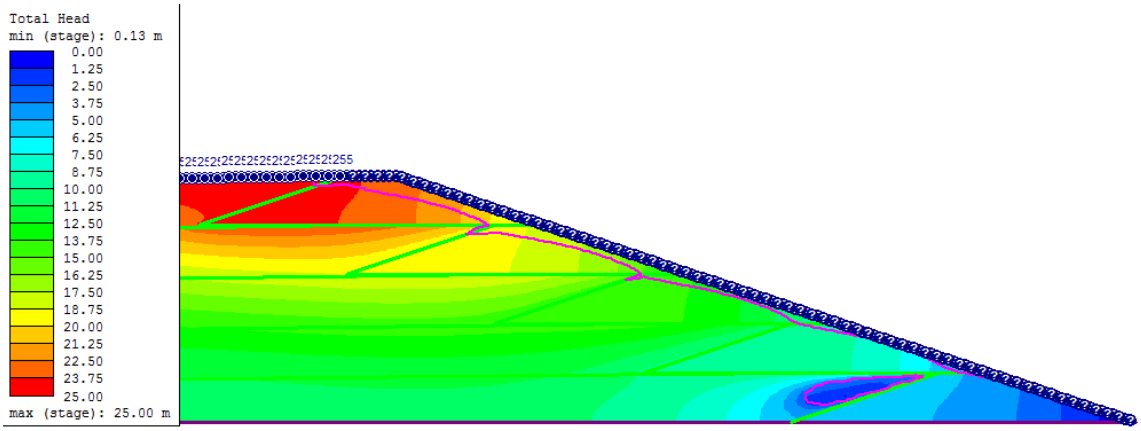

Figure 4.12: Total head distribution and phreatic surface for year 20.

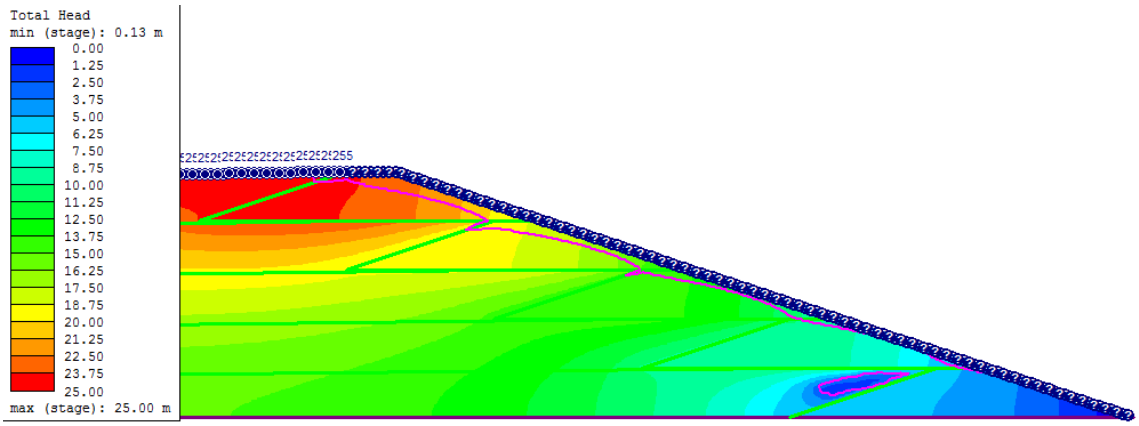

Figure 4.13: Total head distribution and phreatic surface for year 50.

Years 20 and 50 show a similar trend of the seepage face breakout stabilizing.

4.4.1 Models with 3:1 Slope – Anisotropy Set 1

As seen from the previous set of figures, by year 50 the low total head pocket shrinks and the breakout point stabilises, which is also evident from Figure 4.14, which shows the evolution of seepage face as a function of time for an embankment raising of 5m/year (Model 1). Thus, we can conclude that the upward migration of seepage face breakout stops around year 20 for this model, about 15 years after the termination of dam raising and pond filling. Considering the rest of models shown on Figure 4.14, we can observe that as the beach width (L/H) gradually increases, the groundwater condition changes. It appears that the location of phreatic surface rises sharply within the first ten years for all models, in particular for Model 2 (L/H of 5), then gradually decreases for Models 2 through 4 for the remaining 40 years. This decrease in the seepage face breakout can be attributed to the increasing beach width. Therefore, is can be concluded that farther the pond is, lower the location of seepage face breakout would be.

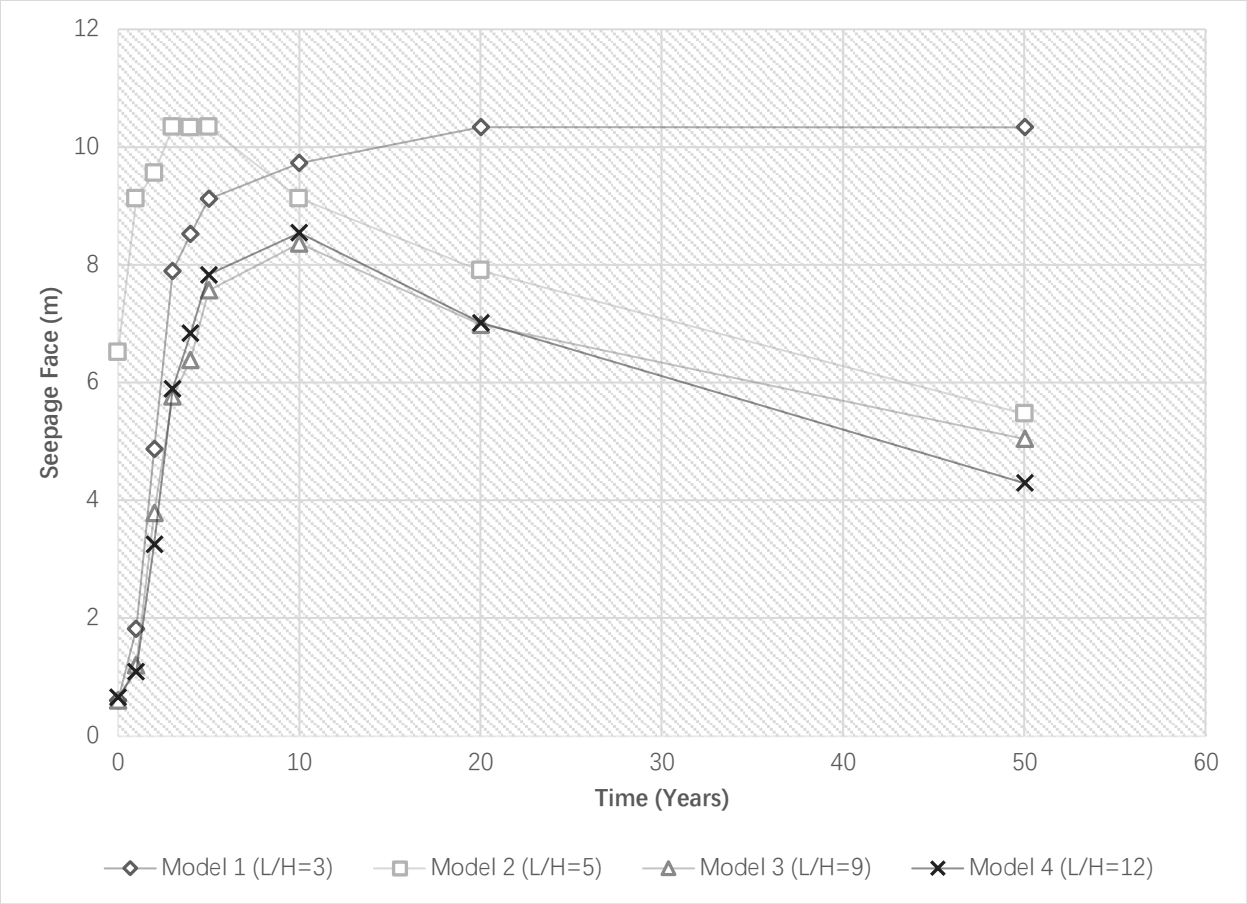

Figure 4.14: Seepage face breakout convergence results for Models 1 - 4 with Anisotropy Set 1, dam raising at rate of 5m/year.

Applying the same approach to construct embankments for the rest of the models, results, as shown in Figures 4.15-4.17, indicate the evolution of seepage face as a function of time for embankment raising of 5, 10, 15 and 20 meters per year with Anisotropy Set 1, respectively.

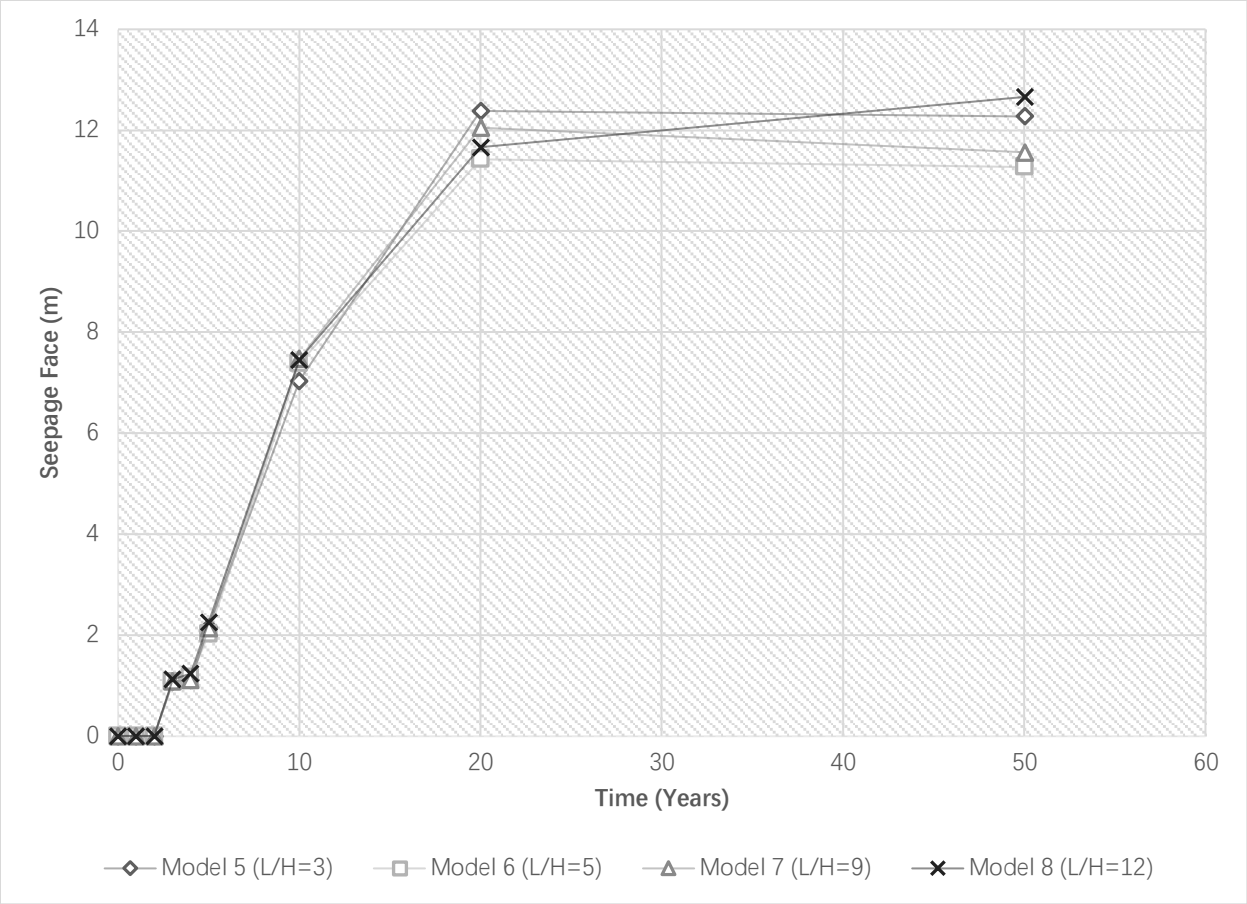

Figure 4.15: Seepage face breakout convergence results for Models 5 - 8 with Anisotropy Set 1, dam raising at rate of 10m/year.

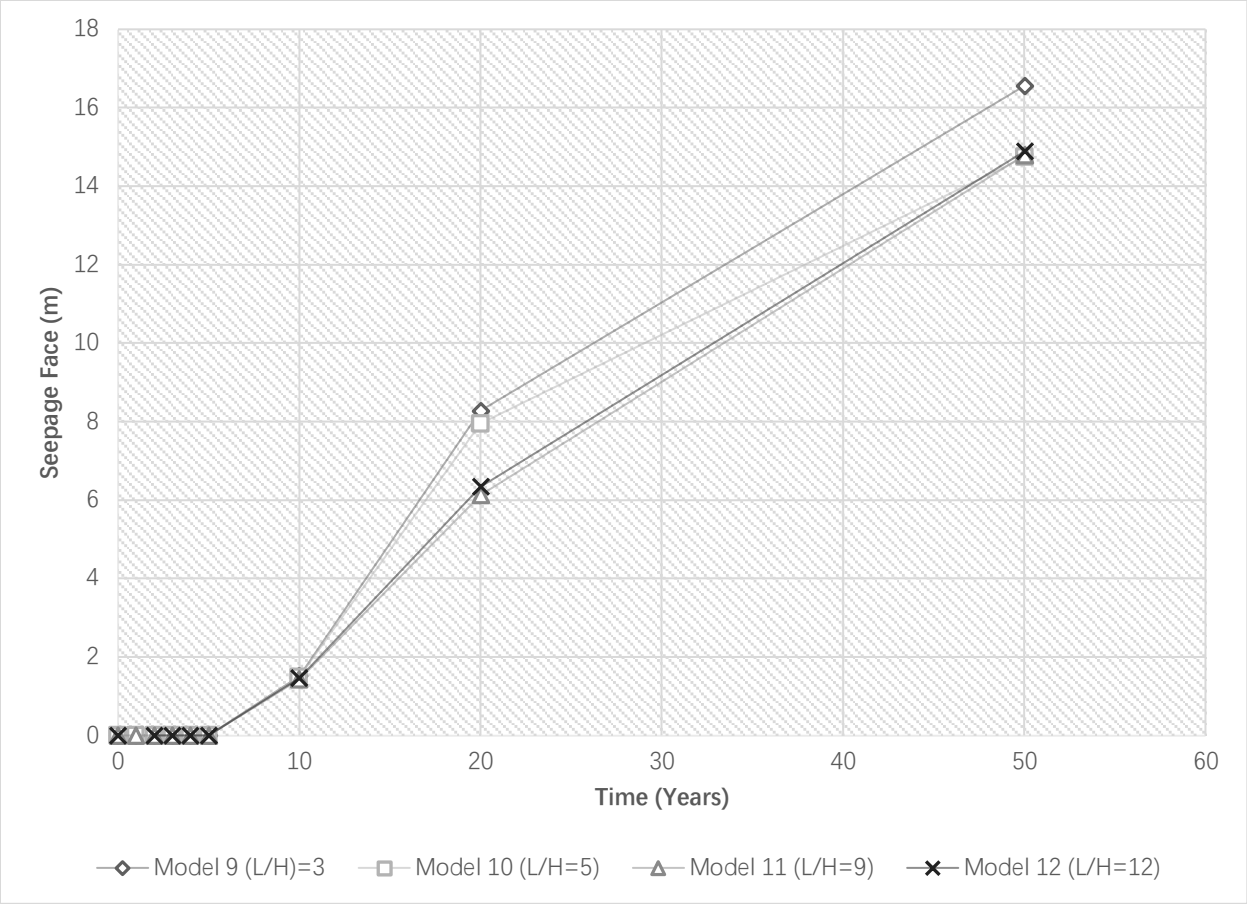

Figure 4.16: Seepage face breakout convergence results for Models 9 - 12 with Anisotropy Set 1, dam raising at rate of 15m/year.

When the dam was raised at a rate of 15m/year, it took five years for the seepage face breakout to appear on the downstream slope of the dam, for all (L/H)-s considered. Afterwards, the seepage face increased as time progressed, and within the 50 years simulation span it had not reached a constant value, like it did for raising rates 5 and 10m/year.

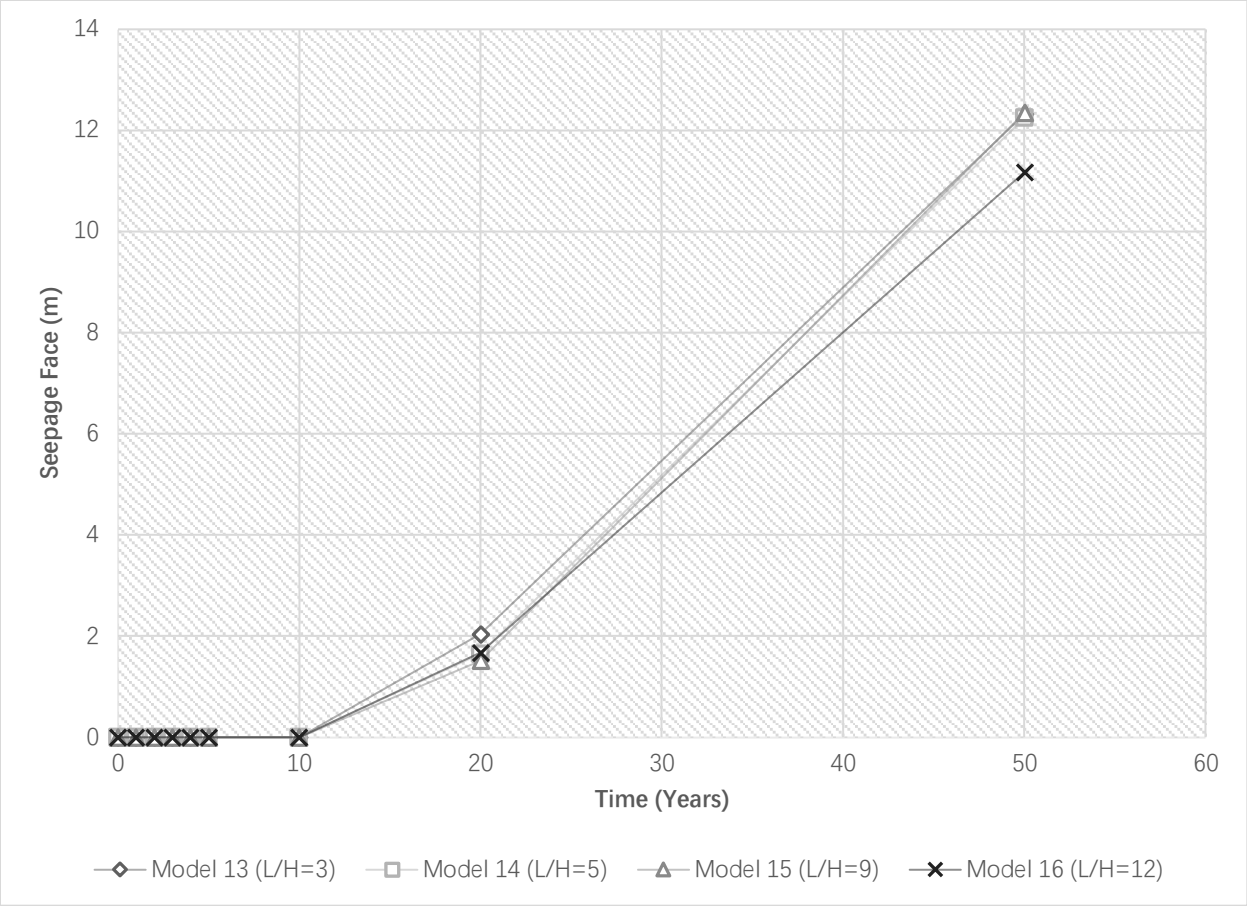

Figure 4.17: Seepage face breakout convergence results for Models 13 - 16 with Anisotropy Set 1, dam raising at rate of 20m/year.

At the fastest raising rate of 20m/year, the seepage face breakout appeared only after 10 years, irrespective of (L/H). Afterwards, it increased in an almost linear fashion not reaching a constant value in 50 years, similar to the raising rate of 15m/year. Although with increasing (L/H), the seepage face breakout location generally decreases, yet it was a much more modest decrease as compared to the raising rate of 5m/year.

4.4.2 Models with 2:1 Slope – Anisotropy Set 1

For a steeper slope of a 2:1 ratio, as defined in Table 4.1 (b), Models 17 though 32 were generated and analyzed. Figures 4.18-4.21 summarize the evolution of phreatic surface and seepage face with respect to time.

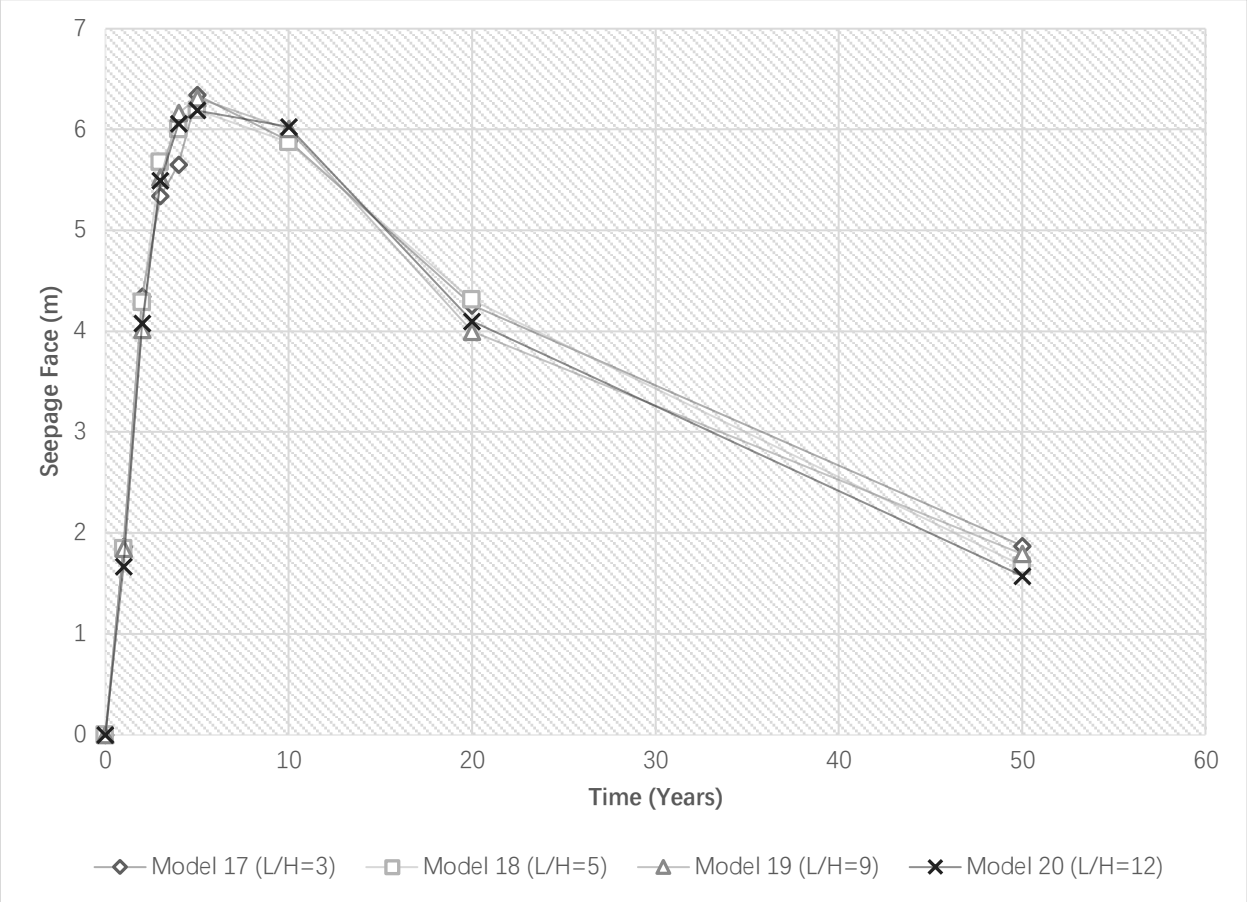

Figure 4.18: Seepage face breakout convergence results for Models 17 - 20 with Anisotropy Set 1, dam raising at rate of 5m/year.

For the 5m/year dam raising, the shape of seepage face breakout is very similar to the 3:1 slope ratio case (Figure 4.14); there is a sharp increase followed by a steady drop. Yet is appears that the steeper slope (2:1) results in a sharper decline of seepage face breakout as time passes.

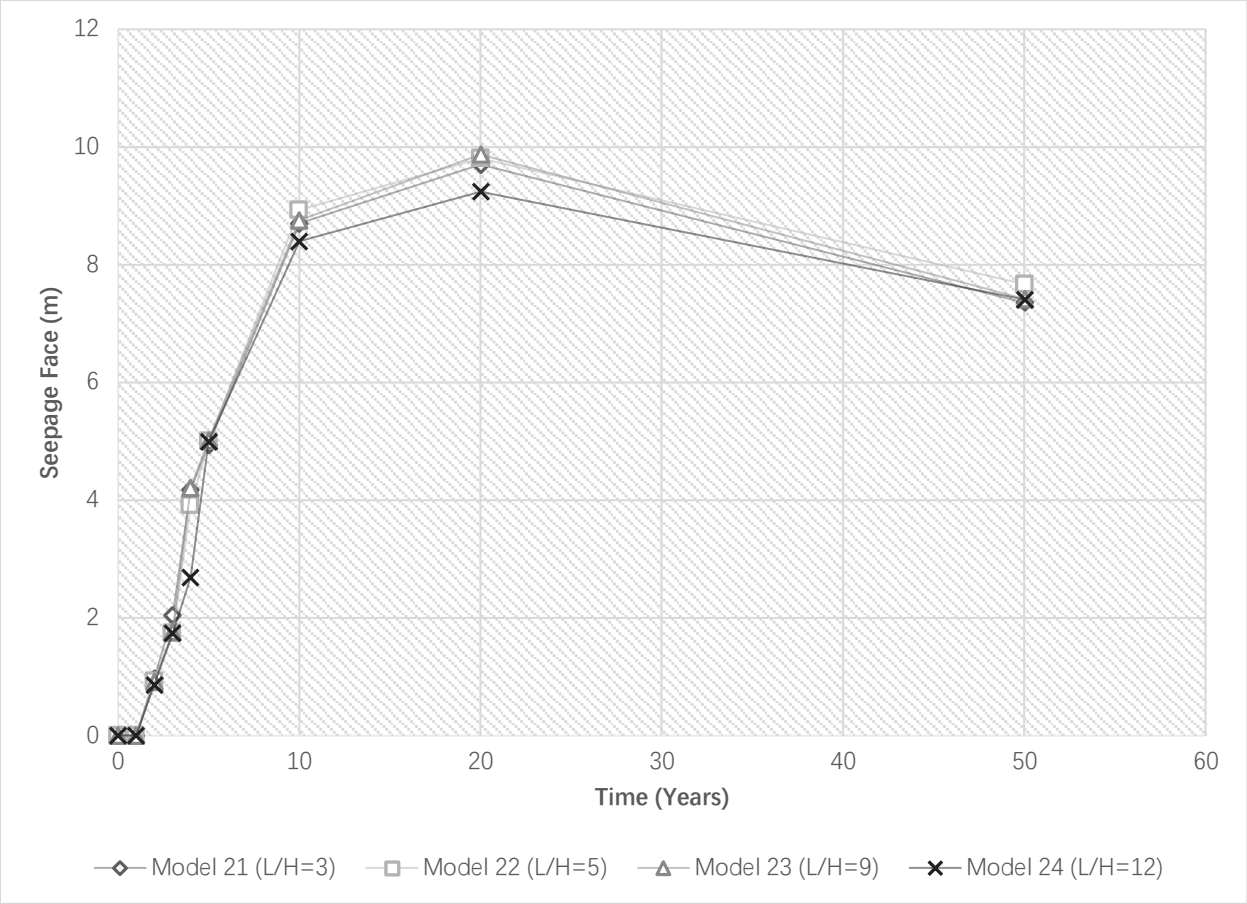

Figure 4.19: Seepage face breakout convergence results for Model 21 - 24 with Anisotropy Set 1, dam raising at rate of 10m/year.

The set of curves, obtained for the raising rate of 10m/year, resemble the 5m/year ones (Figure 4.18), but there is a delay of one year for the seepage face breakout, which is similar to the 3:1 slope case, shown on Figure 4.16. Overall, the (L/H) ratio does not seem to affect the curves. At 50 years, the seepage face breakout is reduced from the 20-year values. In comparison, if the dam raising rate is increased to 15m/year, the long-term behaviour reaches a steady state value, as can be seen in Figure 4.20. As the dam raising rate increased from 10m/year to 15m/year, the first appearance of seepage face breakout was delayed, for this case by at least three years.

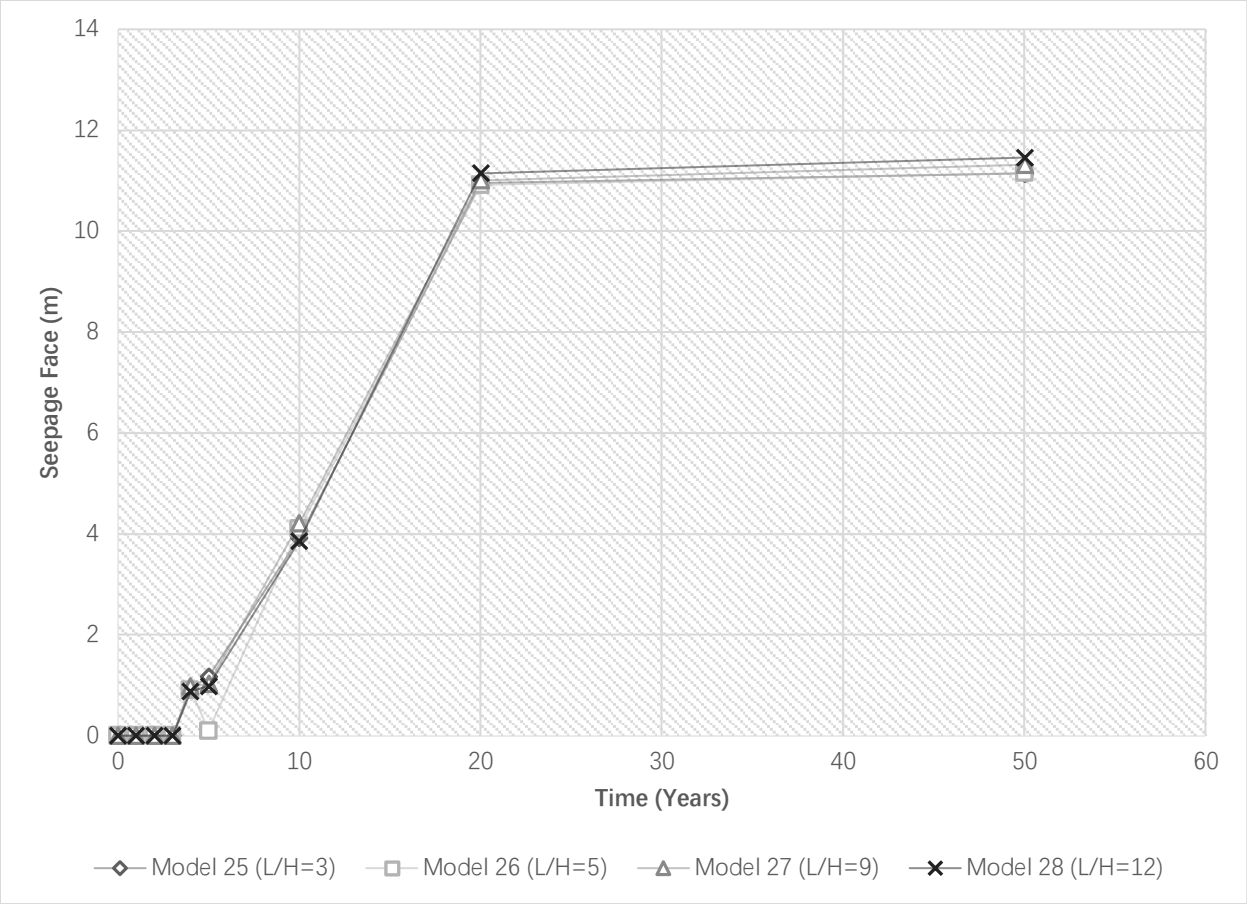

Figure 4.20: Seepage face breakout convergence results for Model 25 - 28 with Anisotropy Set 1, dam raising at rate of 15m/year.

Similar to the 3:1 slope, the dam raising rate of 20m/year resulted in a delay of appearance of seepage face breakout up to five years, followed by an almost linear increase, which did not reach steady-state values in the 50-year investigation window, as can be seen from Figure 4.21.

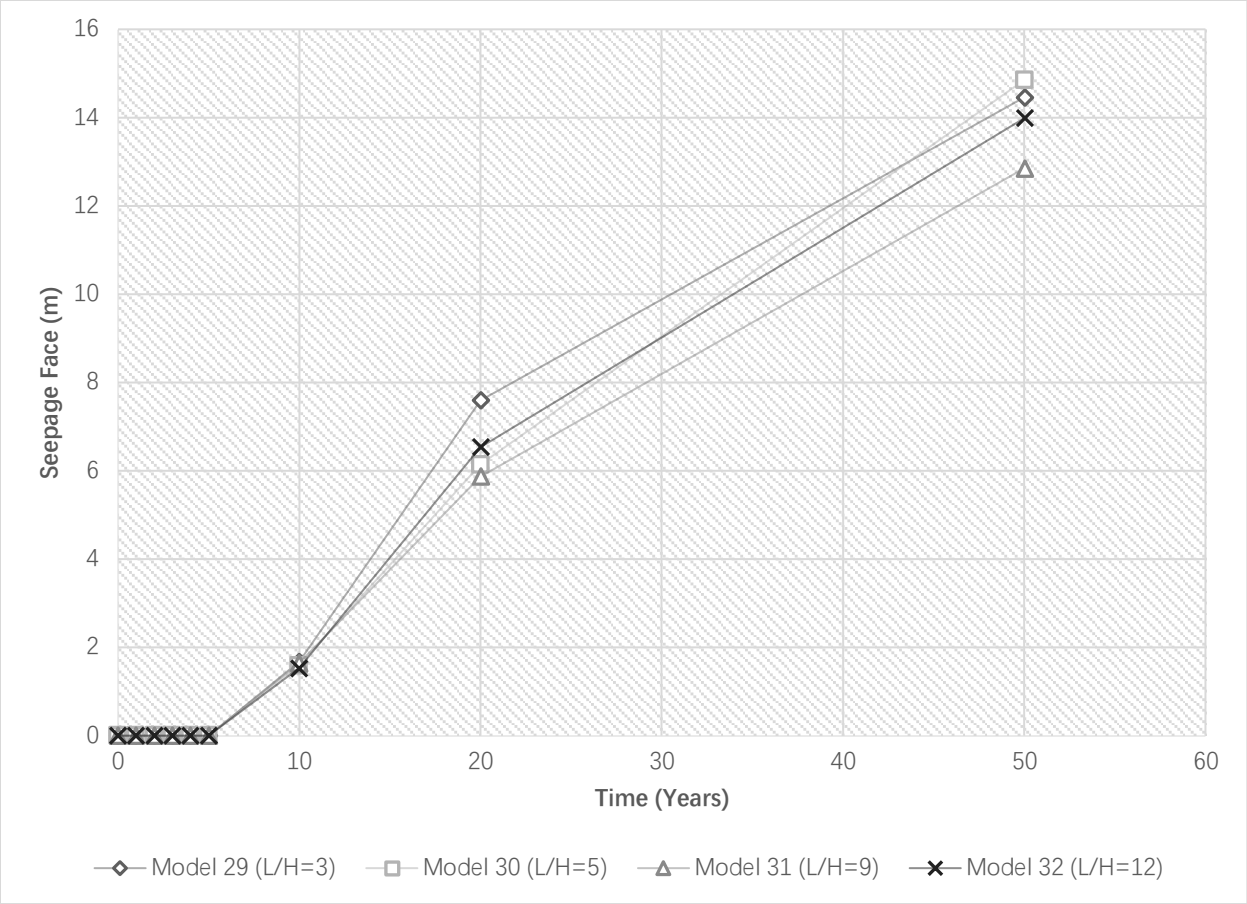

Figure 4.21: Seepage face breakout convergence results for Model 29 - 32 with Anisotropy Set 1, dam raising at rate of 20m/year.

4.4.3 Models with 3:1 Slope – Anisotropy Set 2

For the second set, the permeability anisotropy was changed to 2 for sands and 10 for slimes, respectively. Although the ratio of between sands and slimes was maintained at 5, the individual permeability between the horizontal to vertical direction was doubled (from 1 horizontal to 1 vertical for sands to 2 horizontal to 1 vertical, similarly for slimes from 5 horizontal to 1 vertical to 10 horizontal to 1 vertical). Figures 4.22 through 4.25 show the evolution of seepage face breakout for these models.

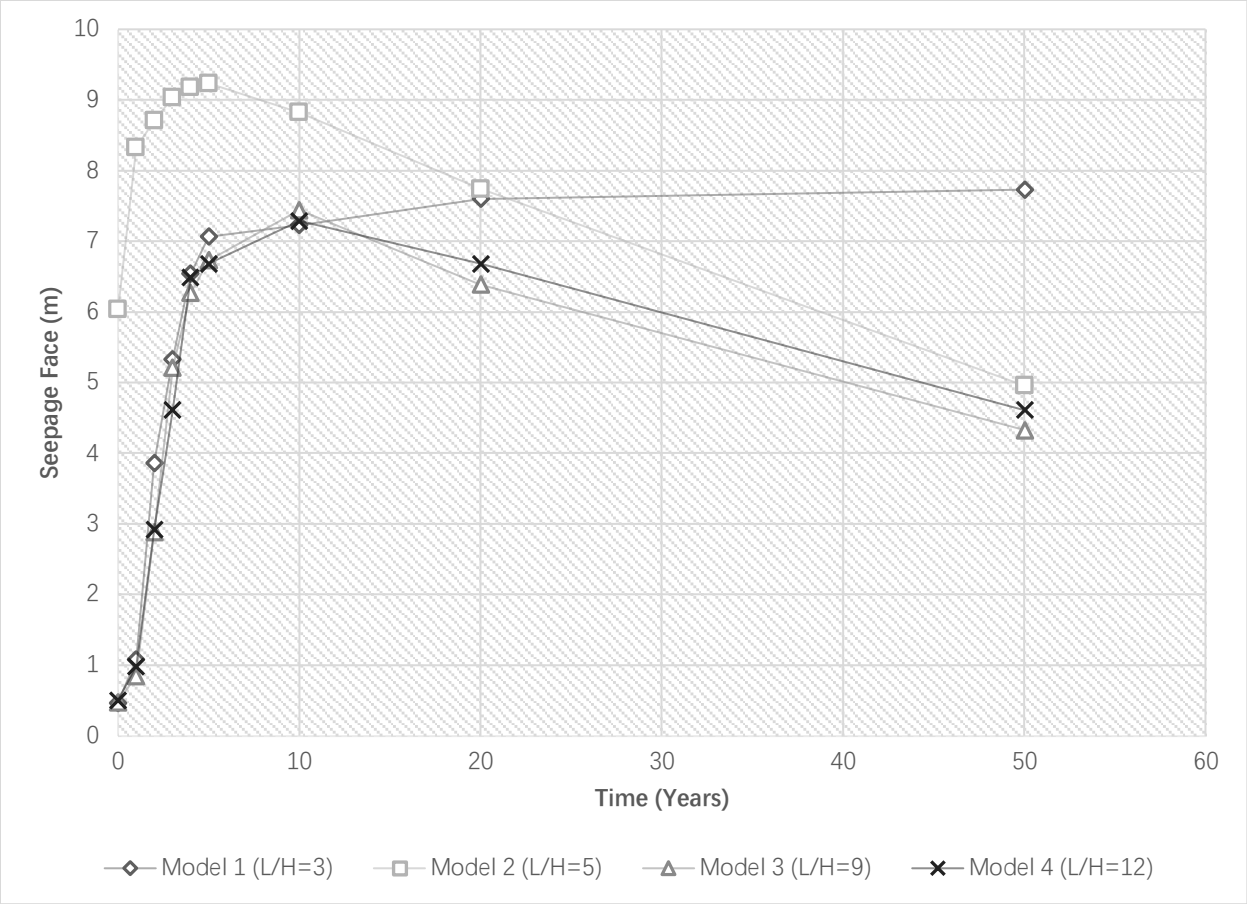

Figure 4.22: Seepage face breakout convergence results for Model 1- 4 with Anisotropy Set 2, dam raising at rate of 5m/year.

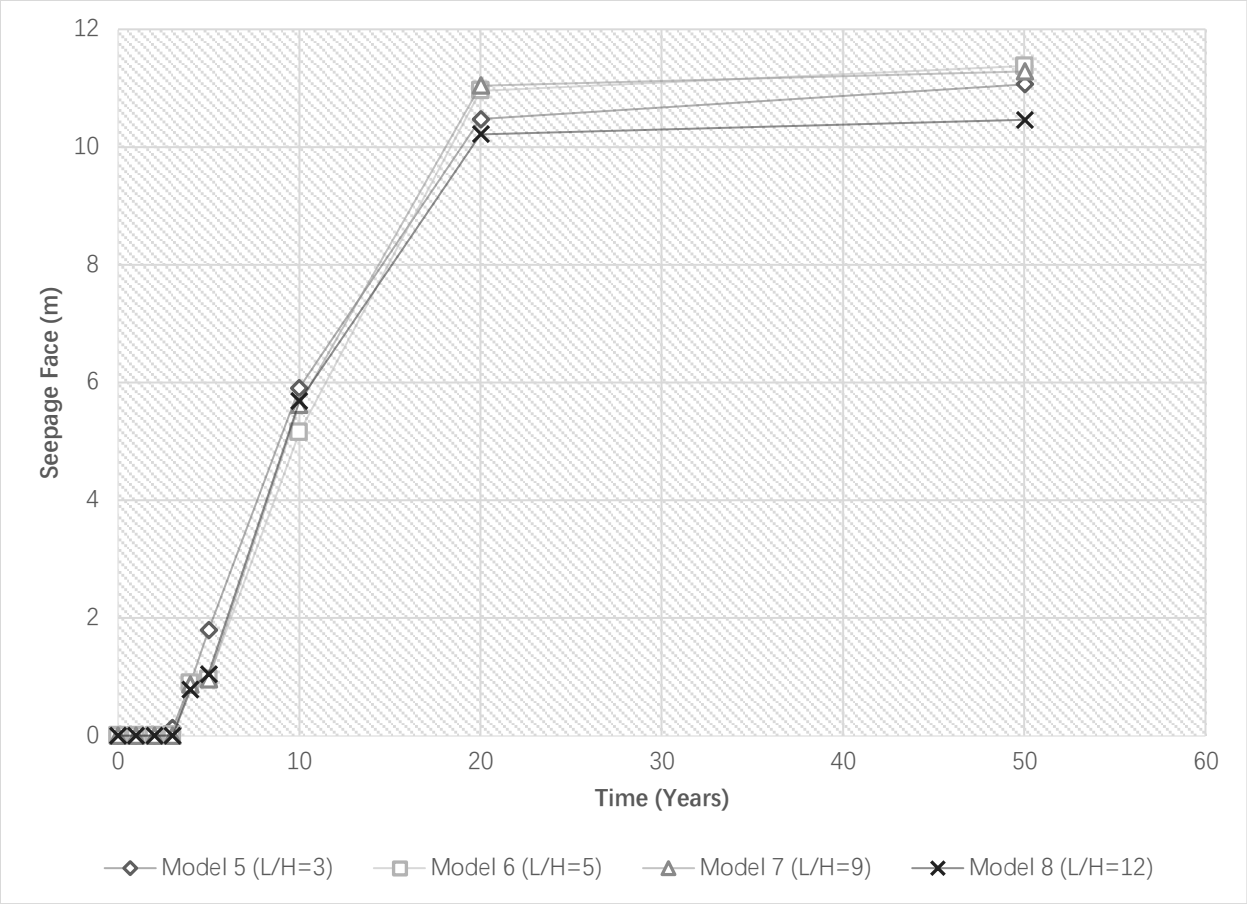

Figure 4.23: Seepage face breakout convergence results for Model 5 - 8 with Anisotropy Set 2, dam raising at rate of 10m/year.

For the 5m/year dam raise, the evolution of seepage face breakout resembles that of those in Anisotropy Set 1; there is an initial sharp increase followed by a gradual drop as time progresses (Figure 4.22). Similarly, when the raising rate increases to 10m/year, the curves do level off like for the Anisotropy Set 1 models. The first appearance of seepage face breakout is delayed to year 3.

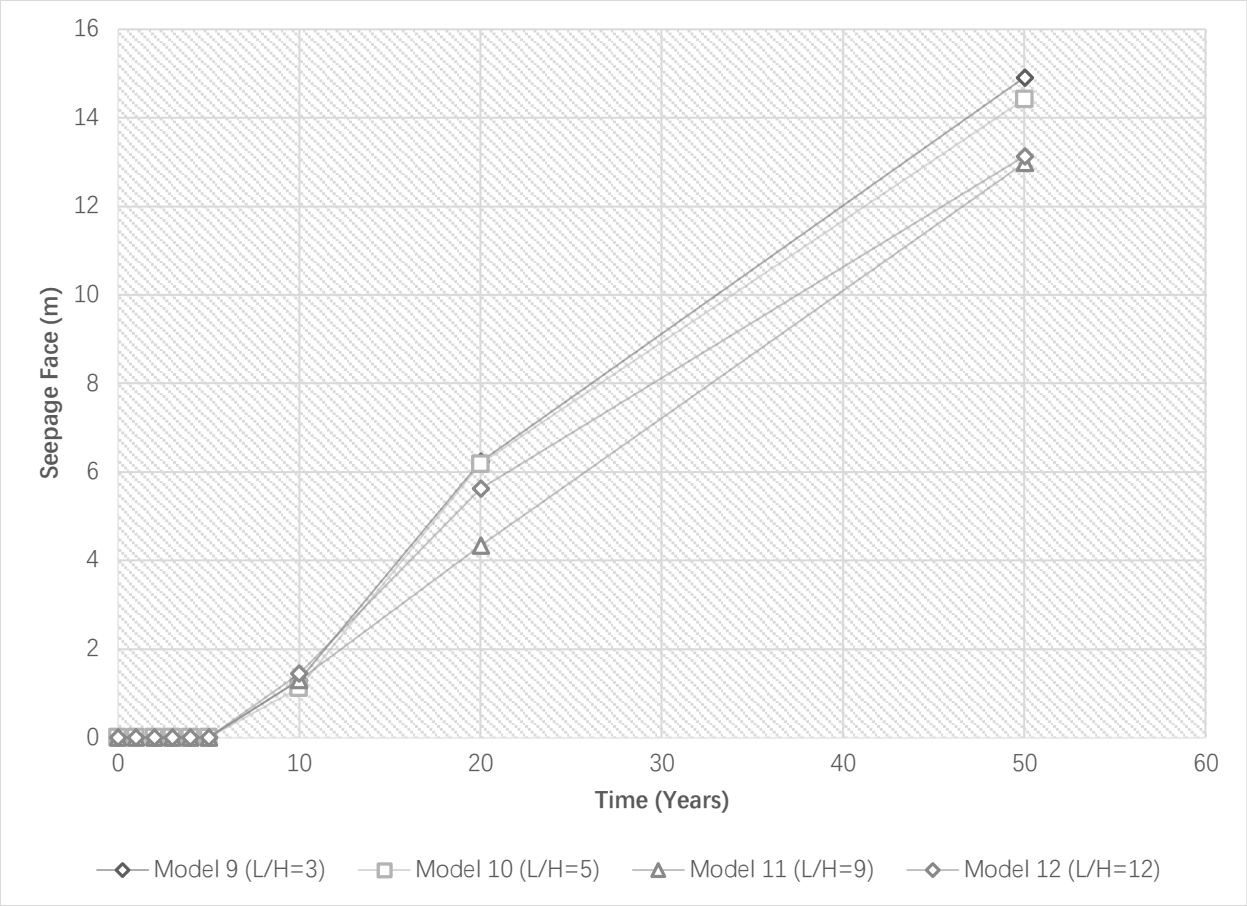

Figure 4.24: Seepage face breakout convergence results for Model 9 - 12 with Anisotropy Set 2, dam raising at rate of 15m/year.

When the dam raising rate increases to 15m/year, the seepage face breakout appears in year 5 and almost linearly increases as time progresses. The beach width (L/H) does not seem to affect the results considerably.

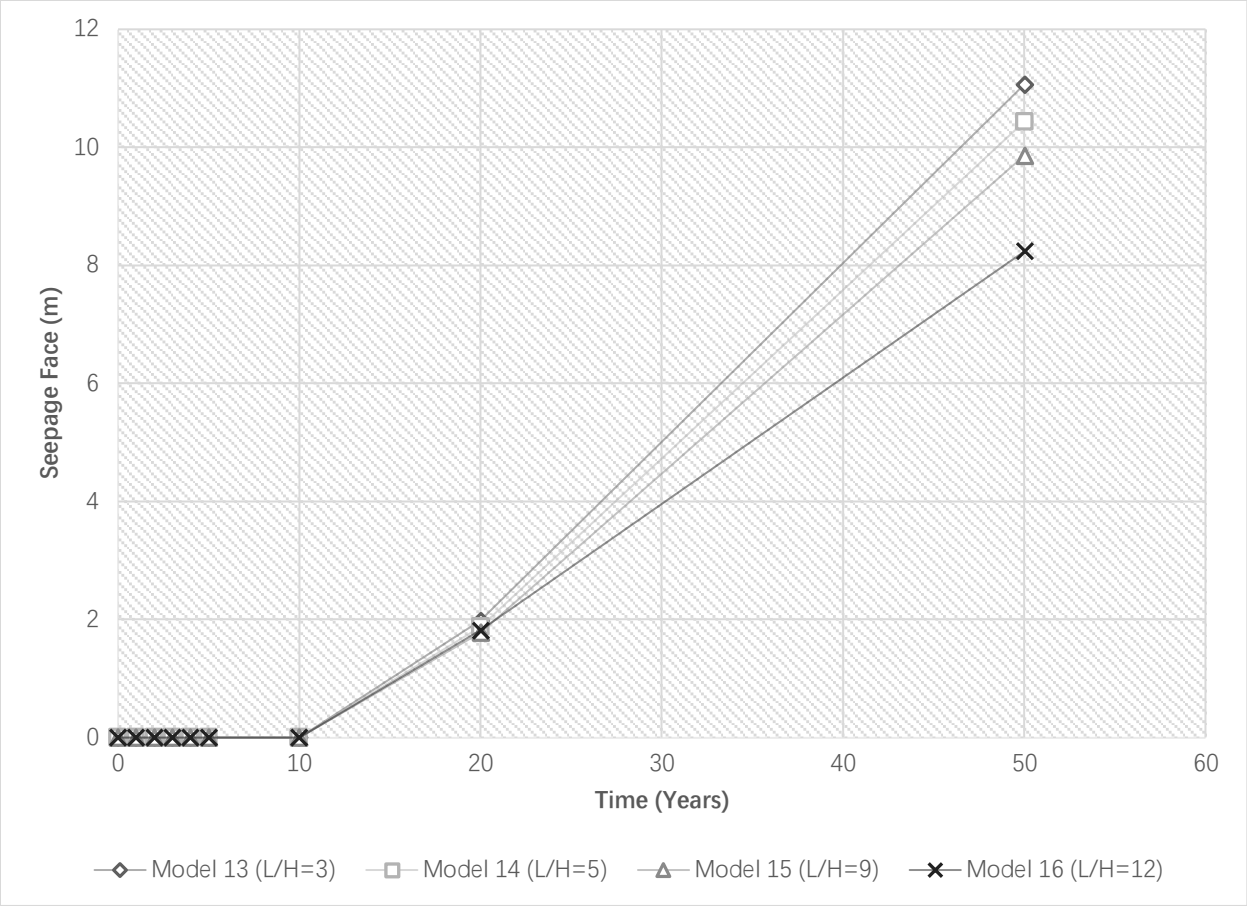

Figure 4.25: Seepage face breakout convergence results for Model 13 - 16 with Anisotropy Set 2, dam raising at rate of 20m/year.

When the dam raising rate is 20m/year, the seepage face appears only in year 10 and increases linearly as time progresses. The (L/H) ratio differentiates the seepage face breakout only in year 50, with higher values of (L/H) result in lower seepage face breakout locations, as expected.

4.4.4 Models with 2:1 Slope – Anisotropy Set 2

For steeper slopes, with Anisotropy Set 2, Figures 4.26 to 4.29 summarize the evolution of seepage face breakout with time. Even though the permeability anisotropy has changed, the same shapes

of curves were obtained. For embankment dam raising rate of 5m/year, there is a sharp increase, followed by a peak and a decline. The beach width (L/H) does not seem to differentiate the curves.

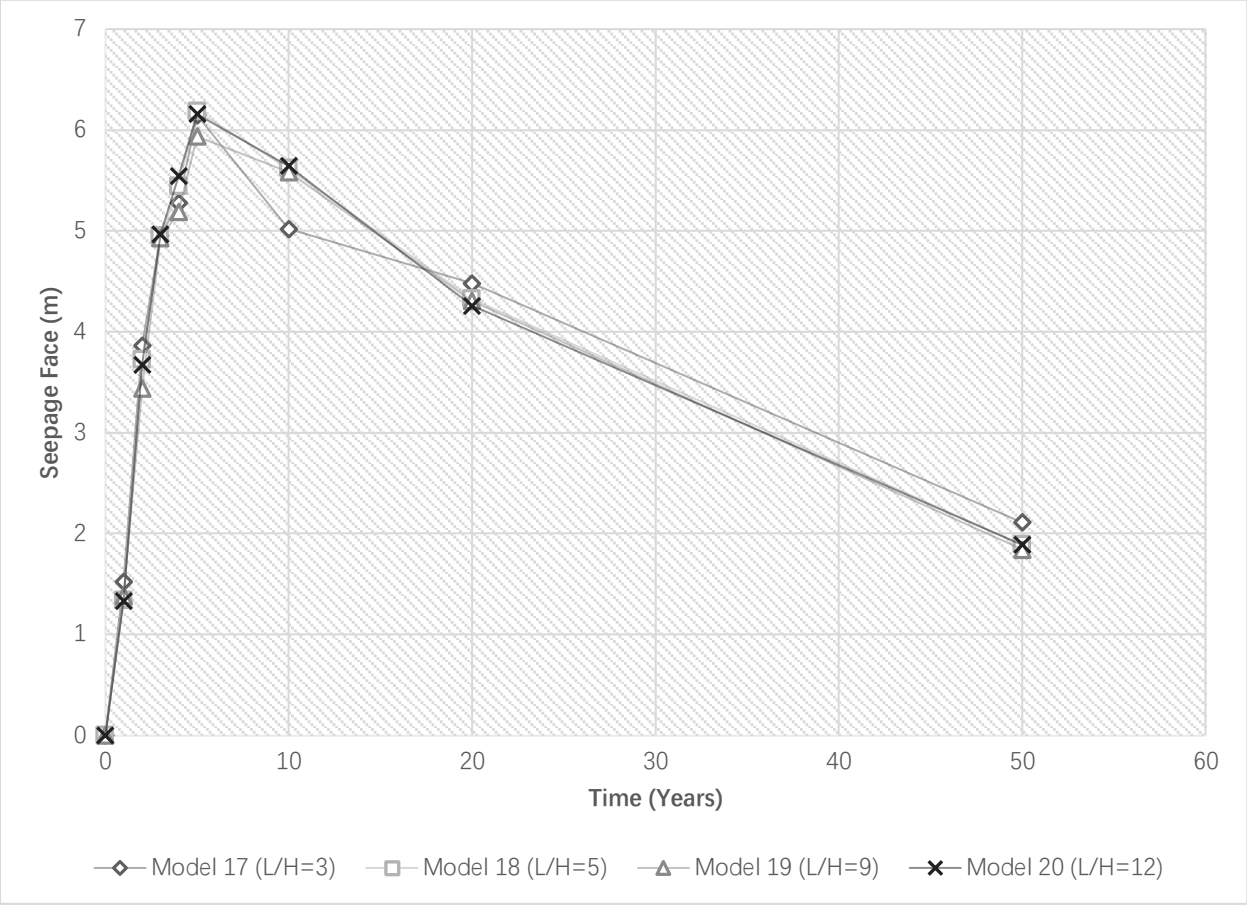

Figure 4.26: Seepage face breakout convergence results for Model 17 - 20 with Anisotropy Set 2, dam raising at rate of 5m/year.

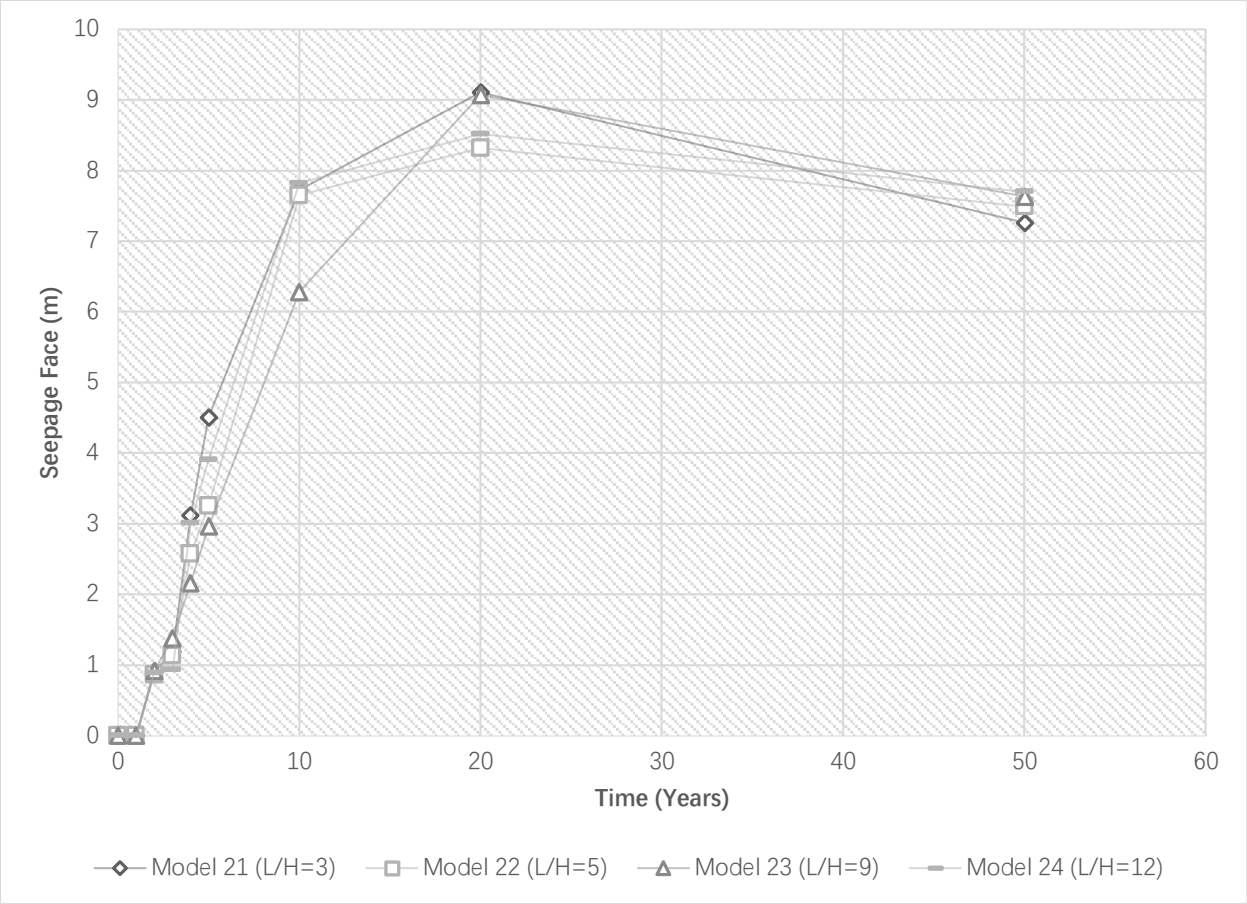

Figure 4.27: Seepage face breakout convergence results for Model 21 - 24 with Anisotropy Set 2, dam raising at rate of 10m/year.

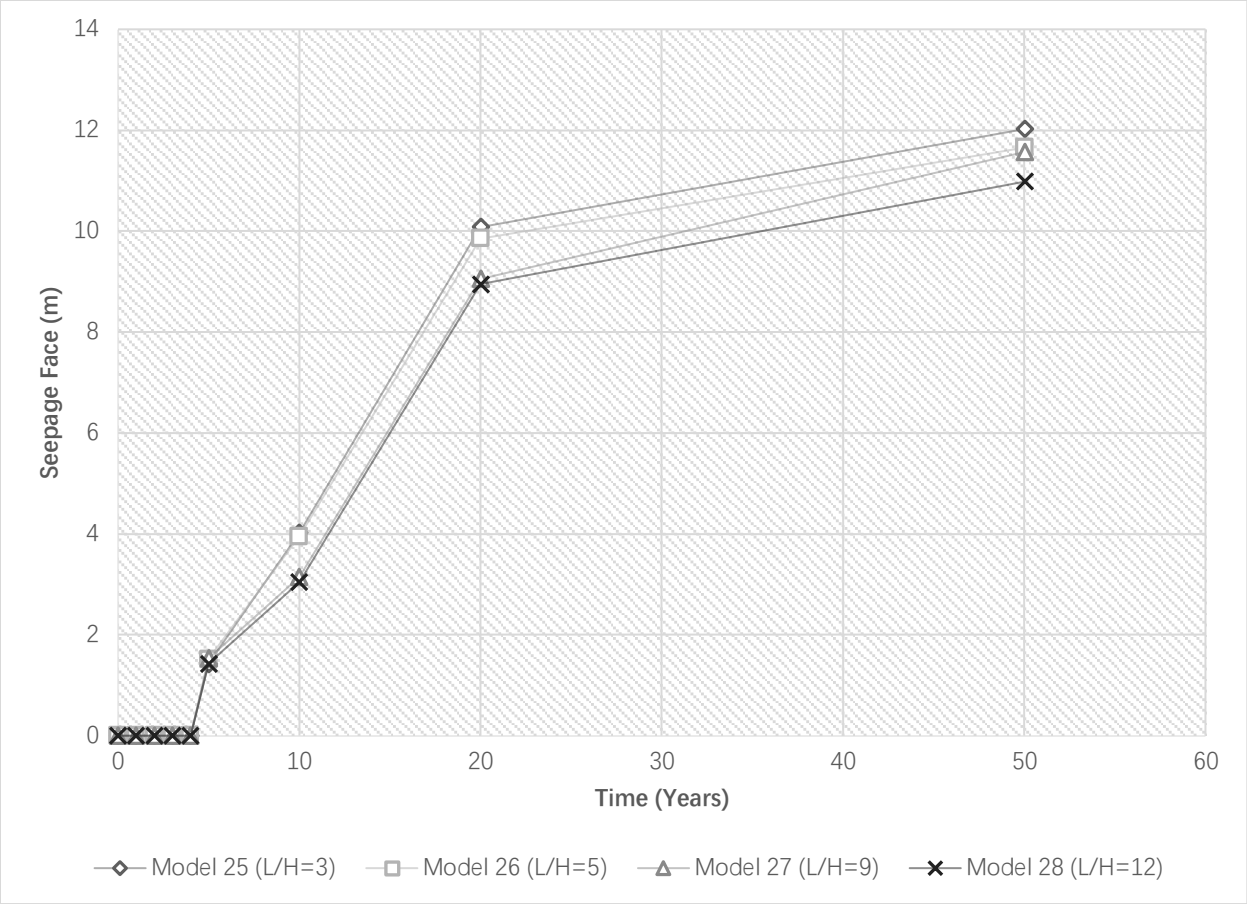

Figure 4.28: Seepage face breakout convergence results for Model 25 - 28 with Anisotropy Set 2, dam raising at rate of 15m/year.

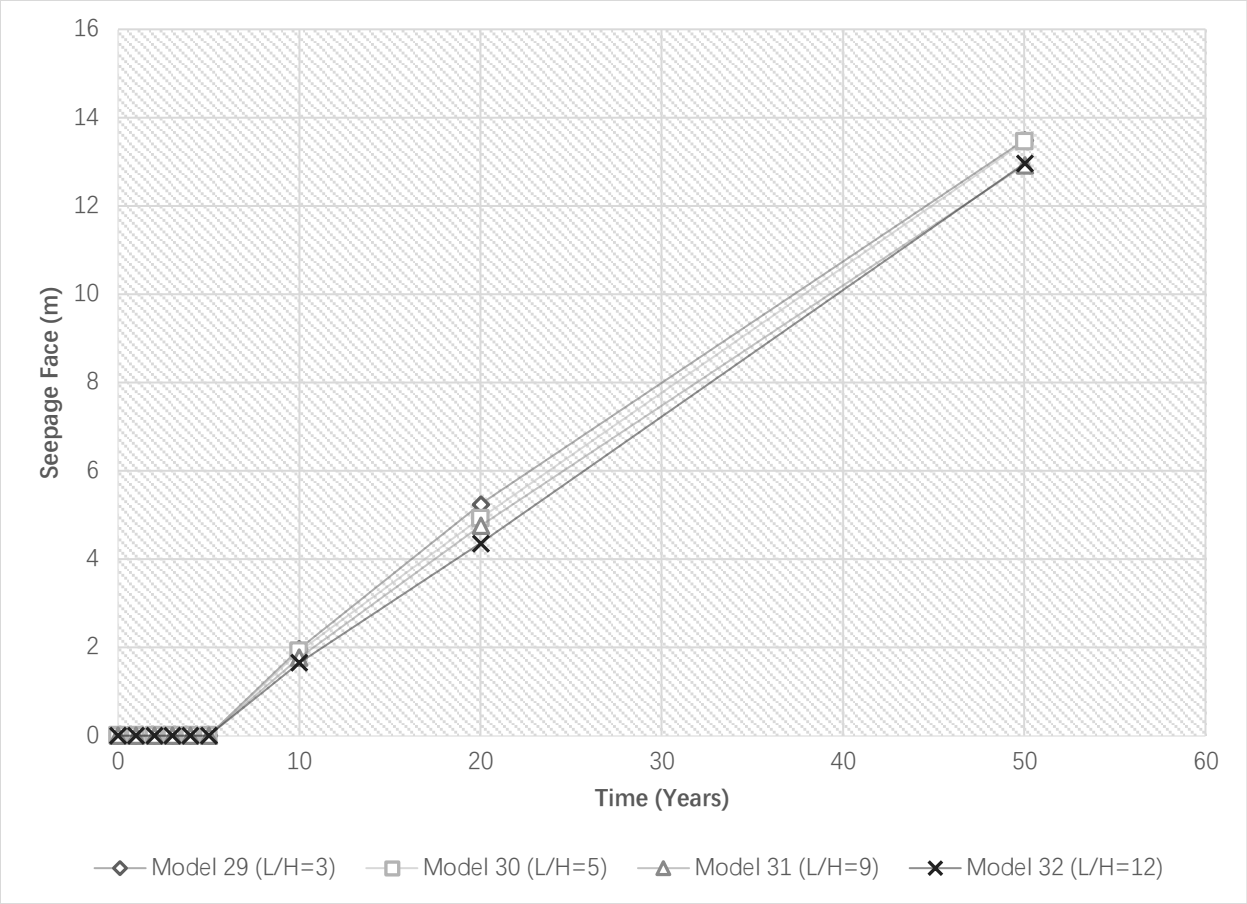

Figure 4.29: Seepage face breakout convergence results for Model 29 - 32 with Anisotropy Set 2, dam raising at rate of 20m/year.

As the embankment raising rate increases to 10m/year, the seepage face breakout is delayed by a year. The curves peak then drop down, similar to previous cases. While for rates of 10m/year and 20m/year the delay of seepage face breakout is 4 and 5 years, respectively and the shape of curves is more or less linearly increasing with time.

4.4.5 Models with 3:1 Slope – Anisotropy Set 3

When the permeability anisotropy increased to 5 for sands and 10 for slimes, the ratio of the two actually decreased from 5 (2:10 in Set 2) to 2 (5:10 in this set). However, the horizontal to vertical ratios have more than doubled for both sands and slimes.

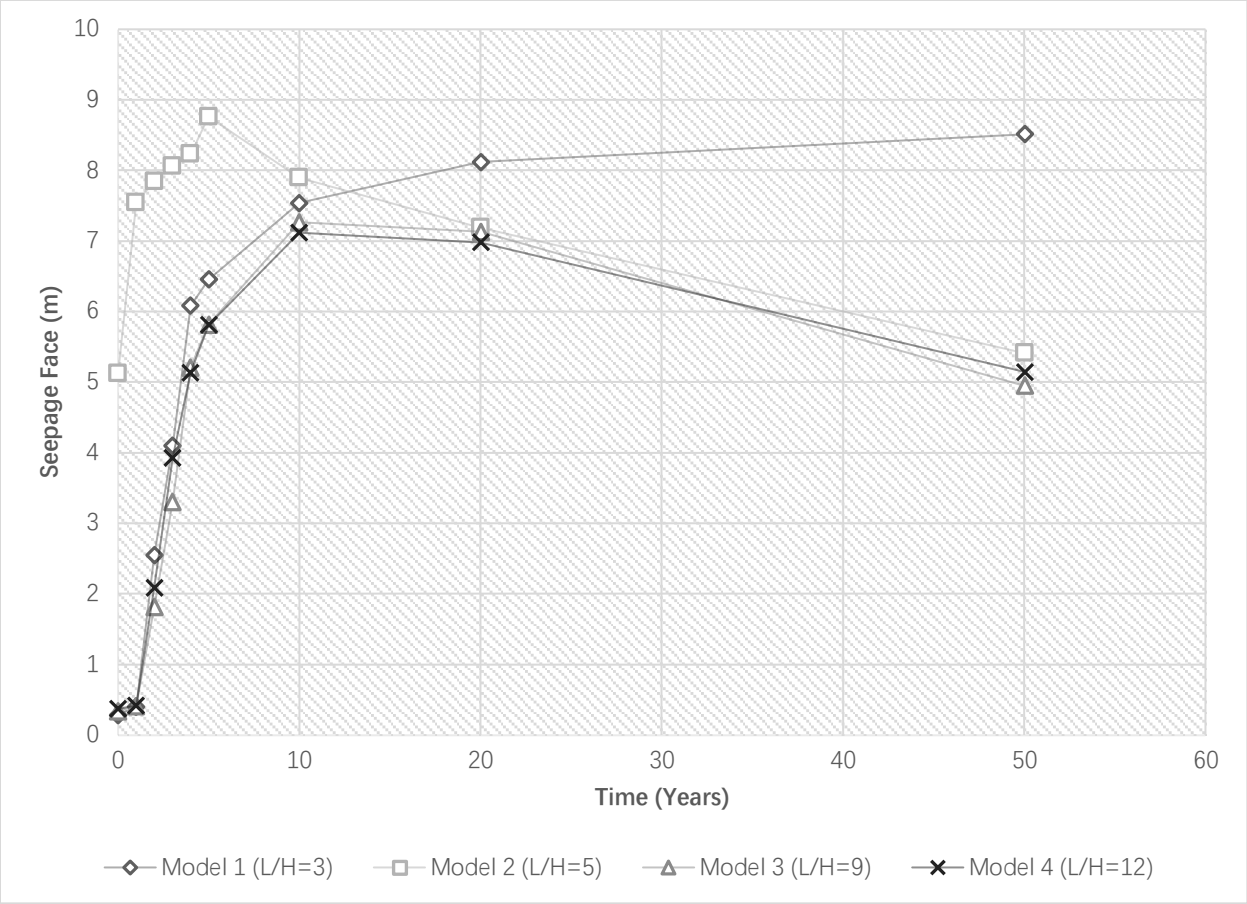

Figure 4.30: Seepage face breakout convergence results for Model 1 - 4 with Anisotropy Set 3, dam raising at rate of 5m/year.

As can be seen in Figures 4.30 to 4.33, curve shapes like before were obtained in the analysis. A sharp increase, peak and some levelling off for the 5m/year raising rate. While the 10m/year ones

have a 3-year delay, followed by a linear increase that eventually level off and reach steady-state at 50 years. Higher embankment raising rates (15 and 20m/year) result in even longer delays (5 and 10 years, respectively) and an almost linear increase with time and no steady-state in 50 years.

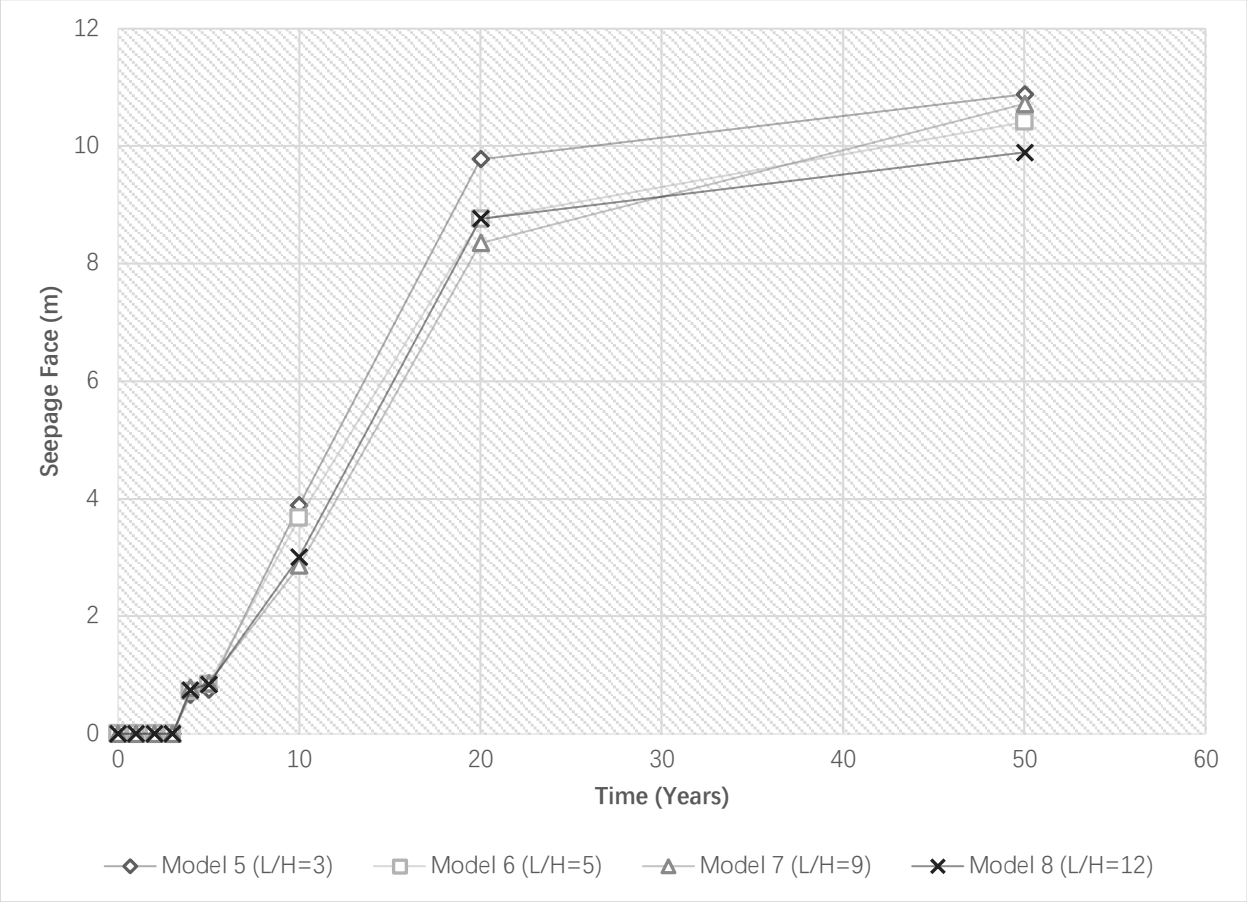

Figure 4.31: Seepage face breakout convergence results for Model 5 - 8 with Anisotropy Set 3, dam raising at rate of 10m/year.

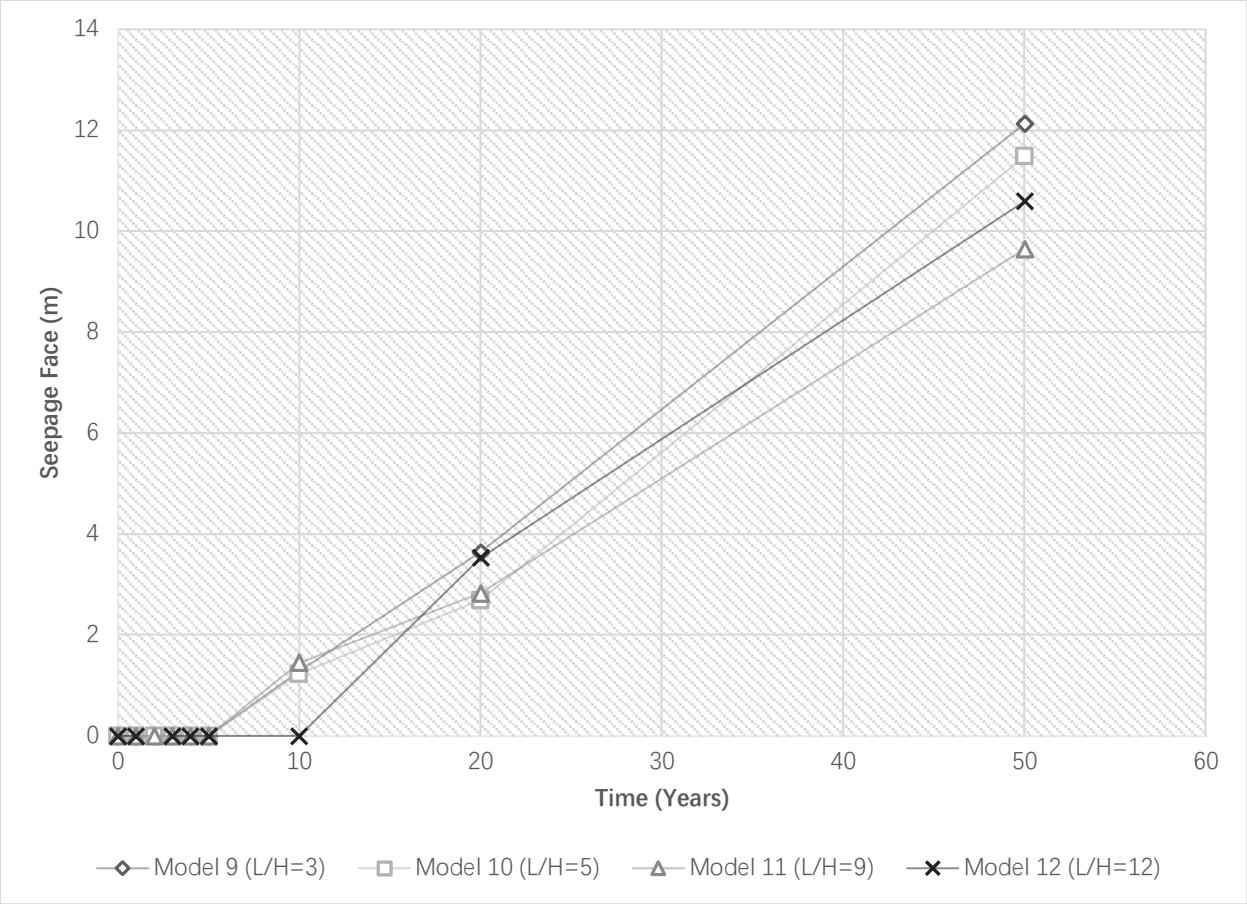

Figure 4.32: Seepage face breakout convergence results for Model 9 - 12 with Anisotropy Set 3, dam raising at rate of 15m/year.

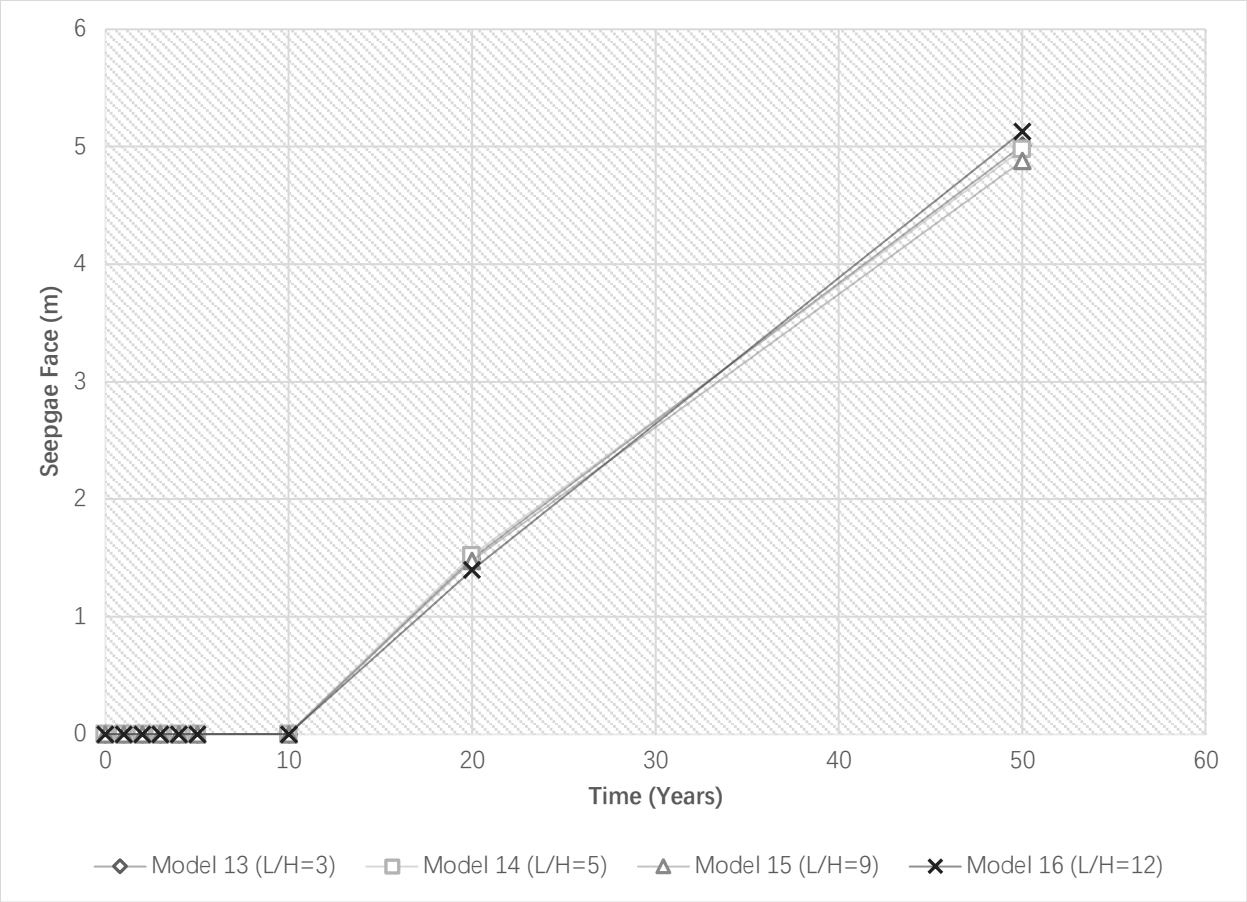

Figure 4.33: Seepage face breakout convergence results for Model 13 - 16 with Anisotropy Set 3, dam raising at rate of 20m/year.

4.4.6 Models with 2:1 Slope – Anisotropy Set 3

For models with steeper slopes, the increased anisotropy resulted in the set of curves shown in Figures 4.34 through 4.37. For the embankment raising rate of 5m/year, all curves peak at about 10 years and then drop off. The (L/H) ratio does seem to affect the seepage face breakout location, but by not much. For the 10m/year raise rate, the seepage face breakout appears at year 2, increases and becomes steady-state by year 20. However, for rates 15 and 20m/year, the seepage face breaks out in years 5 and 10, respectively. Similar to all other models for this type, the seepage face breakout never reaches steady-state in the span of 50 years.

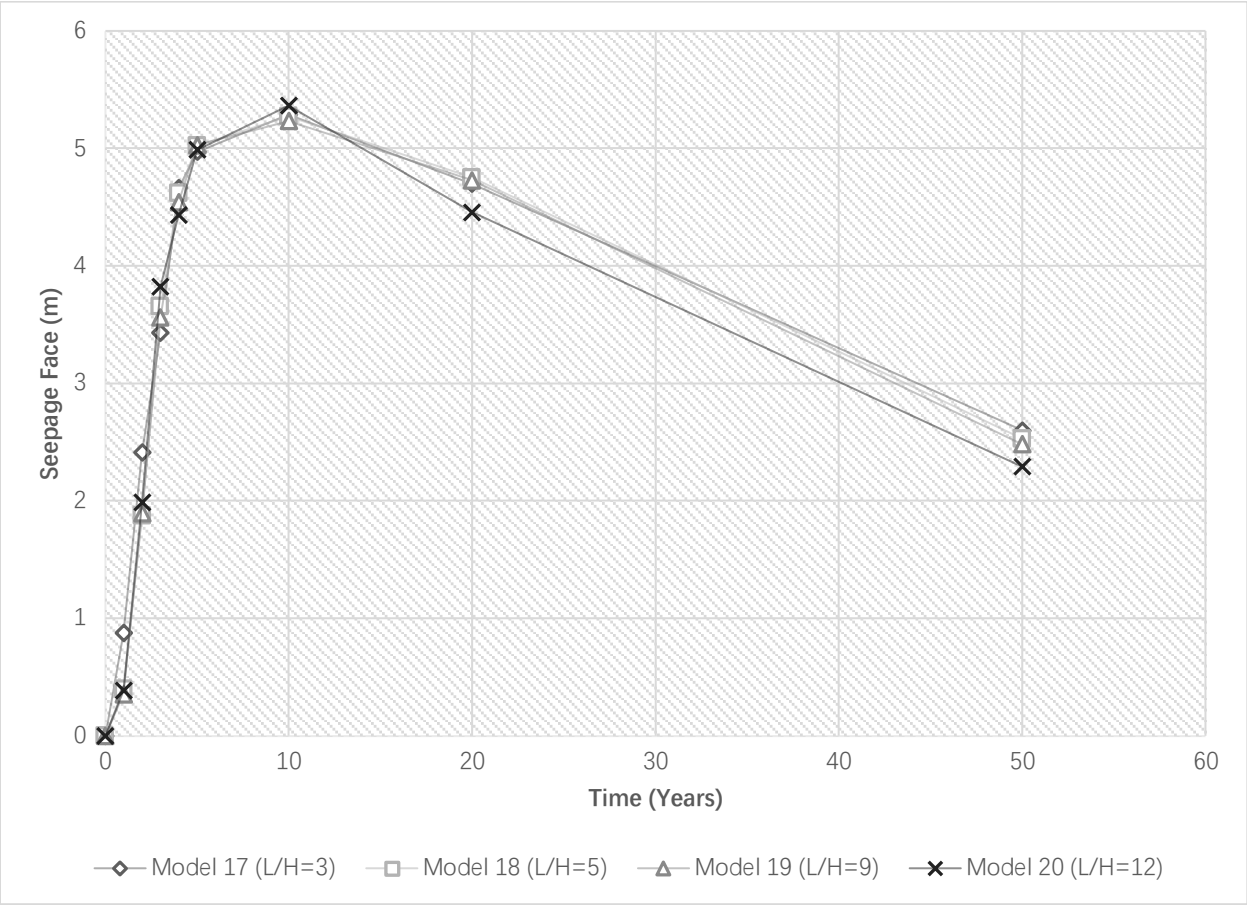

Figure 4.34: Seepage face breakout convergence results for Model 17 - 20 with Anisotropy Set 3, dam raising at rate of 5m/year.

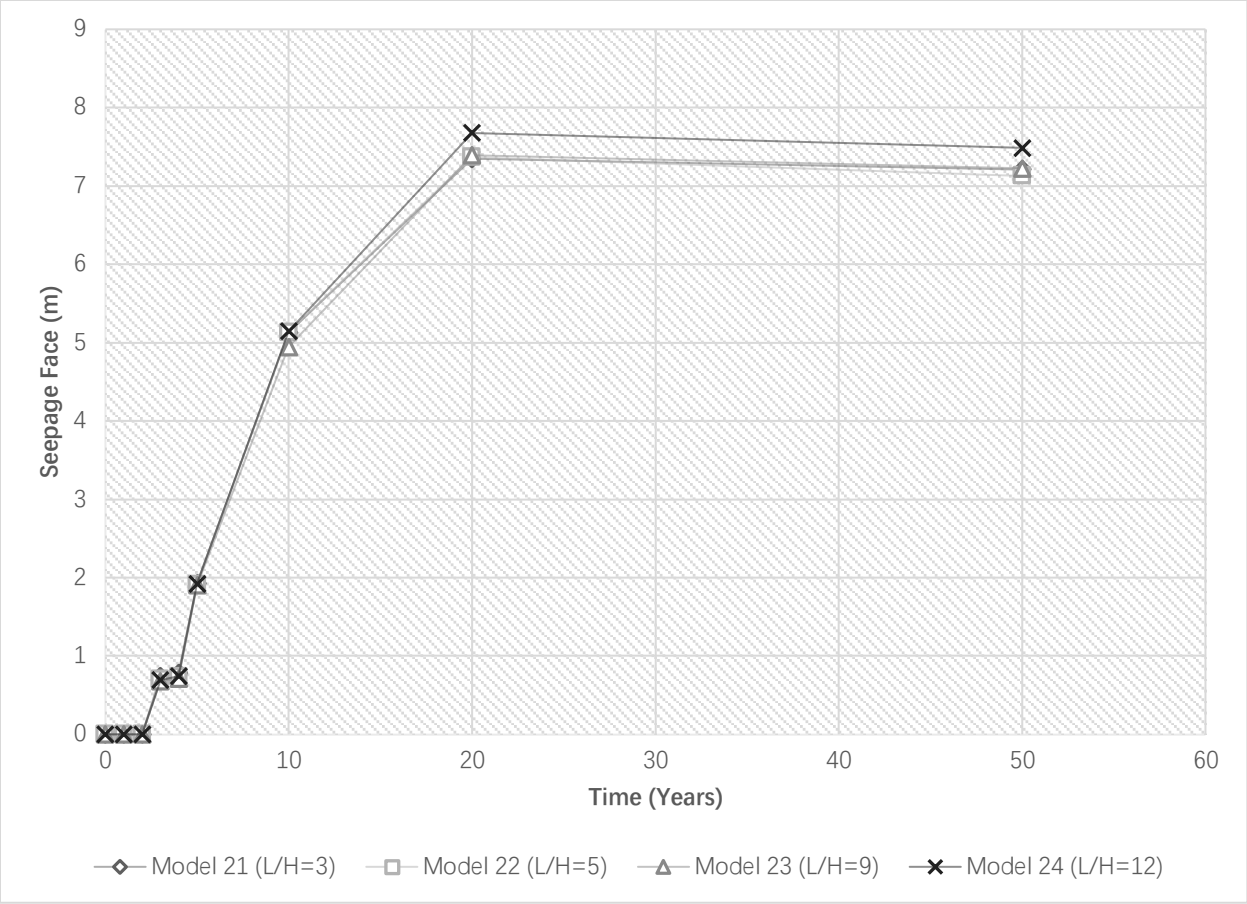

Figure 4.35: Seepage face breakout convergence results for Model 21 - 24 with Anisotropy Set 3, dam raising at rate of 10m/year.

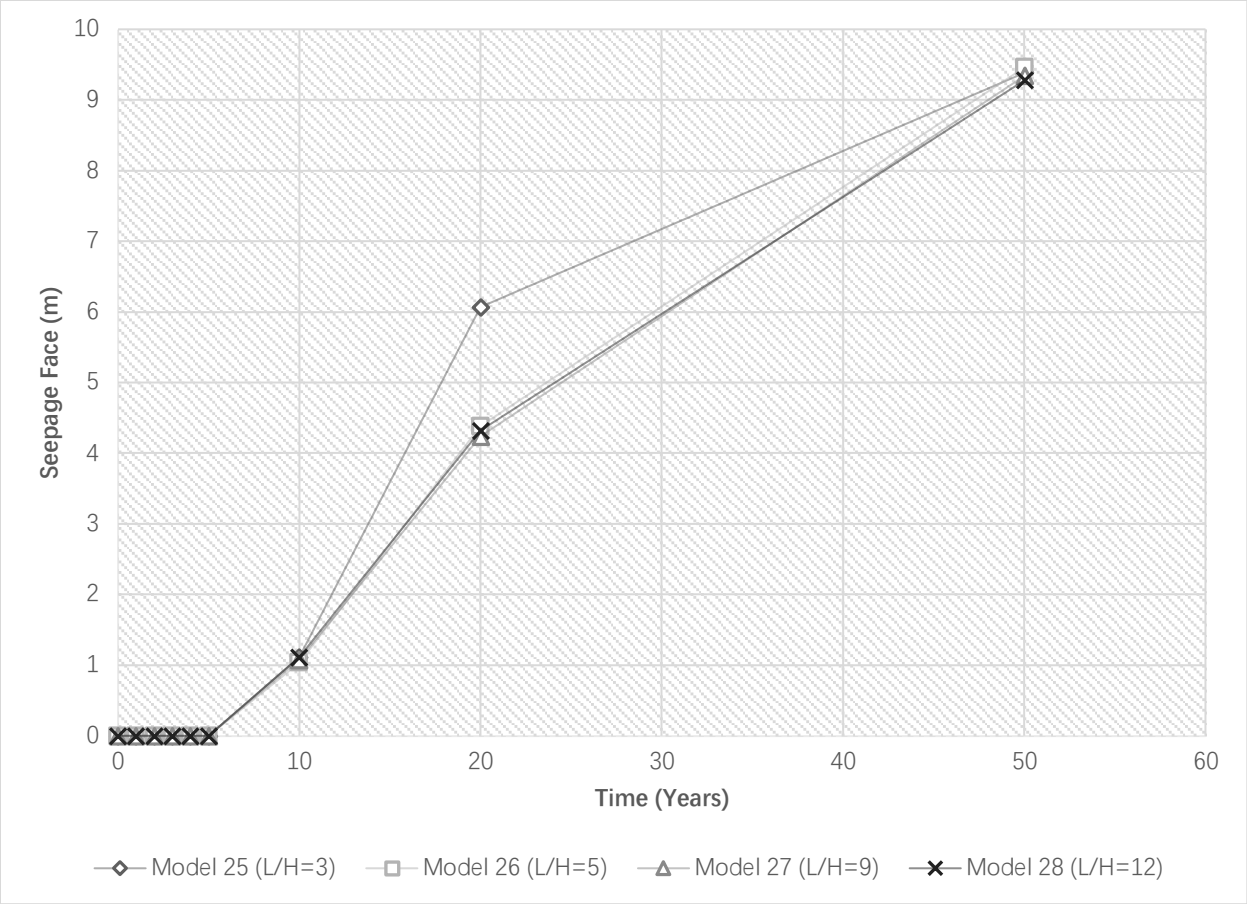

Figure 4.36: Seepage face breakout convergence results for Model 25 - 28 with Anisotropy Set 3, dam raising at rate of 15m/year.

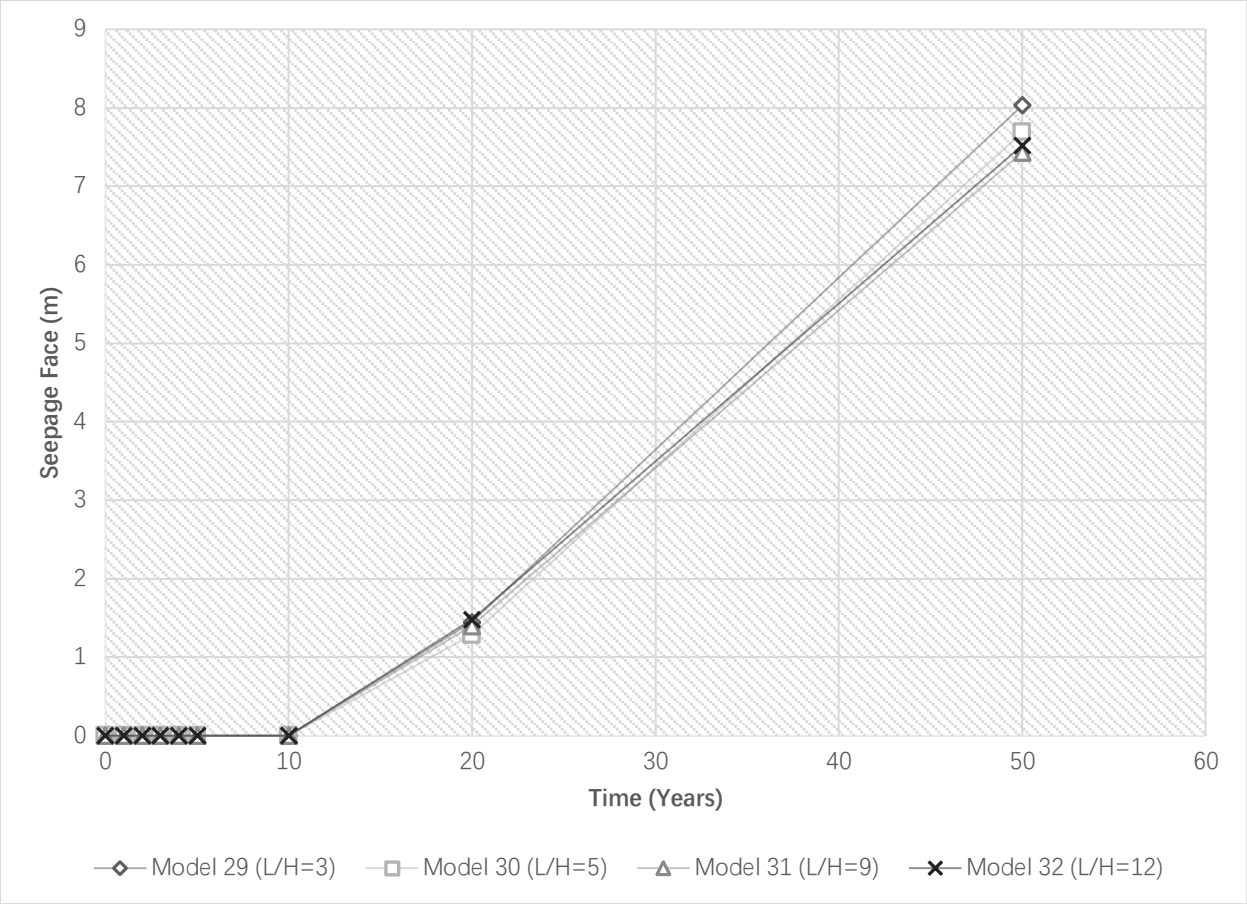

Figure 4.37: Seepage face breakout convergence results for Model 29 - 32 with Anisotropy Set 3, dam raising at rate of 20m/year.

4.4.7 Observations Based on Model Results

The preceding subsections have presented the results of analysis for models without underdrain. Although all curves of seepage face evolution were shown, it is quite difficult to draw conclusions based on individual figures. Thus, the purpose of the next subsections is to look at individual parameters, evaluate their effect on the appearance of seepage face breakouts and draw conclusions.

4.4.7.1 First Time Appearance of Seepage Face Breakout

The appearance of water breaking out on the downstream slope can signal a serious condition that can result in slope instability and collapse of an embankment dam. For dams with no underdrains or underdrains that became clogged, it is particularly important to know when the seepage is expected to break out on the slope face. The higher it breaks out, the more the downstream shell of an embankment dam is saturated, resulting in the reduction of the soil's shear strength. In the current study, the time of first appearance of seepage face breakout will be taken as the year (for which data is available) before the first non-zero value was obtained. Although this perhaps predicts the appearance of seepage face breakout earlier than it actually occurs, it has to be appreciated that the true value falls somewhere between the chosen year and the next year where non-zero computed results are available. Thus, it presents a conservative estimate. Tables 4.4 to 4.6 summarize the appearance of seepage face breakout for each model.

Model Set I – Anisotropy Set 1				
Slope inclination	3 horizontal: 1 vertical			
Crest	6.1m (20ft)			
Embankment raising rate (m/year)	Beach width (L/H)			
	3	5	9	12
5	0	0	0	0
10	2	2	2	2
15	5	5	5	5
20	10	10	10	10

Table 4.4 (a) First appearance of seepage face breakout of Model Set I - Anisotropy Set 1, note values in the table are in years.

Model Set II – Anisotropy Set 1				
Slope inclination	2 horizontal: 1vertical			
Crest	6.1m (20ft)			
Embankment raising rate (m/year)	Beach width (L/H)			
	3	5	9	12
5	0	0	0	0
10	1	1	1	1
15	3	3	3	3
20	5	5	5	5

Table 4.4 (b) First appearance of seepage face breakout of Model Set II - Anisotropy Set 1, note values in the table are in years.

Model Set I – Anisotropy Set 2				
Slope inclination	3 horizontal: 1 vertical			
Crest	6.1m (20ft)			
Embankment raising rate (m/year)	Beach width (L/H)			
	3	5	9	12
5	0	0	0	0
10	2	2	2	2
15	5	5	5	5
20	10	10	10	10

Table 4.5 (a) First appearance of seepage face breakout of Model Set I - Anisotropy Set 2, note values in the table are in years.

Model Set II – Anisotropy Set 2				
Slope inclination	2 horizontal: 1vertical			
Crest	6.1m (20ft)			
Embankment raising rate (m/year)	Beach width (L/H)			
	3	5	9	12
5	0	0	0	0
10	1	1	1	1
15	4	4	4	4
20	5	5	5	5

Table 4.5 (b) First appearance of seepage face breakout of Model Set II - Anisotropy Set 2, note values in the table are in years.

Model Set I – Anisotropy Set 3				
Slope inclination	3 horizontal: 1 vertical			
Crest	6.1m (20ft)			
Embankment raising rate (m/year)	Beach width (L/H)			
	3	5	9	12
5	0	0	0	0
10	3	3	3	3
15	5	5	5	5
20	10	10	10	10

Table 4.6 (a) First appearance of seepage face breakout of Model Set I - Anisotropy Set 3, note values in the table are in years.

Model Set II – Anisotropy Set 3				
Slope inclination	2 horizontal: 1vertical			
Crest	6.1m (20ft)			
Embankment raising rate (m/year)	Beach width (L/H)			
	3	5	9	12
5	0	0	0	0
10	2	2	2	2
15	5	5	5	5
20	10	10	10	10

Table 4.6 (b) First appearance of seepage face breakout of Model Set II - Anisotropy Set 3, note values in the table are in years.

Based on the tables, the following observations can be made:

1. It appears that the beach width (L/H) has no effect on the first appearance of seepage face breakout. For a given embankment raising rate, all models with the same (L/H), for a specified anisotropy set, resulted in the same values, as read across the rows.
2. The embankment raising rate has a considerable influence on the seepage face appearance; higher raising rates delay the seepage breakout. For almost all models there is a sharp increase (doubling of values) between rates of 15 and 20m/year. This can be attributed to the increasing volume of tailings and water to be retained, and to the non-linear increase in volume of embankment that the water has to flow through for each raise. Please see Figure 2.5, illustrating that the volume of embankment grows as the area of a trapezoid.
3. The permeability anisotropy does not seem to affect the first appearance of seepage face, since across the three sets' values (years) show very little variation, if any.

4. The first anisotropy set (1:5 ratio for sands and slimes) and 2:1 slope ratio resulted in an earlier appearance of seepage face breakout for higher dam raising rates; 3 years instead of 5 years (15m/year) and 5 years instead of 10 years (20m/year). Thus, other than this case, it appears that the slope inclination does not affect the seepage breakout in any considerable way.

4.4.7.2 Maximum Height of Seepage Face Breakout

Not only the earliest time the seepage appears on a slope face, but its maximum value is important, so affected parties can prepare remedial measures, among them carrying out slope stability analysis. Thus, based on the generated dataset, it is possible to observe what parameters affect the height of seepage face breakout. However, the definition of a 'height' of seepage face breakout requires further explanation. In the analysis, the distance from the toe of the slope to the point where the phreatic surface touches the downstream slope face (the location of breakout) was measured. Also, the time (in years) was noted when this has occurred. Readily, it can be appreciated that taller the dam, potentially higher the seepage face breakout would be. Thus, all measured values were normalized by the calculated slope length (function of time because of embankment raising rate) at the time when the maximum seepage face breakout was measured.

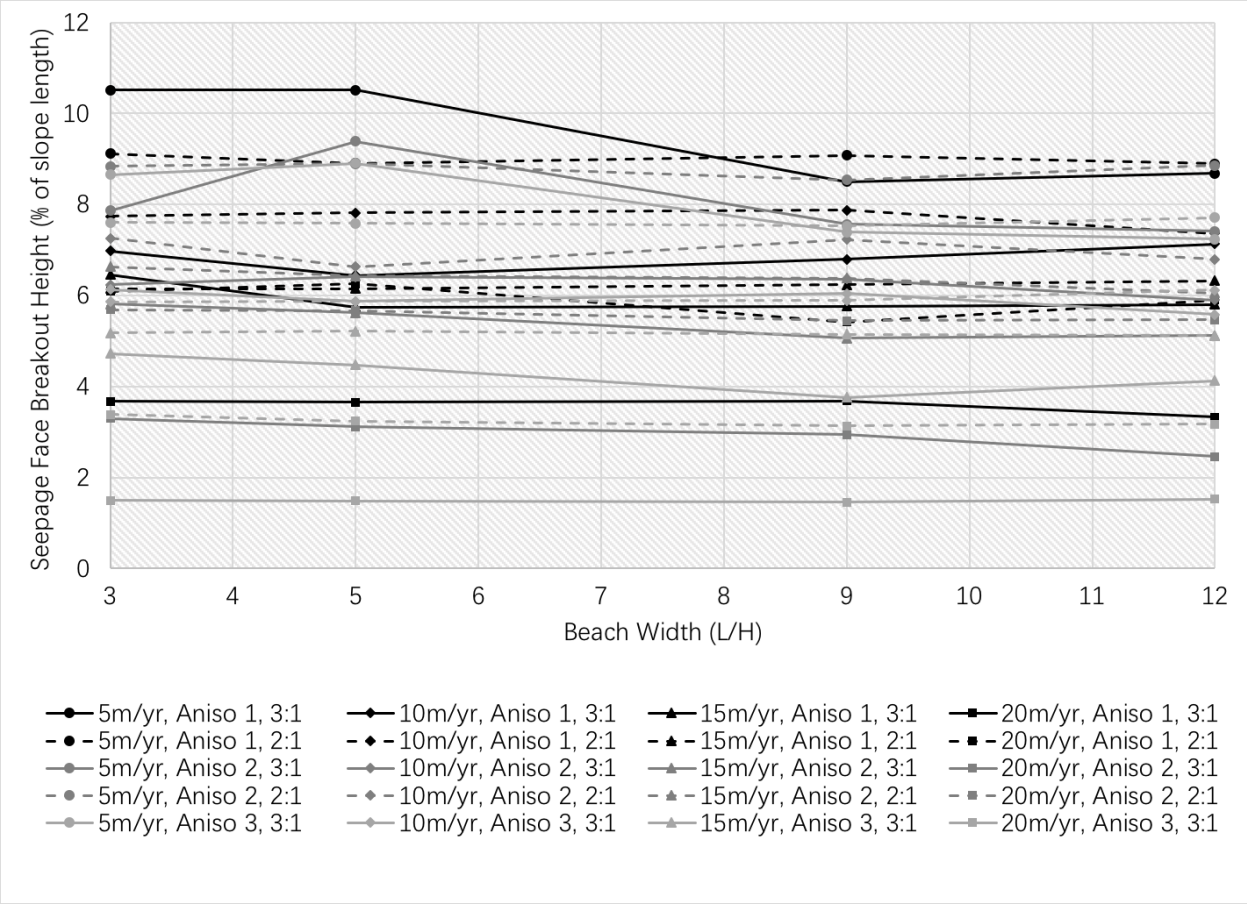

Figure 4.38: Maximum height of seepage face breakout.

Although somewhat cluttered, Figure 4.38 contains a lot of information, that otherwise plotted in separate figures might be more difficult to comprehend. What is shown is the seepage face breakout (as a percentage of slope length) as a function of beach width (L/H) for all considered cases. The figure is organized as follows; The shades denote the anisotropy set (1-black, 2-dark grey, 3-light grey), solid lines refer to 3:1 slopes, while dashed lines are for 2:1 slopes. Finally, the markers specify the embankment raising rate (circle – 5m/year, diamond – 10m/year, triangle – 15m/year, square – 20m/year).

Thus, the following observations can be made:

1. The maximum height (~10.6% of slope length) of seepage face breakout occurs for Anisotropy Set 1, for beach widths of 3 and 5 for a 3:1 slope.
2. It appears that the beach width (L/H) does not influence the maximum height of seepage face breakout to any appreciable extent, except for a few cases. The greatest variation for any given rate of raise was about +/- 20% from their average over the (L/H) range. Further discussion of this is deferred to Section 4.4.7.5.
3. The rate of embankment raising is the most influential factor affecting the height of seepage face breakout; it was found that the higher the rate of raise, the lower the height of seepage face. Thus, the relationship is inversely proportional. It will be investigated further in Section 4.4.7.6.
4. The permeability anisotropy affects the location of maximum seepage face breakout. It was observed that the highest maximum seepage face breakouts occur for Set 1 (Sand/Slimes of 1:5) and decrease for Set 2 (Sand/Slimes of 2:10) and Set 3 (Sand/Slimes of 5:10), in that order. It is understood that what is manifested is the combined effect of horizontal to vertical permeability for each material along with the ratio of anisotropies for the two materials making up the tailings storage facility.
5. The slope inclination (3:1 and 2:1) does seem to affect the maximum seepage face breakout to some extent. Gentler slopes (3:1) tend to have higher seepage face breakouts. This is due to how the seepage face breakout is measured; if a seepage face breaks out at a certain elevation above sea level, from a given dam base elevation, the distance along the slope face is longer for gentler slopes than for steeper slopes. Thus, this ‘artifact’ is acknowledged,

since it is customary (in literature) to measure the seepage face breakout along a slope face, it is not considered further, since this effect was treated by normalizing by the slope face length.

6. Although not plotted up, but the time (in years) at the maximum seepage face breakout reveals some interesting trend; the earliest maximum occurred in the same year (year 5) when mining operations ceased, while over 70 percent of cases were at the end of time span, at 50 years. Thus, while tailings are actively deposited, the seepage face breakout will not reach its maximum in most cases. This further reinforces the need for monitoring the tailings facility for a duration well beyond the active mining operation.

4.4.7.3 Height of Seepage Face Breakout at 50 Years

In conjunction with the preceding subsection, the height of seepage face breakout at 50 years is a good indicator of the state of seepage flow though the tailings embankment, particularly for long-term seepage assessment. Since the 50-year mark is often considered as a point when the tailings facility is decommissioned, it is important to know the state of the system at that point to plan for future remedial measures. Figure 4.39 summarizes the 50-year seepage face breakout heights. The same definition was adopted for 'height' of seepage face breakout as in the previous section; distance along the slope face, normalized by the slope length, expressed as a percentage.

Based on the figure, the following observations can be made:

1. The highest seepage face breakout at 50 years occurs for models with 5m/year raising rate and beach widths (L/H) of 3. The height is also affected by the permeability anisotropy; Set 1 (1:5) was the highest, followed by Set 3 (5:10) and Set 2 (2:10).

2. Beyond what was established under point 1 above, it appears that the beach width (L/H) does not influence the seepage face breakout location considerably, as can be seen from Figure 4.39, where most lines are horizontal.

3. Similar to findings of the previous section, the rate of embankment raising appears to affect the height of seepage face breakout the most. As the rate increases, the seepage face breakout height decreases. It will be investigated further in Section 4.4.7.6.

4. In contrast to the findings of Section 4.4.7.2, the permeability anisotropy has a more moderate (about 30% of what was found on Section 4.4.7.2) effect on the location of seepage face at 50 years. Nevertheless, it was observed that on average, the highest seepage face breakouts occur for Set 1 (Sand/Slimes of 1:5) and decrease for Set 2 (Sand/Slimes of 2:10) and Set 3 (Sand/Slimes of 5:10), which is the same order as in Section 4.4.7.2.

5. Similar to the preceding section, the slope inclination (3:1 and 2:1) does seem to affect the seepage face breakout at 50 years to some extent; gentler slopes (3:1) tend to have higher seepage face breakouts. It is believed that for the same reason as stated in Section 4.4.7.2.

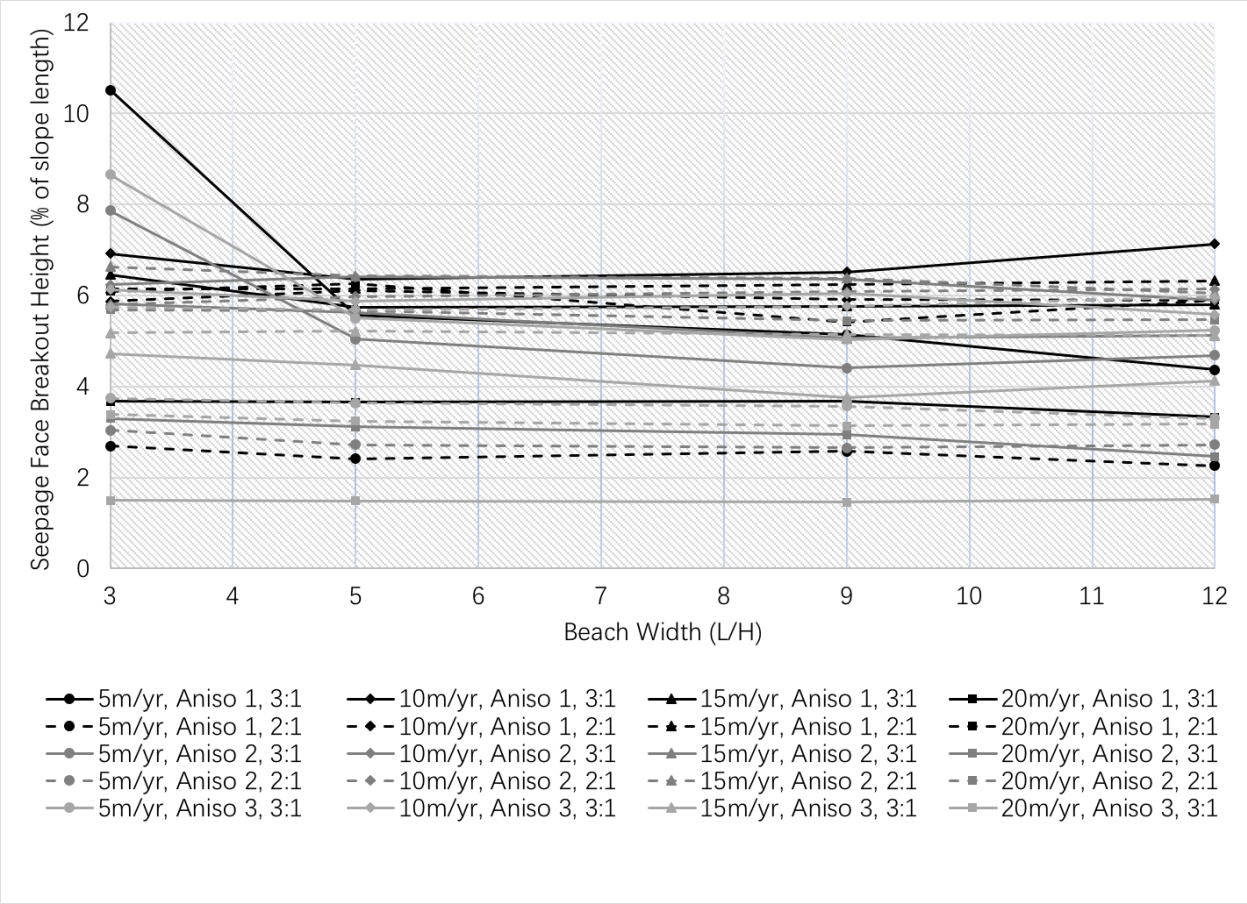

Figure 4.39: Height of seepage face breakout at year 50.

4.4.7.4 Change in the Shape of Seepage Face Height vs. Beach Width Curves

Although not anticipated at the onset of modeling, it was observed that the shape of seepage face breakout height versus beach width (L/H) curves take on characteristic forms as a function of embankment raising rate. Typical curves, selected from the dataset, are plotted up side-by-side on Figure 4.40.

From this Figure, across all slope inclinations and permeability anisotropies, the following can be observed:

1. For embankment raising rates of 5m/year, all related curves take on the same shape: initial

sharp increase, peaking relatively early, often while the embankment raising and tailings pond filling is still underway, followed by steady-state or drop in the seepage face breakout height, as years progress.

2. For the rate of 10m/year, the curves' start year shifts to the right (delayed) and the slope decreases with respect to 5m/year raising rate. At later years, the steady-state and drop are still observable.

3. For the 15m/year rate, the start delay further increases and the slope of the curve decreases. Within the 50-year window, there is no peak observed.

4. Finally, for the 20m/year rate, the first appearance of seepage face breakout is further delayed and similar to the other rates, the slope of the curves further decreases. No peak was observed in the 50-year period.

Thus, based on the four points above, it can be stated that; a.) the first appearance of seepage face breakout is delayed as the embankment raising rate increases (label a in Figure 4.40) and b.) the slope of seepage face breakout versus time curve decreases as the embankment raising rate increases (label b in Figure 4.40). The delay in the seepage face breakout is attributed to the increasing path of flow that the water has to traverse, since with the increasing raising rate, the volume of dam increases as well (area of a trapezoidal dam cross-section). Note, however that the preceding observations are based on a 50-year window addressed in the simulation, which is, as discussed earlier, quite reasonable time frame in the life of a mine and its associated tailings facility. Nevertheless, it could be that what actually observed is nothing but the same curve shape for all raising rates, but shifted to the right (delayed) with a decreasing slope (stretched out in time). However, the rest of the curve (beyond the 50-year window) is not seen. This could be further investigated in a follow-up study.

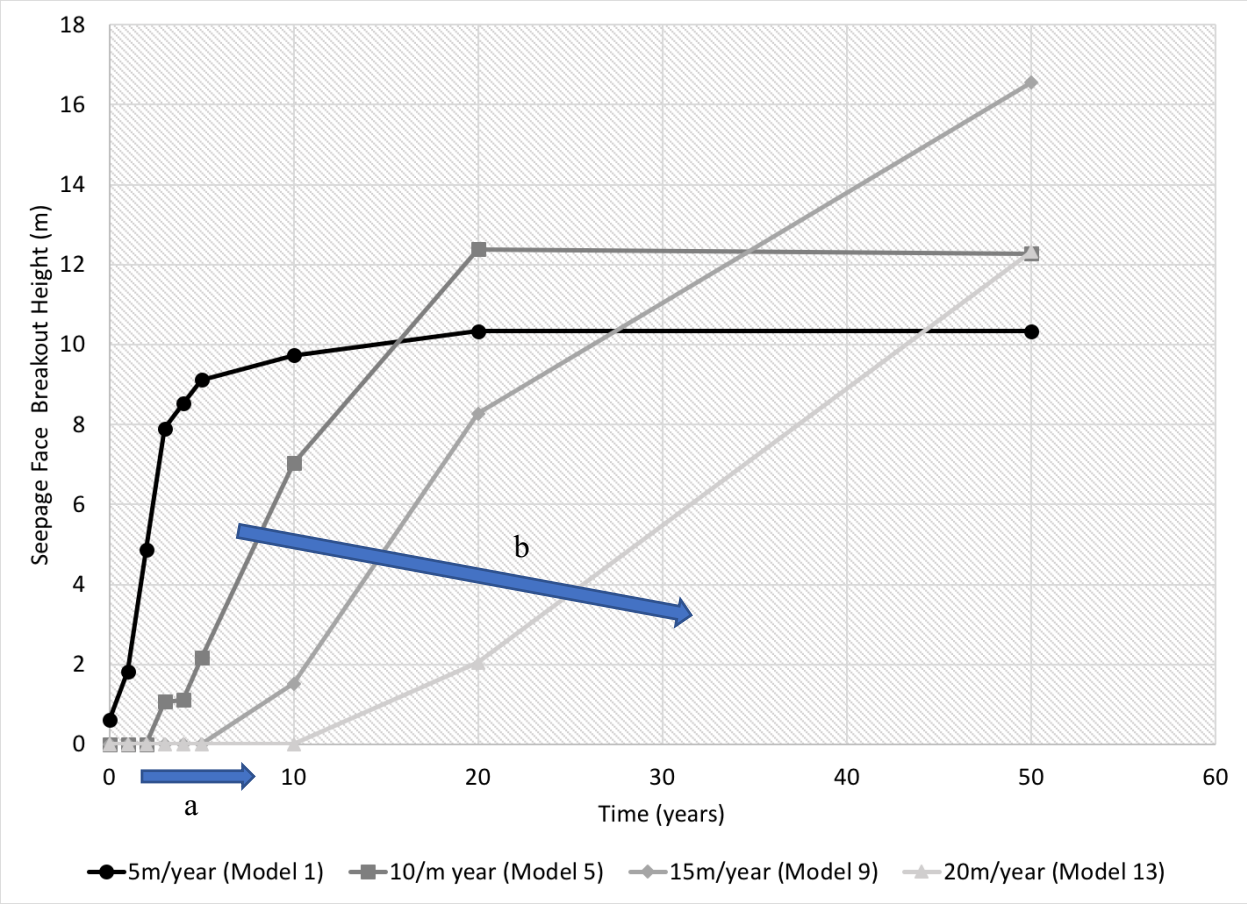

Figure 4.40: Seepage face breakout curves for various embankment raising rates.

4.4.7.5 Effect of Beach Width (L/H)

The beach width (L/H) was one of the key parameters selected in Section 3.1.4, since Vick (1983) identifies (L/H) ratios less than 9 leading to seepage face breakouts in tailings embankment dams. In the simulation sets, ratios of 3, 5, 9 and 12 were considered to explore a wide range of values. In summary, models based on the dataset led to the following conclusions:

1. As already briefly discussed in Section 4.4.7.1, the beach width does not seem to affect the first appearance of seepage face breakout in transient simulations. Across all models with a same embankment raising rate, irrespective of slope inclination or permeability anisotropy, the same value was obtained. Thus, is can be concluded that beach width does

not influence the first appearance of seepage face breakout.

2. Low values (3 and 5) of beach width appear to result in high seepage face breakout values for low raising rates (5m/year) if compared to the rest of models, as observed in Section 4.4.7.2, further confirming Vick's (1983) observations. However, other than these few cases, the majority of models showed very little sensitivity to (L/H) ratios, not more than 20% deviation from their mean values across the (L/H) range.
3. Similarly, the height of seepage face at 50 years is affected by low (value of 3) ratios of (L/H), shown in Figure 4.39 (Section 4.4.7.3). For other combinations, (L/H) does not appear to produce a discernable effect of seepage face breakout. In less than 40% of cases, it was observed that (L/H) values of 9 and 12 result in somewhat reduced seepage face breakout heights (15% lower on average from their mean values across the (L/H) range).

Thus, it can be concluded that beach width (L/H), other than low ratios of 3 and 5 for certain cases, does not affect the height of seepage face breakouts.

4.4.7.6 Effect of Embankment Raising Rate

Undoubtedly, the rate of embankment raising has a substantial effect on the performance of a tailings storage facility. From the standpoint of mining operations, faster the embankment is raised, the more storage is available for tailings, thus if possible, the rate of ore extraction can increase. However, from the perspective of seepage through a tailings embankment dam, the rate of raising was identified as a potential key parameter, as discussed in Chapter 2. Subsections 4.4.7.1 through 4.4.7.4 already established that the rate of embankment raising affects the first appearance of seepage face breakout along with the maximum and 50-year seepage breakout height as well. Thus,

this parameter deserves further investigation. Using the dataset obtained from the simulations, it is possible to look at the effect of raising rate on the seepage face breakout across all models. Figures 4.41-4.46 show the relationships for both the maximum seepage face breakout height and the 50-year value, grouped by anisotropy sets.

Based on the figures, the following conclusions can be made:

1. For gentler slopes (3:1) it appears that there is a peak seepage face breakout height corresponding to the raising rate of 15m/year (Figures 4.41-4.46). This is valid, irrespective of the values of permeability anisotropy and it is present for both maximum seepage face breakout height and 50-year height. Note that these heights are often the same, e.g. the 50-year value is the maximum value, as discussed in a preceding section.
2. For steeper slopes (2:1) and permeability anisotropies belonging to Set 1 (Sand/Slimes of 1:5) and Set 2 (Sand/Slimes of 2:10) the seepage face breakout height approximately linearly increases with the raising rate (Figures 4.41, 4.42, 4.44 and 4.45). However, for Set 3 (Sand/Slimes of 5:10), it peaks at the raising rate of 15/year and then falls off (Figures 4.43 and 4.46).

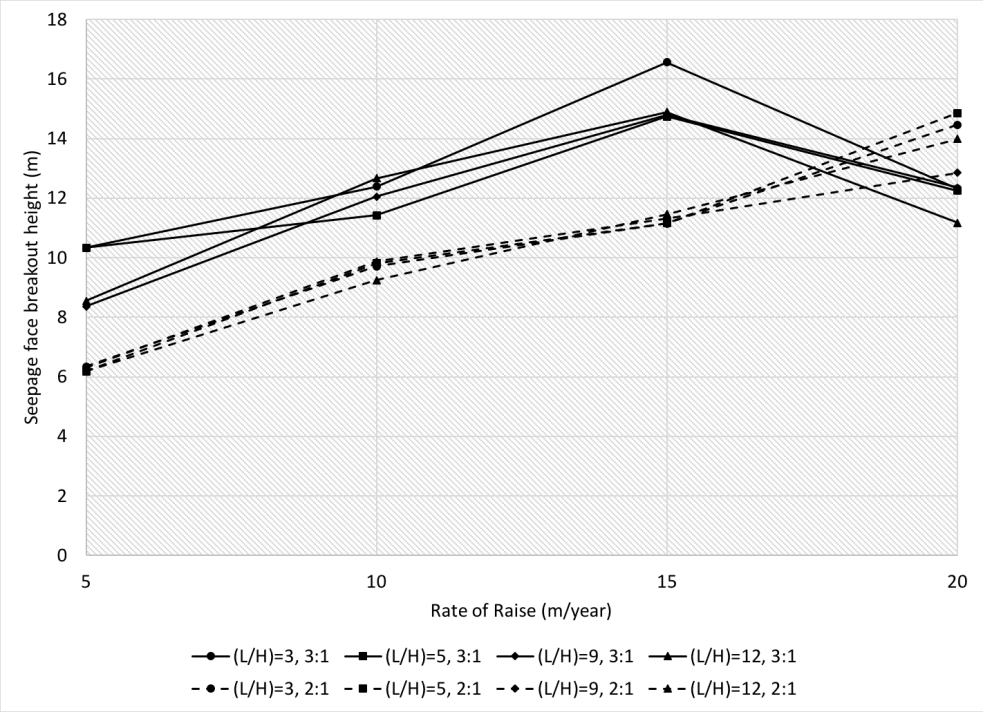

Figure 4.41: Maximum seepage face breakout as a function of embankment raising rate – Anisotropy Set 1.

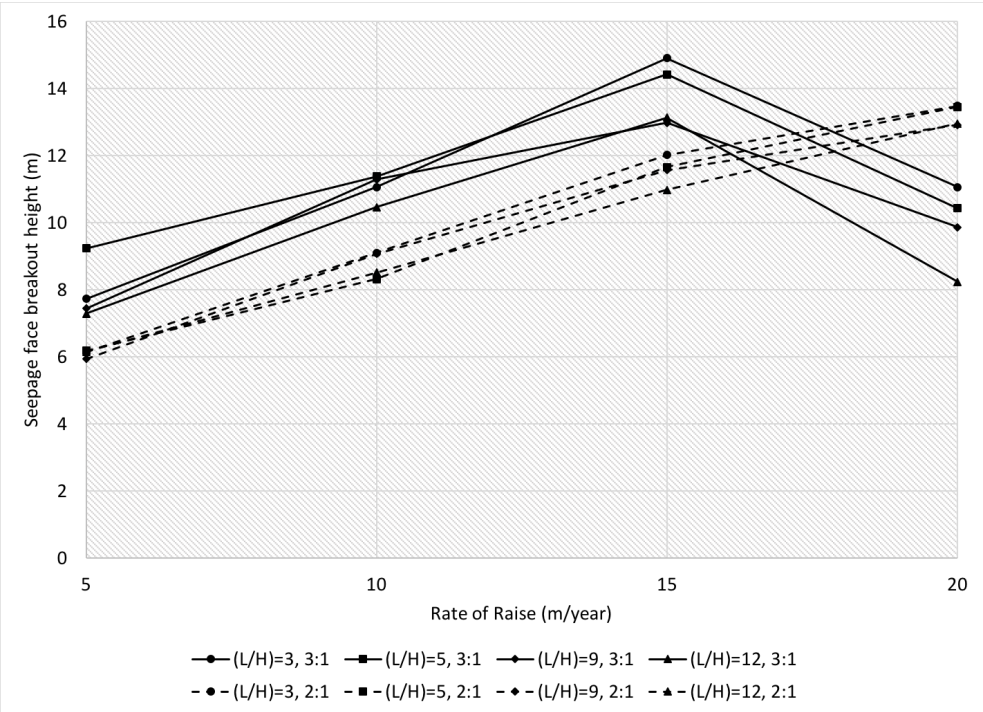

Figure 4.42: Maximum seepage face breakout as a function of embankment raising rate – Anisotropy Set 2.

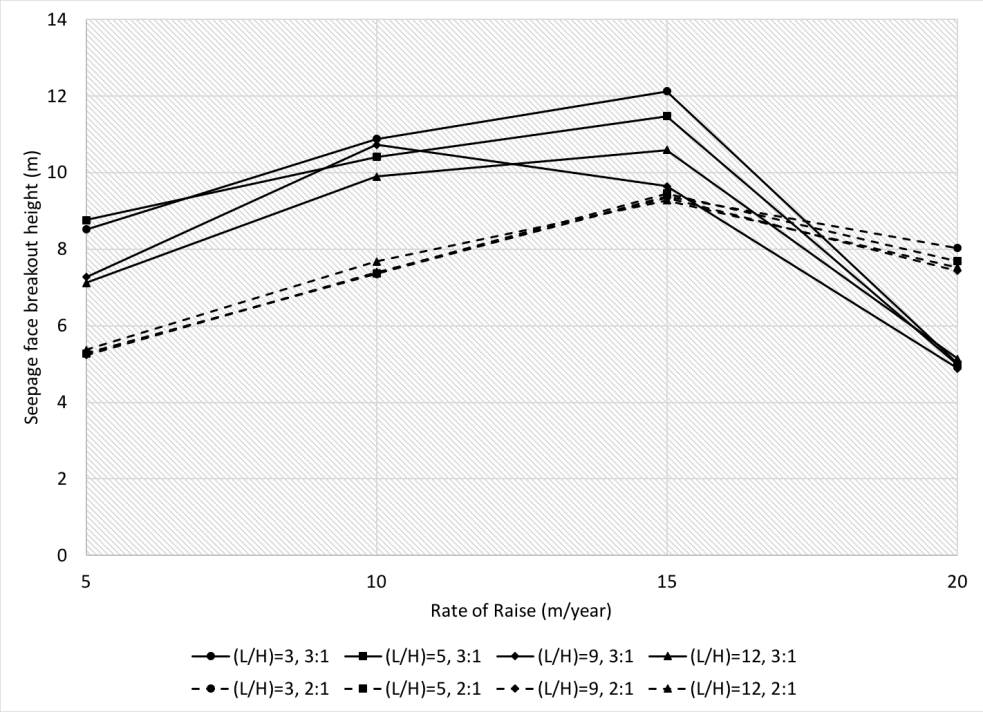

Figure 4.43: Maximum seepage face breakout as a function of embankment raising rate – Anisotropy Set 3.

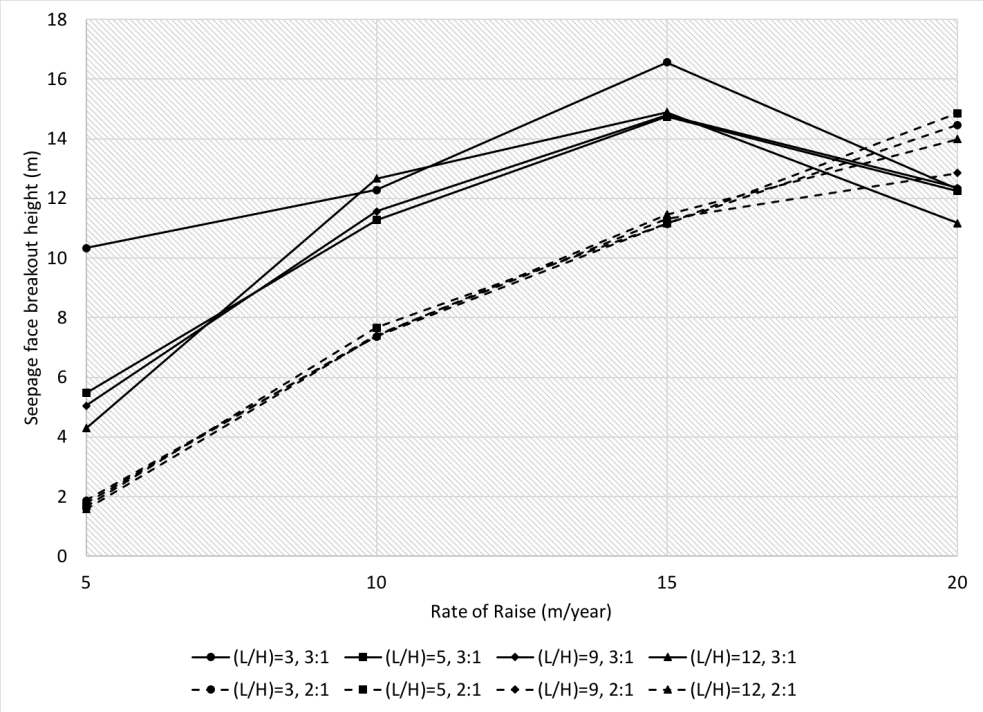

Figure 4.44: Seepage face breakout at 50 years, as a function of embankment raising rate – Anisotropy Set 1.

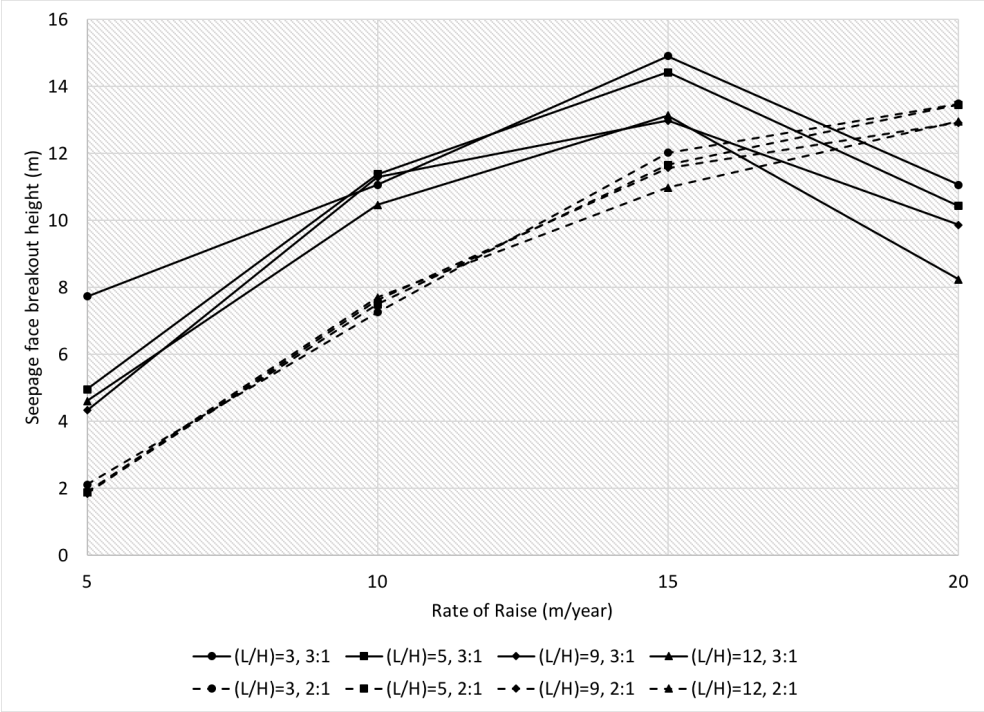

Figure 4.45: Seepage face breakout at 50 years, as a function of embankment raising rate – Anisotropy Set 2.

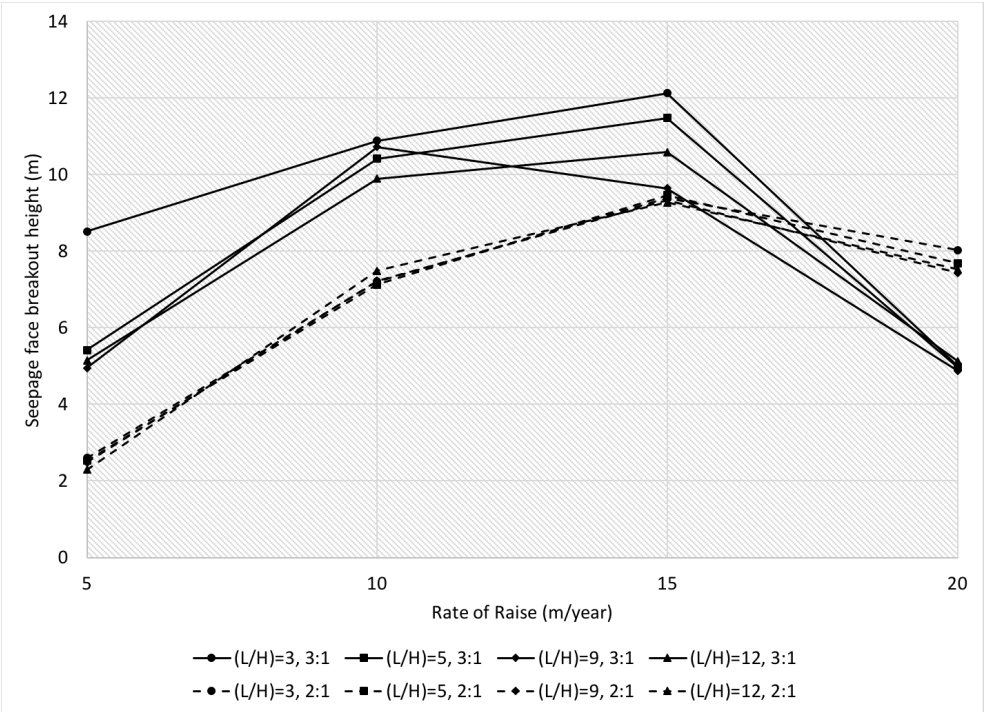

Figure 4.46: Seepage face breakout at 50 years, as a function of embankment raising rate – Anisotropy Set 3.

4.4.7.7 Effect of Permeability Anisotropy

Permeability of various materials making up the tailings facility is recognized to have an effect on seepage flow. Not only the difference in horizontal and vertical rate of permeability within a single material, but the ratio of permeabilities of dissimilar materials, like slimes and sands, needs to be considered. The models developed for this research used three different permeability sets; Set 1 (Sand/Slimes of 1:5), Set 2 (Sand/Slimes of 2:10) and Set 3 (Sand/Slimes of 5:10). Their inclusion as variables led to the following observations:

1. As noted in Section 4.4.7.1, the permeability anisotropy does not seem to affect the first appearance of seepage face, there is little variation with respect to the three sets.
2. Permeability anisotropy affects to some extent the location of maximum seepage face breakout on a slope face. The highest maximum seepage face breakouts occur for Set 1 (Sand/Slimes of 1:5) and decrease for Set 2 (Sand/Slimes of 2:10) and Set 3 (Sand/Slimes of 5:10), in that order, as explained in Section 4.4.7.2.
3. For the 50-year seepage face breakouts, it was observed in Section 4.4.7.3, that Set 1 (Sand/Slimes of 1:5) results in the highest values, followed by Set 2 (Sand/Slimes of 2:10) and Set 3 (Sand/Slimes of 5:10) last. However, the effect of permeability anisotropy is less pronounced than what was found for the maximum seepage face breakout height.
4. In conjunction with slope inclination and the rate of embankment raising, it was found that for steeper slopes (2:1) and permeability anisotropies belonging to Set 1 (Sand/Slimes of 1:5) and Set 2 (Sand/Slimes of 2:10) the seepage face breakout height approximately linearly increases with the raising rate (Section 4.4.7.6). However, for Set 3 (Sand/Slimes of 5:10), there is a peak at the embankment raising rate of 15/year, which was not observed

for other anisotropy sets.

4.4.7.8 Effect of Slope Ratio (2:1 and 3:1)

The inclination of an embankment slope plays an important role in the stability of a slope; generally, the gentler the slope, the higher the factor of safety against slope failure. However, the gentler slope results in increased volume of material needed to construct an embankment, thus raising both the cost and footprint requirement. For upstream embankment dams considered in this thesis, the gentler slope means less space is available for the tailings pond, since the construction proceeds toward the center of the pond (upstream direction, see Section 2.2.2). Thus, the modeling of seepage flow had considered two representative slope inclinations: 2-to-1 and 3-to-1. Based on results from the preceding subsections (in Sections 4.4.6 and 4.4.7), the following conclusions can be drawn;

1. It was found that slopes with 2:1 slope ratio resulted in an earlier appearance of seepage face breakout for higher dam raising rates as compared to ones with 3:1 (Section 4.4.7.1).
2. The slope inclination (3:1 and 2:1) affects both the maximum and the 50-year seepage face breakout and; gentler slopes (3:1) tend to have higher seepage face breakouts (Section 4.4.7.2 for an explanation).

Although, it is shown that slope inclination does affect the seepage face breakout, the effect is considerably less than other parameters' (c.f. rate of embankment raising).

4.4.7.9 Effect of Inclusion of Underdrain in the Models

All models considered in the preceding discussions had no underdrain present beneath the downstream shell of the embankment dam, representing situations when either no underdrain was installed at the inception of a project or it has become clogged or otherwise damaged, thus non-functioning. Properly designed and functioning underdrains should, by their virtue, provide a high-permeability path for the seepage water to escape without ever resulting in a seepage face breakout. Nevertheless, as a verification, all models (see Tables 4.1(a) and 4.1(b)) had an infinite-permeability underdrain installed and were re-analyzed. The underdrain was modeled using a boundary condition where the pressure was set to be zero (atmospheric pressure) and it was located under the outer 1/3 of the downstream shell. This is a customary method of defining free drainage in a finite element model for seepage simulation of embankment dams (Rocscience Inc., 2018). Figure 4.47 shows a typical model with an underdrain defined.

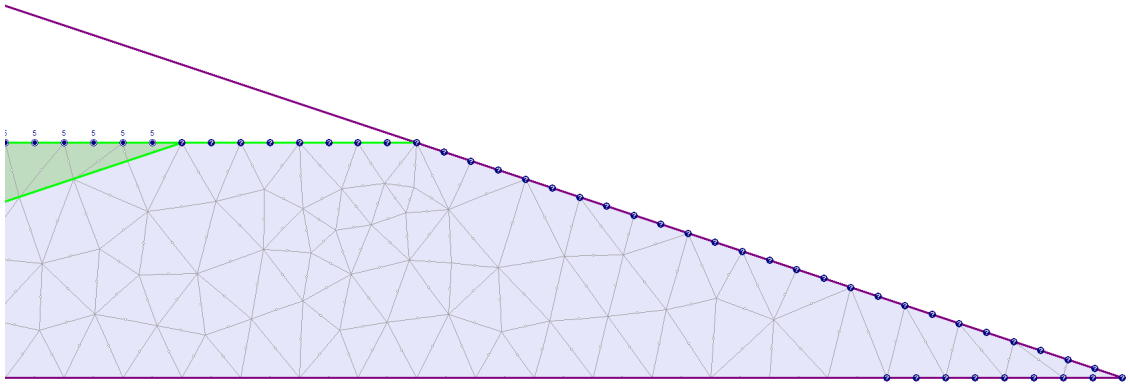

Figure 4.47: Definition of an underdrain for a typical finite element model using free drainage boundary conditions.

As expected, all models with an underdrain resulted in no seepage face breakouts on the downstream shell, further reinforcing the importance of underdrains. Figure 4.48 shows the pressure head distribution and the location of the phreatic surface for a typical model. It can be observed, that the phreatic surface terminates at the leftmost end of the underdrain and no seepage flow occurs above it in the downstream shell, thus no seepage face breakout develops.

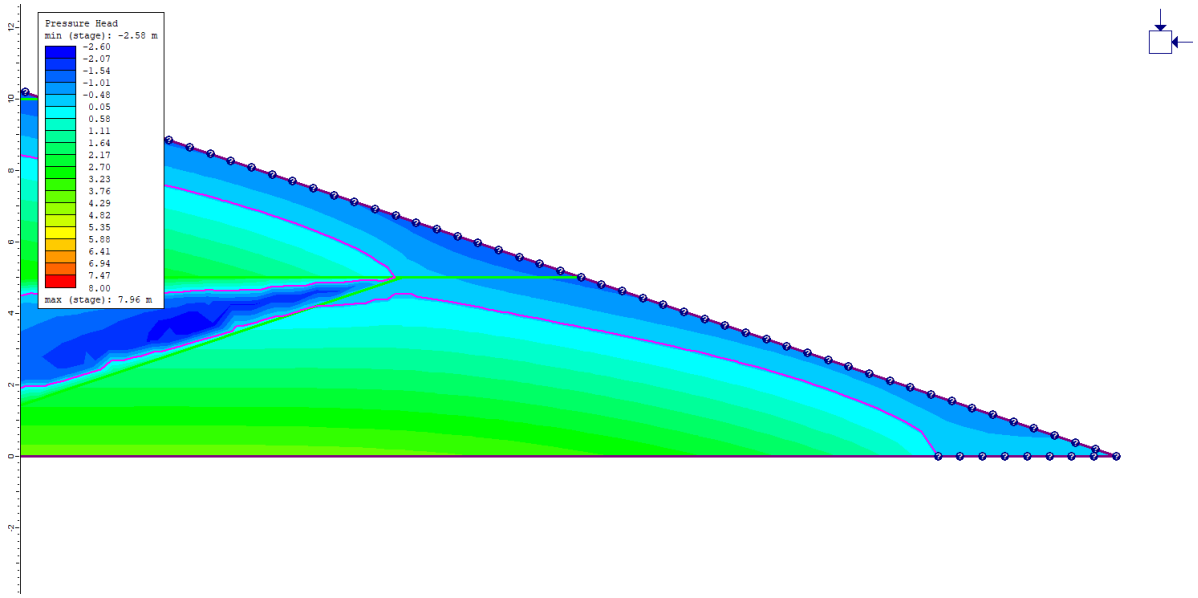

Figure 4.48: Pressure head distribution and location of phreatic surface for an embankment dam with an underdrain installed.

Chapter 5: Conclusion and Recommendations

In this thesis, the long-term evolution of seepage conditions for upstream tailings dams were investigated using numerical modeling to study the effect of damaged or non-existent underdrains. Observations in the preceding chapter revealed that the long-term seepage performance can be impacted by not only individual factors but often by some combination of them. Some models showed less sensitivity to factors like beach width and slope ratio. But, values of beach width (L/H) less than 5 resulted in a problematic phreatic surface location with breakout of seepage face on the downstream face. Also, it was found that the breakout height is considerably lower for tailings dams with a long beach width (in the range of 9 to 12). However, the first-time appearance of seepage face breakout does not seem to be affected by beach width and permeability anisotropy.

Also, materials with low anisotropy ratio in the transition beach zone are relatively insensitive to layering. From the long-term observation, both the maximum seepage face breakout height and 50-year seepage face breakout height results in the highest value for permeability anisotropy of 1:5 for sand/slimes and followed by sand/slimes anisotropy of 2:10 and anisotropy of 5:10. However, in the case of steeper slopes (2:1), the higher anisotropy of sand/slimes (5:10) results in the highest seepage face breakout for embankment raising rates of 15m/y.

The most important factor influencing phreatic surface location is the rate of embankment raising during the operation of a mine. The raising rate acts in combination with slope ratio and anisotropy permeability; the faster the dam is raised, the more likely to results in a high breakout face in the downstream shell of an embankment. However, 15m/y appears to be a critical embankment raising rate, resulting in the highest seepage breakout height for the majority of models for both maximum

and 50-year seepage breakout height. For rates above this, the height of breakout face is less. This peak is due to the imbalance between seepage rate and the rate of excess tailings being impounded, driving the flow. In addition, for the case of steeper slopes with lower anisotropy permeability (Sets 1 and 2), the seepage face breakout height is proportional to the raising rate.

Overall, it appears that the slope ratio affects the seepage face breakout the least. However, the obversions showed that the first-time appearance of seepage face breakout is earlier for steeper slopes. Even though a gentler slope is more stable and expensive to construct than a steeper one for long-term evolution of tailings embankment, but there is still an opportunity for a high seepage face breakout.

The above observations were based on the fact that no functioning underdrain is available. Once tailings dams constructed with an underdrain, there will be no seepage face breakout on the downstream shell.

According to the conclusions above, the following recommendations can be given to control seepage face breakout;

- Beach width is an operational factor that can be controlled during tailings impoundment, and it is recommended to be kept in the range from 9 to 12.
- Materials with higher anisotropy ratios may contribute to lower the phreatic surface location for upstream embankments.
- Underdrains are the most efficient remedy against high seepage face breakout available to a designer. However once constructed, there are no means to correct any flaw in them.

Despite all of this, each tailings dam is constructed with unique characteristics, siting, requirements and other inherent conditions. In fact, there could be too many variables during the construction

and operation process that cannot be controlled and predicted ahead of time. Thus, the approach used in this thesis allows engineers to perform a better comparison of model parameters affecting the long-term seepage performance of tailings dams and also raises issues that tailings facility designers and operators need to consider seepage face breakout both during and after the cessation of mining operation to ensure safe and sustainable tailings disposal practices.

Future research, building on this work, should include investigation of the effect of coupled seepage and stress analysis not only to examine seepage-induced instability, but to perform slope stability assessment in which a factor of safety can be established based on deformation and pore water pressure.

References

1. Asadzadeh, M. (2010). *An introduction to the Finite Element Method (FEM) for differential equations in 1D*. Retrieved from http://www.math.chalmers.se/~mohammad/teaching/PDEbok/Draft_I+II.pdf
2. Bhanbhro, R. (2014). *Mechanical properties of tailings: Basic description of a tailings material*, Licentiate dissertation, Department of Civil, Environmental and Natural Resources Engineering, Lulea University of Technology, Sweden. Retrieved from http://urn.kb.se/resolve?urn=urn:nbn:se:ltu:diva-16952
3. Breitenbach, A.J. (n.d.). *Improvement in the stability of upstream method phosphate tailings dams with rock fill shells*. Retrieved from https://www.ausenco.com/download/628
4. Byrne, P., Hudson-Edwards, K., Macklin, M., Brewer, P., Bird, G., & Williams, R. (2015). The long-term environmental impacts of the Mount Polley mine tailings spill, British Columbia, Canada. Geophysical Research Abstracts, 17(EGU2015-6241)
5. Chambers, D. (2016). Post-Mount Polley. Ottawa, Ontario: MiningWatch Canada.
6. Chapuis, R., & Aubertin, M. (2001). A simplified method to estimate saturated and unsaturated seepage through dikes under steady-state conditions. *Canadian Geotechnical Journal*, *38*(6), 1321-1328. doi: 10.1139/t01-068
7. Coil, D., Lester, E., Higman, B., & Mattox, A. (2014). *Mine tailings*. Retrieved from http://www.groundtruthtrekking.org/Issues/MetalsMining/MineTailings.html
8. EC (2004). *Draft Reference Document on Best Available Techniques for Management of Tailings and Waste-Rock in Mining Activities*. European Commission, Edificio EXPO, Seville, Spain: 563
9. El-Salam, A.R.A. (2012). *Mining Tailings and managements*. Retrieved from http://sci.tanta.edu.eg/files/Aya.pdf
10. Fredlund, D., Rahardjo, H., & Fredlund, M. (2012). *Unsaturated soil mechanics in engineering practice*. Somerset: Wiley.
11. Hamade, T. (2013). *Geotechnical design of tailings dams - a stochastic analysis approach,* Ph.D. dissertation, Department of Mining and Materials Engineering, McGill University.
12. Henzel, Y., Bréard, J., Lang, D., & Trochu, F. (1999). *A standard characterisation of saturated and unsaturated flow behaviours in porous media*. Retrieved from https://www.researchgate.net/publication/268400137_A_Standard_Characterisation_of_Saturated_and_Unsaturated_Flow_Behaviours_in_Porous_Media
13. ICOLD (2001). *Tailings dams: Risk of dangerous occurrences: lessons learnt from practical experiences*. Commission Internationale des Grand Barrages, Paris, France.
14. Kealy, C., & Busch, R. (1971). *Determining seepage characteristics of mill-tailings dams by the finite-element method.* Washington D.C.: U.S. Dept. of the Interior, Bureau of Mines.
15. Klohn, E. (1979). *Seepage control for tailings dams*. Retrieved from https://www.imwa.info/docs/imds_1979/IMDS1979_Klohn_671.pdf
16. Lambe, T. W., & Whitman, R. V. (1969). *Soil mechanics*. New York: Wiley.
17. Linnitt, C. (2018). *It's Official: No Provincial Charges for Mount Polley Mine Spill, One of Largest Environmental Disasters in Canadian History | The Narwhal*. Retrieved from

https://thenarwhal.ca/it-s-official-no-provincial-charges-mount-polley-mine-spill-one-largest-environmental-disasters-canadian-history/
18. Mesri, G., Terzaghi, K., & Peck, R.B. (1996). *Soil mechanics in engineering practice*. (3rd ed.) New York City: Wiley.
19. Mittal, H., & Morgenstern, N. (1975). Parameters for the Design of Tailings Dams. *Canadian Geotechnical Journal*, *12*(2), 235-261. doi: 10.1139/t75-028
20. Ritcey, G.M. (1989). *Tailings management: problems and solutions in the mining industry*. Elsevier Science Publishers; New York: Elsevier Science Pub. Co. [distributor for U.S. and Canada], Amsterdam
21. Rocscience Inc. (2018), RS2 User's Manual, www.rocscience.com
22. Singh, A.N., Srinivas, M., & Naik, B.N. (2015). Forcasting the impact of surface mining on surroundings using cloud computing. *Journal of Computer Sciences and Applications*, *3*(6), 118-122.
23. Tan, Q. (2008). *Study on the Optimization Theory and Key Mechanics Problems of High Centerline Tailings Dam*, Ph.D Dissertation, College of Civil Engineering, Chongqing University, People's Republic of China.
24. Thygesen, K. (2017). A mining operation, illustrating a typical process in an open pit mine, from excavation to waste disposal, From collection: Mine Tailings Storage: Safety Is No Accident, http://www.grida.no/resources/11415.
25. U.S. Environmental Protection Agency, Office of Solid Waste. (1994). *Technical report: Design and evaluation of tailings dams.*, Washington DC, USA.
26. Vick, S. G. (1983). *Planning, design, and analysis of tailings dams*. New York: John Wiley & Sons.
27. Wang, H. & Anderson, M. (1982). *Introduction to groundwater modeling*. New York: W.H. Freeman.
28. Whitman, R. (2000). Organizing and evaluating uncertainty in geotechnical engineering. *Journal of Geotechnical And Geoenvironmental Engineering*, *126*(7), 583-593. doi: 10.1061/(asce)1090-0241(2000)126:7(583).
29. WILLIS, (2012). *Mining market review*. Retrieved from https://www.willis.com/naturalresources/pdf/MiningMarketReview2012.pdf.
30. Zardari, M.A. (2011). *Stability of tailings dams: focus on numerical modelling*, Licentiate dissertation, Department of Civil, Environmental and Natural Resources Engineering, Lulea University of Technology, Sweden Retrieved from http://urn.kb.se/resolve?urn=urn:nbn:se:ltu:diva-18427.